THE MODELLING AND DESIGN OF SOLID-STATE TRANSFORMER FOR SMART ENERGY

by

ADIMCHINOBI DANIEL ASIEGBU

Dissertation submitted in partial fulfilment of the requirements for the degree

Master of Engineering: Energy (MGENRC)

in the Faculty of Engineering & the Built Environment

at the Cape Peninsula University of Technology

Supervisor: Dr Ali Almaktoof

Bellville

May 2023

DECLARATION

I, Adimchinobi Daniel Asiegbu, declare that the contents of this dissertation represent my own unaided work, and that the thesis/dissertation has not previously been submitted for academic examination towards any qualification. Furthermore, it represents my own opinions and not necessarily those of the Cape Peninsula University of Technology.

	13/05/2023
Signed	Date

ABSTRACT

This research presents the modelling and design of a solid-state transformer (SST) for smart energy, by scrutinizing and analyzing the problems associated with Low-Frequency Transformers (LFT) and presenting the SST as a model and solution in the smart energy system.

The behaviour of the SST in dynamic conditions that is suitable to a smart energy system was carried out, through the analysis of the SST vital components (converters) and their parameters which should be designed first. This is done by an erudite mathematical analysis, culminating in various equations representing their behaviour, function, and their ratings. The required voltage, current and power rating of each component is represented by corresponding equations that unveils the impedance matching requirement, ensures that maximum power is transferred between connecting components of the SST in the smart energy system. The components of the SST analyzed include the Cascaded Hybrid Bridge (CHB) converter which converts AC to DC and connects to the Dual Active Bridge (DAB) through a DC link capacitor. The DAB is another converter that uses a high frequency transformer situated in between the DC - DC and transforms DC/AC to AC/DC, while ensuring galvanic isolation in the SST high voltage side and low voltage side, and it links to the Three Phase Four Leg (3P4L) converter through a DC link capacitor. The 3P4L DC/AC converter links the SST to the load or grid. The equations, mathematical functions, and algorithms developed in this study will help in the design of converters DC links, and the combinations of these components culminating in the design of the SST.

To assist in retrieving the converters filter parameters, the algorithms are written in simple but engineering and mathematical problem-solving centered methodology, for easy implementation in the various programming language. The efficiency analyses of the SST are performed using the POET framework. The verification, modelling and design are done using MATLAB Simulink. Hence, the potential use or applications of SST as a component of a power grid, modern house, and smart energy is unveiled.

ACKNOWLEDGEMENTS

I wish to thank:

- Dr Ali Almaktoof, my supervisor for his guidance and perseverance in all the research I did, conference presentations, publications, and this dissertation.
- Prof Khaled Aboalez, my lecturer in Energy Efficiency and Energy Audit. The knowledge gained in these modules is indispensable in energy efficiency classification and energy auditing of a Solid-State Transformer (SST), residential, commercial, and industrial infrastructures.
- Prof Raji Atanda, my lecturer in Generation, Distribution and Transmission (GDT) of smart energy and co-lecturer of energy access module. This module elucidates the advanced engineering (advanced power electronics, advanced power systems, advanced control engineering, advanced automation and simulations for the smart grid, advanced engineering mathematics, and advanced electrical machines) behind the SST, and for solving complex engineering problems in creative and innovative procedures.
- Dr Marco Adonis, my lecturer for Alternative and Sustainable Renewable Energy Technologies (ASRE) and co-lecturer in Energy Access. The knowledge gained in this module consist of the erudite analysis of advanced hybrid microgrid system in smart energy system consisting of advanced wind energy, solar photo-voltaic energy, hydro-energy, geothermal energy, waste-to-energy, nuclear energy, fuel cell, hydrogen energy, hydrokinetics, biomass energy, solar heating, and cooking engineering technology. The modelling and simulation of the smart energy hybrid system using HOMER software and simulator, reveals the need for the SST in smart grid system.
- Prof Tariq Kahn, my Energy Modelling lecturer. This module helped me to understand modelling of energy system and smart grid calculations, hydrogen energy, ammonia energy, biodiesel, fuel cell, energy block chain, energy trading and energy economics, troubleshooting and design of power system using power world Simulink software.
- South African Wind Energy Association (SAWEA) For WindAc Conference sponsorship award, and conference presentation opportunity in Cape Town, SA.
- World Intellectual Property Organization (WIPO) and National Intellectual Property Management Organization (NIPMO) for Sponsorship award to attend the advanced summer school on intellectual property.
- Enlit Africa, for Enlit Africa 2023 sponsorship award as a conference speaker.
- My family (my parents, brothers, sisters, children, and wife) for their understanding and support.
- The financial assistance of Liquid Telkom South Africa (LTSA), Energy Institute, and Cape Peninsular University of Technology (CPUT) Center for Post Graduate Studies (CPGS) towards this research is acknowledged.
- Everyone that contributed to the success of this research.

DEDICATION

This dissertation is dedicated to God, my parents (Rev. Leo Chibugwu Asiegbu and Mrs. Grace Uche Asiegbu), my children (Zinachidimma Divine Asiegbu and Chimdindu Haziel Asiegbu), and my wife (Mrs. Chioma Vivian Asiegbu (NRF-UNISA Exceptional Skills Doctoral Scholar)) for their support and believe in me.

TABLE OF CONTENTS

Contents

LIST OF FIGURES

LIST OF TABLES

ABBREVIATIONS AND ACRONYMS

Acronym	Meaning
A, B, C or a, b, c	High voltage side phases or low voltage side phases
AC/DC or AC - DC	Alternating Current to Direct Current
a-factor	Steady state gain (the ratio of input line currents il_{dc} and ih_{dc})
AI	Artificial Intelligence
φ	The phase angle between P and S vector components
Δ	The phase angle between the MV grid and the CHB voltages.
CHB	Cascade Hybrid Bridge
C_{3P4L}	Three Phase Four Leg Capacitor for DC Link
3P4L	Three Phase Four Leg
C_{DAB1}	Total of CCHB2s and CDAB1s
C_{DAB1s}	DAB Capacitor from the CHB side
C_{DAB2s}	DAB capacitor from 3P4L side
$C_{f\text{-}3P4L}$	3P4L filter capacitor
C_e	The equivalent Capacitance
$C_{(inv)}$	Control circuit filter capacitor
$C_{min\text{-}DAB}$ and $C_{min\text{-}sin}$	DAB minimal capacitance and minimal capacitance
D	Duty cycle
DAB	Dual Active Bridge
D_{DAB}	DAB phase-shift (duty cycle)
DC/AC	Direct Current to Alternating Current
DC_{RATIO}	DC conversion ratio
DF	Distortion Factor
DFIG	Doubly-Fed Induction Generator
DG	Distributed Generation
DPDS	Dual Primary Dual Secondary
DPSS	Dual Primary Single Secondary
e_{g1}^{abc} and e_{g2}^{abc}	Network feeder voltages
e_{g1r}^{abc} and e_{g2r}^{abc}	Network reference feeder voltages
$e_g(t)$	Network feeder voltage
$e_i(t)$	Network feeder current
EPT	Electronic Power Transformer
F or f	Frequency
f_{CHB}	Switching frequency of the CHB
$f_{CHB\text{-}effective}$	Effective switching frequency of CHB
f_{DAB}	Switching frequency of DAB
FF	Form Factor
f_{grid}	frequency of the grid
FREEDM	Future Renewable Electric Energy Delivery and Management
f_s or f_{sw}	Switching frequency
g and g'	Control power selector handle with values between 1 and 0
h	harmonic order
HB	Number of Hybrid Bridges
HEART	The Highly Efficient and Reliable smart Transformer
HFT	High frequency transformer
i	input
i_1 and i_2	3P4L converter output and Grid side/load side phase currents
i_{DAB1}	CHB side current of the DAB
i_{DAB2}	3P4L side DC current from DAB

i_{DC1}	Sum of CHB and DAB currents
i_{DC2}	Sum of current on 3P4L DC-side
$i_{DC\text{-}3P4L}$	3P4L DC-side current
$i_{DC\text{-}CHB}$	CHB H-bridge DC-side current
$i_{g1}(t)$ and $i_{g2}(t)$	Switching function to control the rectifier's currents
i_{g1}^{abc} and i_{g2}^{abc}	The corresponding feeder link currents
i_{g1r}^{abc} and i_{g2r}^{abc}	The reference network link currents
IGBT	Insulated Gate Bi-Polar Transistors
$i_{(inv)}\ (t)$	The filter inverter input current
I_L	Load current
il_{dc} and ih_{dc}	Control scheme Input current and high DC current
$I_{ph\text{-}LV}$	Phase-current of the LV-grid
$I_{ph\text{-}MV}$	Phase-to-neutral MV grid current
$i_r(t)$	represents current flow to the load, managed by the control scheme as a disturbance
I_{sc}	Short circuit current
iSST	Isolated Solid-State Transformer
IUT	Intelligent Universal Transformer
IEEE	Institute of Electrical and Electronics Engineers
IGBT	Isolated-Gate Bipolar Transistor
[J]	A 2X2 vector matrix consisting of [0, -1, 1, 0]
LF	Low Frequency
LFT	Line Frequency Transformer
L_{DAB}	Transformer leakage inductance
$L_{DAB'}$	Primary referred, total leakage inductance of the transformer
L_{DAB1}	Leakage inductance of the primary winding
L_{DAB2}	Leakage inductance of the secondary winding
$L_{f1\text{-}3P4L}$	3P4L filter inductor on converter side
$L_{f2\text{-}3P4L}$	3P4L filter inductor on grid/load side
L_{g1} and L_{g2}	Input inductances
$L_{(inv)}$	Control circuit inductance of the filter
L_M	transformer magnetizing inductance
LVMV	Low Voltage to Medium Voltage
$m_{a\text{-}CH}$	CHB modulation index
MIMO	Multiple Input Multiple Output
MPC	Method Predictive Control
m(t)	represents the modulation index (as known as the input controller)
MVLV	Medium Voltage to Low Voltage
N_m	Number of H-Bridges in each phase of the CHB
nTr	Transformer turns-ratio
o	output
P	Active power or real power
P_{DAB}	Power transferred through the DAB
P_{DAB1}	Power of the DAB on the CHB side
P_{DAB2}	Power of the DAB on the 3P4L converter side
$P_{DAB\text{-}rated}$	Rated power of the DAB
PI	Proportional Integral control
P_{rated}	Rated active power
PLL	Phase Locked Loop
PV	Photo-Voltaic Cell

Q	Reactive Power
R_c	Core Magnetic Resistance
R_{DAB1}	Primary winding resistance
R_{DAB2}	Secondary resistance winding
$R_{(inv)}$	Resistance output parameter of the filter
R_{g1} and R_{g2}	Input resistances
$R_{(pu)}$	Per unit resistance
S	Apparent power
S_{max}	Maximum apparent power
SPSS	Single Primary Single Secondary
$V_{abc\text{-}cf\text{-}3P4L}$	Voltage across the filter capacitor on the AC-side of the 3P4L converter
$V_{ac\text{-}DAB1}$	Transformer primary side voltage
$V_{ac\text{-}DAB2}$	Transformer secondary side voltage
V_{CHB}	AC-side voltage of the CHB
V_{DAB1}	DC-voltage between the CHB and the DAB
V_{DAB2}	DC-voltage of the DAB on the side of the 3P4L converter
V_{Dc}	DC link Voltage
v_{hdc} and v_{ldc}	Control scheme high voltage DC and output DC voltage,
vh_{icr}	The reference high DC voltage.
V_{in}	Input voltage
V_{out}	Output voltage
$v_{1(n1)}$ and $v_{2(n2)}$	Voltage switching function to control the rectifier's voltage
$V_{ph\text{-}LV}$	Phase-voltage of the LV-grid
$V_{ph\text{-}MV}$	Phase-to-neutral MV grid voltage
$v_o(t)$	Output 3P4L converter voltage
v_{or}	Desired output voltage reference
ΔV	DC peak to peak ripple voltage
ω_o	The angular frequency in radians of the voltage and current outputs respectively
ω_{s1} and ω_{s2}	signal angular frequency for the control of the current input of the rectifier
s	supply
SH	Smart House
SG	Smart Grid
GHGs	Green House Gases
SISO	Single Input Single Output
SPDS	Single Primary Dual Secondary
SST	Solid State Transformer
TAB	Tri-Active-Bridge
$t_{on\text{-}DAB}$	Switch ON delay time
$T_{s\text{-}DAB}$	DAB switching period
TTr or ttr or Ttr	Transformer Turn Ratio
X_{cf}	3P4L output capacitive reactance
X_{Lf2}	3P4Lgrid or load side inductive reactance
X_{LfN}	3P4L output inductive reactance
Z_e	Equivalent Load impedance
Z_L	Grid or Load Impedance

CHAPTER ONE: INTRODUCTION

1.1 Introduction

The next generation distributed transmission grid, called smart grid (SG), is the backbone of modern electrical power infrastructure, mimicking neural networks, and designed to solve the problem of integration of energy sources, which is crucial (Sooriyabandara, Ekanayake; 2010). These energy sources generate and transmit Electrical power at multiple frequencies and multiple voltages (Maitra, Sundaram, Gandhi, Bird, Doss; 2009). The power quality problems like voltage sags, voltage and current spikes from lightning, power factor issues, downtime, reliability issues, and efficiency of the power system (because of losses and waste of electrical energy) cannot be mitigated by the current grid but by the SG and the Solid-State Transformer (SST).

Modern technology and advances in technology demand more energy in a purer form. The recent decarbonization policy and various policies to improve efficiency and reduce energy consumption from biomass and fossil fuel energy sources coupled with the decrease in cost of renewable energy sources like wind turbines, hydro-dam, hydrokinetics, photo-voltaic (PV) cells and concentrated solar power (CSP) results in high penetration of renewable energy technologies and generation. Also, the development of electrical vehicles and modern storage facilities like highly efficient deep-cycled batteries and molten salt technology, directly put stress on the current grid infrastructure, especially in withstanding the electrical power factor, frequency, voltage, and current variations, respectively.

The SST with bidirectional transmission capability, Artificial Intelligence (AI), and multilayer applications is needed to mitigate the problems associated with current lines or low-frequency transformer and can be designed to function in the medium and low voltage region of 10KV and above, by combining different SST topologies and control strategies (Sabahi, Goharrizi, Hosseini, Sharifian, Gharehpetian; 2010). Hence, A Power Electronic-Based Distribution Transformer like the SST can also be referred to as a High-Frequency Transformer (HFT) (Roman, Sudhoff, Glover, Galloway; 2002), Intelligent Universal Transformer (IUT), and Electronic Power Transformer (EPT) due to its unique and indispensable features and characteristics using high-frequency power electronic switches.

1.2. Research problem

1.2.1 Background to the research problem

Electricity is an important clean energy source, and a smart energy. Access to electrical energy is a major indicator of the presence or absence of energy poverty, and quality of life in general.

Energy consumption is not unconnected with socio-economic growth. Increase in electrical energy consumption is an indicator of growth in economic activities and an improved standard of living.
Economic, health and sustainability factors favor the generation of electricity from renewable sources. These sources can be influenced by the weather, climate, season of the year and other natural effects, leading to a variable rate of generated electrical energy output from these sources (energy transducers).
These present problems with the coordination and integration of different variations in the generation of electricity from diverse sources. Some of the sources like wind turbine generate Alternating Current (AC) electrical energy which has sinusoidal or semi-sinusoidal waveform, while others like photo-voltaic cells (PVC) generate Direct Current (DC) electrical energy, which is horizontally linear in shape or waveform. The problem is that due to unavoidable variations in the input energy, the output electrical energy is not steady, resulting in electrical energy output that varies and fluctuates with respect to time. On the load side or electrical energy demand side, non-linear loads like Resistive-Inductive-Capacitive (RLC) Load introduce harmonics and distortion to the energy system. This undesirable harmonic current flows to other sources and loads in the distributed generation system. The problem on the grid side is that some effects like thunderstorms and lightening can discharge or inject current of high magnitude for a short period (impulsive current) into the grid system, causing voltage spikes, swell, or sag capable of introducing harmonics into the energy system and destroying insulation or important parts of the energy system.
Energy resources are not located in the same place or vicinity on Earth, weather changes are different in different places, and storage systems can be maintained at the source or load side. The problem of integration of all the renewable energy sources and storage systems (water heads, batteries, hydrogen, ammonia) needs to be mitigated and synchronized to ensure reliability, availability, sustainability of smart energy supply, and most importantly energy access to all in line with the Sustainable Development Goals (SDG) of the United Nations (UN) in general, and South Africa in particular.

1.2.1 Statement of research problem

The need for a smart energy system which includes smart grid and SST that is reliable and sustainable means that the SST which allow bi-directional transmission of energy at high efficiency, reduce electrical disturbances like harmonics from non-linear loads and provides different conversion topologies needed to be developed, and replace the current transformer. SST concept was first proposed as a high-frequency AC/AC power converter link in 1970 by William McMurray (Shamshuddin et al., 2020).

1.3 Significance of problem

The cost and lost time in the economy, associated with power loss, downtime, load shedding, lightning and insulation protection, integration of various energy sources, and other significant problems in the power systems, make the design and modelling of SST imperative. The SST allows a bi-directional flow of electrical energy between source and load and reduces or eliminates harmonic currents and distortions from flowing in the smart energy system. SST minimizes voltage flicker and does not need dielectrics, mineral oil, or liquid. It incorporates different voltage (AC to DC, DC to DC, DC to AC, AC to AC) conversion topologies, it can receive AC/DC input and output DC/AC, mitigate voltage sag, swell, and spike, and can be operated at different frequencies, and it can produce different voltage levels (voltage regulation) (Banaei, Salary: 2014a). The current low-frequency power system transformers cannot solve the above-mentioned problems.

The SST performs VAR compensation, smart protection, active filtering, power factor correction and disturbance isolation. There is increasing attention to the matrix converters as a variable frequency and variable voltage AC to AC power system, that can be applied to areas that demands easier maintenance, smaller size, and higher power density (Lee, Nguyen, Chun: 2008; Hooshmand, Ataei, Rezaei: 2012). To address these problems and improve the reliability and efficiency of the distributed generation, a solid-state transformer is designed based on the knowledge of the advanced power system, control system, power electronics, electrical machines, protection technology, engineering mathematics, and high voltage engineering, respectively. It can make decisions to improve performance and efficiency and can be digitally and remotely operated by a computer for solving complex smart energy or power system engineering problems.

1.4 Research objectives

The main objective of this research is to model and design a SST for smart energy, that will mitigate issues like source-load integration, voltage regulation, losses in the grid system, fault and failures detection and prevention, and improvement of the distributed generation in the smart energy system.

To achieve the above objectives the following sections must be done:

1. The review of the SST and line frequency transformer (LFT) from available literature and information repositories.
2. Benefits and cost analysis of SST and FLT to know its viability and economic value.
3. Selecting the best SST architecture for high-efficiency applications.
4. How to combine SSTs for medium and high alternating current and direct current applications.

5. The best possible topology for integrating various sources of electrical energy forms, like SST capable of allowing bidirectional current flow whether it is an alternating current or direct current.
6. Based on the above objectives, modelling and design of SST that satisfies the requirements mentioned above.
7. The thermal and insulation considerations in smart grid with regards to SST implementation
8. Applications of SSTs in smart energy.
9. Investigation and study of the different parameters of the SST, like the evaluation of components values, useful parameter values, core materials through their magnetic classifications and characterizations (Gupta, Sinha, Vates, Chavan: 2021) and the SST design.
10. To confirm the proposed performance of the SST, computer-aided simulations are done using SIMULINK /MATLAB (Banaei, Salary: 2014b).

1.5 Expected outcomes, results, and the research contributions.

1.5.1 The Expected outcomes

The outcome expected from this research is the design of an energy-efficient SST in an energy system, with minimal losses when operated at high frequency, high power density, high voltage, and high current.

1.5.2 The result

The result of this research is the mitigation of the issues encountered in power integration of various energy sources in distributed smart energy systems from direct current and alternating current, with different frequencies and power densities like from solar photo-voltaic energy sources, wind energy sources, geothermal energy sources etc.

1.5.3 The research contribution

The contribution of this research is as follows:

a. Provision of a universal interface for distributed energy sources with different frequency and voltage, even power density requirements.
b. Replacement of the conventional power transformer to achieve high power quality.
c. To reduce the size, cost, and weight of the conventional power transformer
d. To support a smart energy system with or without storage units.
e. To provide active harmonic filtering and power compensation to any type of load.
f. The model developed can be used as plug and play in a smart energy system.

g. It reduces circulating current and supports power balancing.
h. Provision of reactive power compensation.
i. Provision of maximum power tracking and the option of induction heating with an improved efficiency and power factor.
j. Provision of galvanic isolation of different topologies.

There are many possibilities where SST has proven to be an alternative, thus it is called future “energy router” (Vaca-Urbano et al: 2019) and it is at the heart of the Energy Internet. Energy Internet is the main reason for smart energy systems or electric power systems in which there is ubiquitous sharing, ubiquitous use, and ubiquitous ownership of electrical energy in real-time (Huang: 2019). SSTs support voltage restoration and fault isolation under abnormal conditions. Also, the galvanic isolation with DC ports assists in connecting electric vehicles, this provides fast charging of electric vehicles (Srdic, Lukic, Toward: 2019).

Energy storage can be added in the form of bus capacitors on the HV and LV DC buses, with an added advantage of Input voltage dip and swell compensation, Harmonic filtering, direct current, and high frequency alternating current electrical power supply, significantly improved power quality and efficiency, rapid control of voltage, compensation of the reactive component of apparent power, control of reactive power at the high voltage and low voltage side of the transformer. The designed SST will perform monitoring and management of the power system. Thus, SST is the backbone that integrates various distributed resources located at different places, operating at different electrical behaviors (different frequencies, currents, voltages, and power factors), coordinating, controlling, and detecting faults in the modern power system. SST modelling and design is achieved using different software simulating tools to produce a prototype. The drawback of SST is the low efficiency when compared with LFT, large number of semiconductors needed to design multi-level stages, reliability and energy losses associated with these semiconductors, and few experiences and expertise in the field. Based on the complexity of SST, it is more expensive than low-frequency or LFT counterparts but due to advances in technology as time passes, especially the use of silicon Carbide (SiC) and nanomaterials along with other improvements in technology, SST will be cheaper, well suited and preferred over current bulky conventional low LFT.

1.6 Research questions

This research tends to answer the following research questions:

1. Can the transformer's ability to regulate voltage due to voltage swell, voltage sag, transients, and transmission line voltage drops that result in end-user low voltage be mitigated using SST?
2. Is it possible for the line frequency transformer to be changed to the SST, to improve its ability to handle variable source frequencies, and AC and DC voltage sources?
3. Ways to connect the solid-state transformer serially or in parallel to handle higher voltages.
4. How to identify and select high-performing magnetic core and winding materials.
5. Can the voltage and current capabilities of semiconductor materials be improved?
6. Selection of a better insulator for the transformer.
7. How to improve distributed generation and cogeneration.
8. How to change the traditional grid to a smart grid in a smart energy system.

1.7 Research methodology and design

1.7.1 Introduction

This is the research method used and implemented in other to achieve the stated goal above and solve the research problems in this research, commonly associated with SSTs for the smart energy system. The first research method employed is literature review to fully get the latest and scholarly information on the SST from peer reviewed sources. Secondly, the mathematical models of SST converters, components, and their combined topologies are developed. Thirdly, the developed mathematical model is used to calculate the converters and components values, and a conjecture is made. This is followed by the development of a control scheme for the SST. Lastly, conclusion and recommendation are made. The optimized design of the SST developed is important in minimizing power quality issues and better use of distributed resources in a smart energy system. By using SST model and design, different energy or power sources with their peculiarities and requirements can be integrated and the associated environmental issues can be reduced, for example, liquid dielectric is eliminated in the design of the SST, efficient management of different energy sources is ensured, control and communication topologies are implemented in this design. The research methodology and design are implemented by carefully designing SST conversion topologies, control strategies, high-frequency transformer design with improved efficiency, and computer modelling and simulation.

1.7.2 SST conversion topologies design

The SST conversion topology is designed, considering the conversion requirements to achieve specific outcomes, like medium voltage to low voltage, medium voltage to medium voltage, low voltage to low voltage alternating current or direct current respectively. Also, if the alternating current side is a four-wire (neutral present) or three wire system. The topologies are shown in Figure 1.1 representing the topology for single stage SST, Figure 1.2 representing the topology for two stage SST, Figure 1.3 representing the topology for three stage SST, and Figure 1.4 depicting the configuration of a multilevel cascaded SST and configuration for MV based on MMC (Shri: 2013).

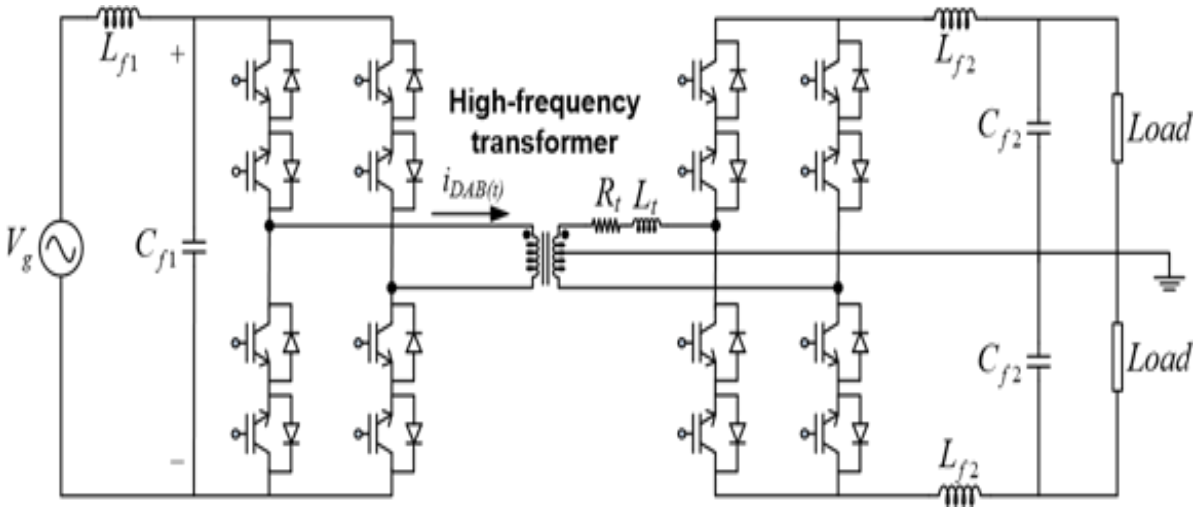

Figure 1.1: Topology for single SST.

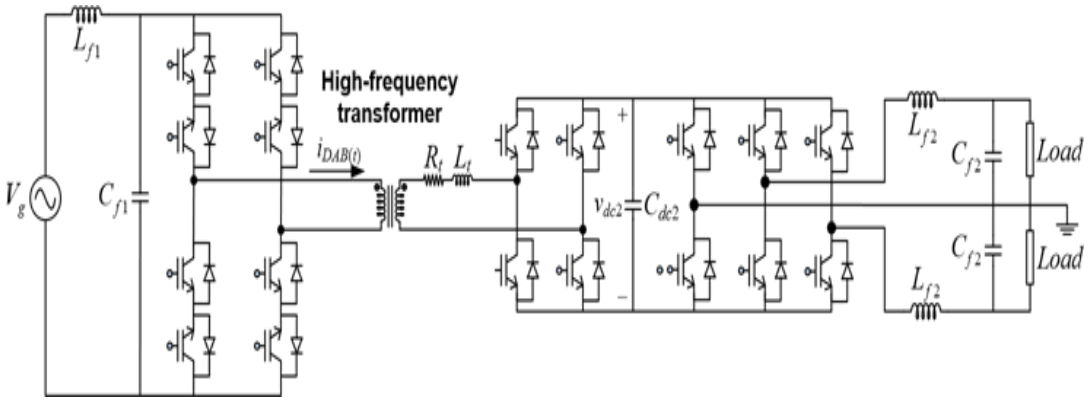

Figure 1.2: Topology for two stage SST.

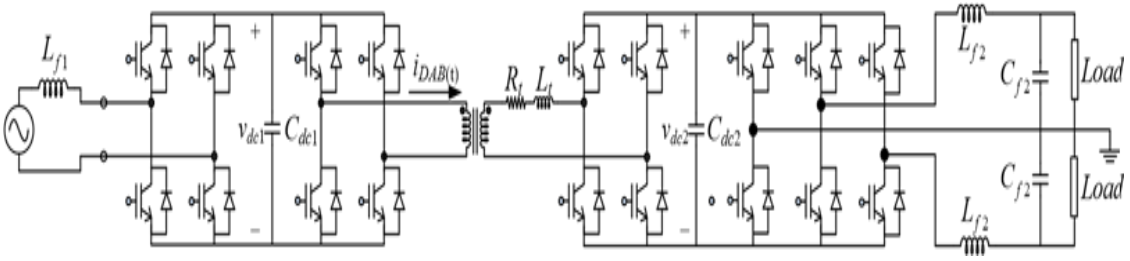

Figure 1.3: Topology for three stage SST.

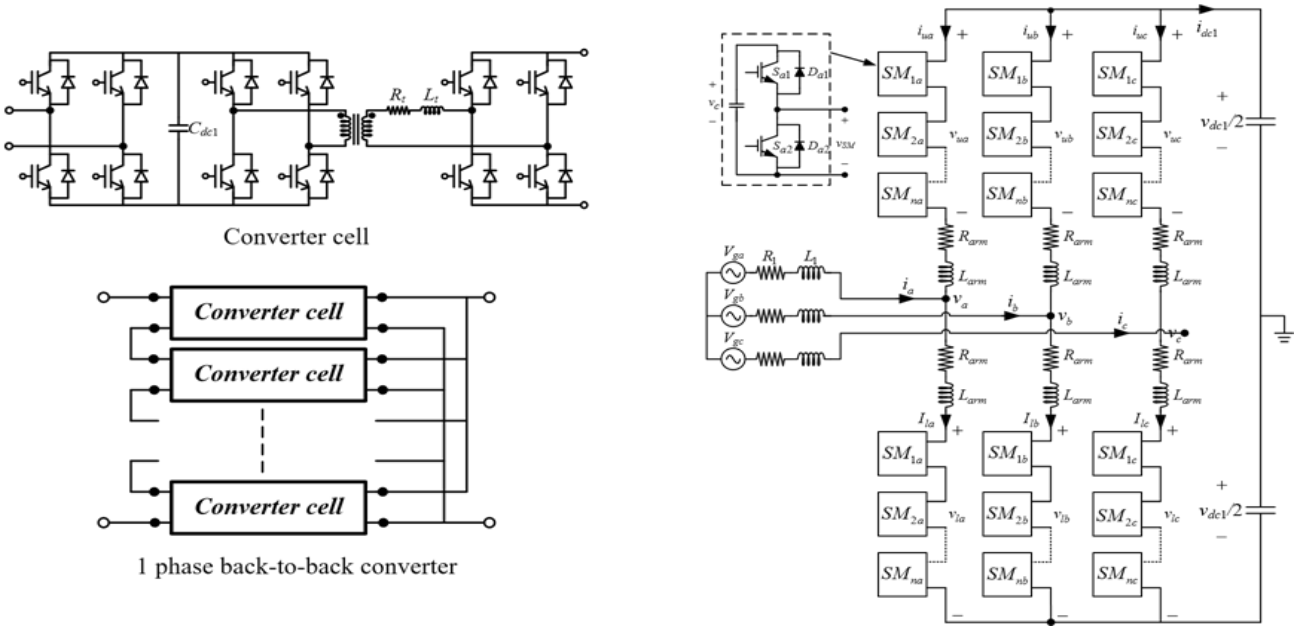

Figure 1.4: The configuration of a multilevel cascaded SST and MV based on MMC.

One stage and two stages can give desired functions with some limitations. Three stages give the best functionality with an added advantage of a simplified control design (Qin and Kimball: 2013). The three-level topology used in this design includes the clamped diode multilevel converter, multilevel converter with flying-capacitor, and converter that is stacked serially (Merwe WVD, Mouton: 2009). For the medium voltage converter level side, the proposed design is the multilevel cascaded H-inverter configuration (Wang et al.: 2016) or the modular multilevel converter (MMC), or the neutral point Converter (González-Molina et al.: 2015). The bidirectional dynamic current is very good because it provides current inverter stages, three-phase alternating current to alternating current power conversion with twelve switches making the input stages and output stages to work with an arbitrary number of frequencies and power factors plus a frequency galvanic isolation (Chen et al.: 2017). This is very useful in designing multiphase direct current and multiphase alternating current systems.

For instance, the 270 kilovolt-ampere SST, which is designed on 10 kilovolt Silicon Carbide metal oxide semiconductor field effect transistor is analyzed to support a 24-kilovolt input voltage with each device capable of blocking 10 kilovolts. To achieve this configuration and design, three flying capacitors is used to operate a zero-voltage switching which is phase-controlled (Shri et al.: 2013).

1.7.3 Control strategies

The linear quadratic regulator method is used to improve dynamic performance, with the integral action feedback to cancel the steady-state errors. A simple predictive control mainly used for multilevel stage control on the low voltage side or high voltage side is explored. This method involves the generation of the reference primary current level and analysis of the delay angle optimized between secondary voltage and primary voltage using a predictive control algorithm. The primary side, secondary side and tertiary side control hierarchy for power management strategy can be used to control direct current microgrid (Moonem and Krishnaswami: 2014). Two communication network control technique is used to control the modularity among the power modules for efficient and proper management of the distributed energy system (Vargas et al.: 2015).

1.7.4 High-frequency transformer

The high-frequency transformer is an important part of the design of a SST, and to achieve the much-needed reduction in the size of the overall system. For a high frequency transformer to achieve high current, high frequency, high power, and voltage operations, the following needs to be considered (Ronanki and Williamson: 2018):

a. To achieve high-frequency operations, magnetic material with high power density and low losses at high frequencies must be selected and used.
b. At high frequency, the windings or coils of the transformer needs to be carefully chosen.
c. To avoid thermal breakdown because of high voltage and high-power applications, the thermal behaviour of the materials used should be carefully considered.
d. Since oil is eliminated in the configuration of the SST, insulation is a challenge. This means the insulators to be used must be carefully tested and proven to be appropriate for the SST.

The two most important ratings are power rating and frequency rating. A 24- or 12-pulse rectifier system with silicon-grained magnetic core, can give a size reduction of about one-third when compared with a conventional transformer operating at 60Hz. Metal glass alloy is the best magnetic core material that will reduce core losses and optimize leakage inductance (Yu Du et

al.: 2010). By using coaxial coils for the medium voltage and applying the finite elements methods, an efficiency of around 99.5% can be obtained.

1.7.5 The efficiency of the SST

The efficiency of the SST can be improved by implementing advanced configuration for the converter stages using control optimized stages for the SST, a well-designed high-frequency transformer, and the use of semi-conductors with wide band gaps like silicon carbide semiconductors.

Energy efficiency can be classified based on performance efficiency, operation efficiency, equipment efficiency, and technology efficiency (POET) as a unifying and complete approach for energy efficiency analysis and classification. Technology efficiency is an indication and measurement of energy generation, conversion, processing, transmission, and utilization efficiencies of the thermal utility often limited by thermodynamic laws that make the overall efficiency less than unity. Technology efficiency is the overriding efficiency, that paves the way for analysis of the other efficiency frameworks. Thus, there will be detailed information regarding energy efficiency and savings opportunities in this section, and it will be used to classify the rest of the components of POET.

Technology efficiency information is retrieved from the dimensions or indicators like the feasibility of the technology, life span cost and ROI (Return on Investment), and the converting/transmission rate of change with time/procession coefficient. The SST is under technology efficiency (T). Performance efficiency is a measure of energy efficiency that is retrieved by external indicators and deterministic system indicators like environmental impact indicators, cost indicators, technical indicators energy sources indicators, and production indicators. The SST can be placed under performance efficiency tier 1 (P1). Operational efficiency is a measure of the system's wide variety of parameters that is evaluated by using the coordination of different dimensions or components of the system. This consists of the human physical, and time coordination parts. The SST is on (O1) because it needs minimal human intervention, when in full operation. Equipment efficiency is showing the output energy of isolated equipment with consideration to the given design specifications of a technology. The equipment is treated as separate equipment from the rest of the system and has low relationship effects with the other equipment or system components and it is evaluated by the following indicators: specifications, maintenance constraints, capacity, and standards. SST falls under Equipment efficiency, but it is not as efficient as the LFT, hence it is falls under second tier of Equipment efficiency (E1).

The POET framework reveals the efficiency and saving opportunities of using equipment like the SST. The checklist of criteria for POET unifying classification of energy system efficiency parameters, where each column represents an energy efficiency group, is shown in Table 1.1.

Table 1.1: POET Framework checklist.

T	0	0	0
E1	E2	0	0
O1	O2	O3	0
P1	P2	P3	P4

Based on the groupings in Table 1.1, SST is classified under column 1 (T, E1, O1, P1) representing the best energy efficiency saving opportunities. The improving technology behind the SST is better than that of the LFT. Since, technology is the overriding parameter in the POET framework, the SST is a better option than the LFT.

1.7.6 Simulation and modelling computer software

Computer software for modelling and simulation like MATLAB/Simulink and MATLAB/PLECS, and SPICE is very useful in studying and design of a complete SST. This is software will be used in this research analysis, design, and modelling of the SST for the smart energy system. The average model for simple direct current and alternating current inverter topology is shown in Figure 1.5, the topology for three stage bidirectional SST design is depicted in Figure 1.6, and the average model of a three-stage SST is shown in Figure 1.7 (Ramachandran et al.: 2014; Zhao et al.: 2009).

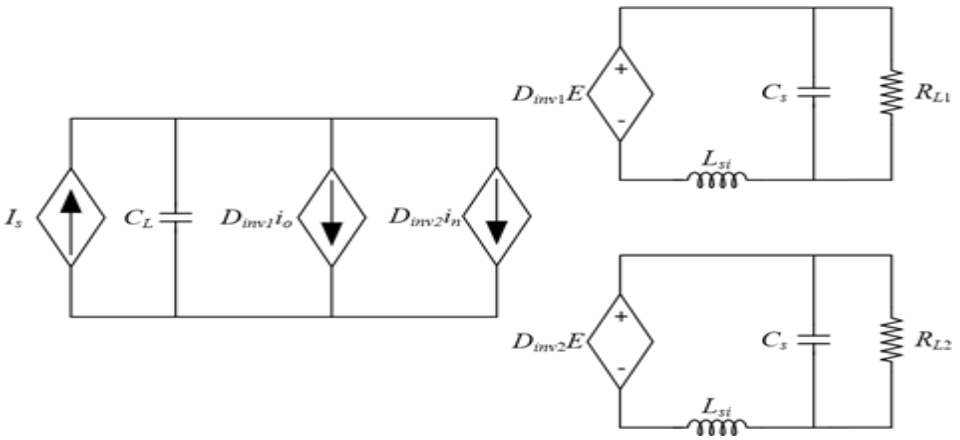

Figure 1.5: The average model for simple direct current and alternating current inverter topology.

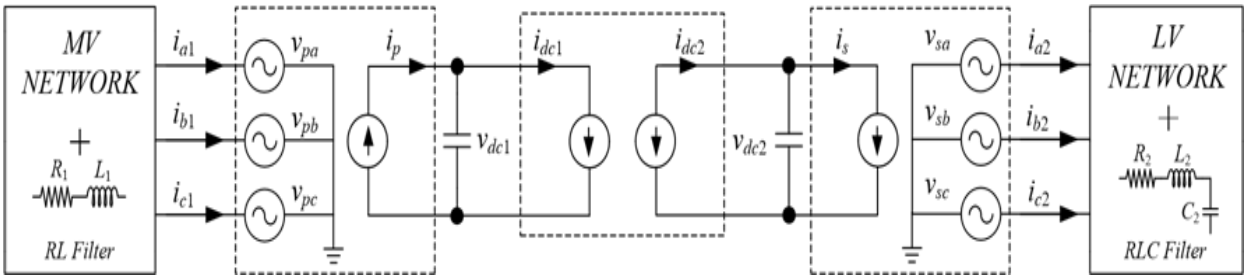

Figure 1.6: The topology for three stage bidirectional SST design.

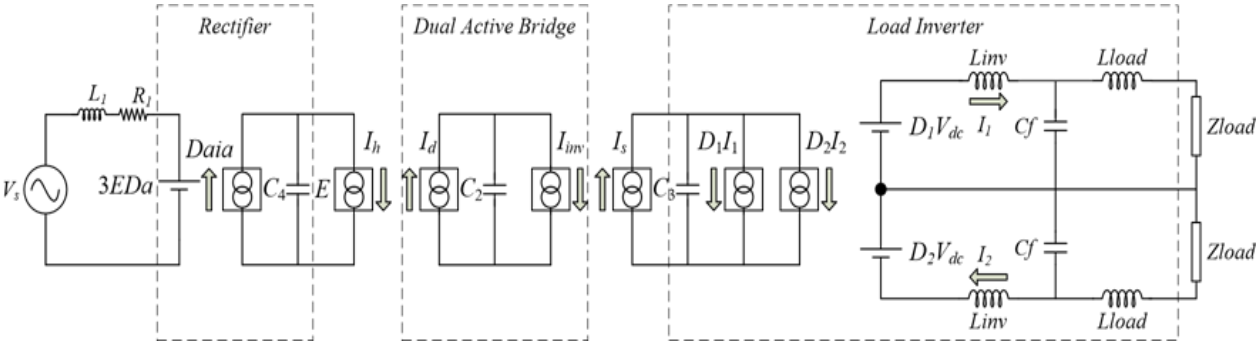

Figure 1.7: The average model of a three-stage SST.

1.8 The comparisons between LFT and SST

The cost of the LFT is less than that of the SST. However, with advances in semiconductor technology, and a decrease in prices of modern power electronics components, SST will become cost-effective and affordable when compared to LFT cost. Because of the complexities of the SST configurations, it may not be reliable when compared to LFT. But the SST modular design allows for faults detection, bypassing and isolation. This means that the reliability of the SST will increase as technological advances are made. The efficiency of the SST is less than the LFT because of the losses in the power electronics components. The efficiency of SST is between 90 - 98 % against that of the LFT, which is greater than 97%. however harmonic reduction and power factor close to unity in SST, enhances the performance of the SST when compared to the LFT performance.

LFT has been very important and useful in the power system but has some drawbacks like the following:

1. Total large size and big weight.
2. The oil used in the transformer can be a contaminant and hazardous to the environment and humans.
3. The magnetic material used in the core is not very efficient resulting in the core being saturated, large inrush magnetizing current, increase in the LFT energy losses in, increase

in the current drawn from the supply, more losses in the transmission lines and emission of more greenhouse gases (GHG).

4. Undesirable effects and variations on the input are carried over to the output.
5. The harmonics in the load side can affect the input side causing more cores loses and system disturbances.
6. If LFT is not operated in the full load mode, the efficiency of the LFT decreases, which means more losses.
7. Relative high losses at their average operation of load. Transformers are usually designed with their maximum efficiency at near to full load. Usually, distribution transformers' average load operation is 30%
8. Most LFTs have voltage regulation problems. Since the voltage regulation is inversely proportional to the FLT rating. Transformers used for the distribution of electricity is of low rating, resulting in poor voltage regulation.

The benefit of Solid-State Transformer includes the following:

1. SST produces voltage regulation better than FLT which uses tap changers.
2. SST has the capacity to compensate voltage sags, interconnect networks with different frequencies, mitigate harmonic problems, serving as an interface between DC and AC port(s).
3. The compensation of reactive power, voltage magnitude resolution, disturbances isolation from the load and source or from source to load.
4. Tap changers and mechanical actuators are not required.

The future lower cost of the SST, and the possibility of the SST replacing some power system components including FLT makes the solid-state transformer economically feasible.

1.9 Dissertation Chapters

The structure and organization of the dissertation consist of six chapters, and the details of the overview of each chapter is given as follows:

1.9.1 Chapter One

In this chapter, the overview of the dissertation is presented, culminating in the background study, problem statement, significance of the problem statement, the objective of the research, research question, and the research methodology used to carry out this research.

1.9.2 Chapter Two

This chapter consist of the literature review of the SST based on the peer reviewed scholarly articles and research in SST applications, interfacing challenges, architectures, combinations options, core materials selection, modular converter level technology, power flow control strategy, classifications, cells, high or medium frequency transformer, winding materials, and construction, respectively. Ongoing research and ethical considerations were reviewed.

1.9.3 Chapter Three

Chapter three analysis and formulates appropriate formulae, assumptions, and conjectures for determining the component values of the SST. The components and parameters determined include the filter values and the required filter types, DC capacitors values, switching frequency, and the Cascaded Hybrid Bridge (CHB), Dual Active Bridge (DAB), Three Phase Four Leg (3P4L) converters, respectively. Also, various currents, voltages, active, and reactive power were calculated. These values and waveforms were verified using MATHLAB Simulink.

1.9.4 Chapter Four

In chapter four, the mathematical and technical functions derived from chapter three is implemented in the component value determination for the individual power electronic components which includes the number of Hybrid bridges required for the design of the filters, CHB, DAB, and 3P4L converters respectively. The DC link capacitor values, and filter components values, culminating in SST design were retrieved.

1.9.5 Chapter Five

Chapter 5 provides the SST control model design parameters for smart energy from the mathematical dimensions, using differential equations to represent the behaviour of the SST in rectifier and regenerative mode of controlled operation. In the rectifier mode, the SST is controlled to allow only active power flow, whereas in the regenerative mode both the reactive and active power flow can be allowed and controlled. The control scheme developed is implemented in MATHLAB, to check the sharing and flow of power through the grid or load and the sources or storage sources. this gives the SST the ability to perform distributed generation.

1.9.6 Chapter Six

Chapter six forms the concluding chapter, where novel achievements from this research are noted, future research areas are recommended, and novel work done on the SST by other sources are covered.

1.10 Summary

In this chapter, an overview and background information of the SST components like the hybrid converters consisting of the CHB, DAB, 3P4L converters, DC links capacitors, filters, and the combinations of these components to form the SST was outlined. The problem statement was identified, and the research questions and objectives of this study were formulated. Lastly, the comparisons between LFT and SST were done. Section 1.1 forms the introductory part of this research, and it shows that based on the current energy demand, and technology trend, the next-generation distributed transmission grid, called smart grid (SG), is the backbone of modern electrical power infrastructure, mimicking neural networks, and designed to solve the problem of integration of energy sources, which is crucial. Section 1.2 representing the research problem statement, presents problems with the coordination and integration of different variations in the generation of electricity from diverse sources, the location of energy sources and storage, undesirable harmonic current flows, and thunderstorms and lightening which can inject current of high magnitude for a short period into the grid system, are analyzed. Section 1.3 is an overview of the significance of the research problem. This is done by considering the cost and lost time in the economy, associated with power loss, downtime, load shedding, lightning and insulation protection, integration of various energy sources, and other significant problems in the power systems. The main objective of this research is to model and design a SST for smart energy, that will mitigate issues mentioned in the problem statement, was introduced in Section 1.4. Section 1.5 deals with the expected outcomes, results, and the research contributions. Section 1.6 tends to answer the research questions. Section 1.7 unveils the research method used and implemented to achieve the stated goal above and solve the research problems in this research. Section 1.8 presents the comparisons between LFT and SST. The cost of the LFT is less than that of the SST. However, with advances in semiconductor technology, and a decrease in prices of modern power electronics components, SST will become cost-effective and affordable when compared to LFT cost. Finally, Section 1.9 presents the structure and organization of the dissertatioin.

CHAPTER TWO
LITERATURE REVIEW

2.1. Introduction

According to (Saponara & Mihet-Popa, 2019) The electrical power system is the cleanest form of energy for easy transmission, distribution, and performing useful work, known as energy utilization by the end-user or demand side. It can be efficiently stored, and converted to other forms of energy, like a different form of electrical energy (pulsating electrical energy, impulse electrical energy, direct current electrical energy, alternating current electrical energy, and electrostatic electrical energy), chemical energy (electrolytic and electrochemical cells), mechanical energy (sound energy, vibrational energy, translational energy, potential energy (water stored at a height under the influence of gravity in dams), kinetic energy (electric vehicles, electric trains, magnetic levitation machines, electric motors etc), and Electromagnetic energy like visible light energy (compact fluorescent Lamps, light emitting diode, incandescent lamps etc) and invisible light energy (X-rays, gamma rays, radio waves, microwaves, ultra-violet rays etc).

(Shadfar et al., 2021) noted that central to the abovementioned modern power system referred to as Smart Grid (SG), Artificial Intelligence (AI), controlled industrial production (smart industry 4.0), and a modern energized house called a smart house (SM), is the SST. All the above combination forms the Smart Energy (SE) System. The SST is a multifunctional equipment at the heart of this microgrid system (A. Hirsch and J. Guerrero, 2018) or SE, that uses power electronics components and a transformer operating at a high frequency to perform isolation and conversion of voltage (Hirsch et al., 2018).

Thus, In (She et al., 2013) SST power electronics and techniques in the distribution system power flow are reviewed, (Abu-Siada et al., 2018) show an analysis of the controller and topology systems in SST, and the applications of the SST in the SE system is discussed in (Yu *et al.*, 2014) in terms of the existing prototypes and modularity of the SST in the microgrid and SE system review of current and existing SE SST design and control schemes or configurations with their merits and demerits, and recognized criteria for selection are explored to unveil the inherent gaps in the SST technology for SE.

The review is presented in five parts in this paper as follows:

- Application of SST according to various peer-reviewed sources, and how the SST meets the requirements from the demand side.
- The configuration of the SST and their topologies, considering the Merits and demerits of the SST architectures according to various implementation schemes.
- The control and coordination of the converters, and other parts of the SST.

- The model and setups of the SST.

conclusion is drawn from these reviews to unveil the gap that needs to be filled in the SST technology for SE.

2.2. The application of SST for Smart Energy (SE)

To support the rapid ongoing development and innovation, like the modern traction system, electric vehicle charging stations (fast charging times), and power requirements of modern devices like plug and play electronics, smart television, cell phone, etc. (She et al., 2013; Kotb et al., 2018; Huang et al., 2011) proposed that the SST should be able to mitigate the following problems:

- The integration to the hybrid grid system (grid connected mode)
- Operate isolated (isolation mode of operation) or Operation in the stand-alone or islanded mode.
- High performance in the power system (transfer of power at unity power factor).
- Transfer of operation from standalone mode to the grid-connected mode.
- Fault isolation and advanced protection of the power system.
- Integration of all the connected power sources, loads, and storage.
- The increase in DC power supply.
- Mitigation of CO_2 and other GHGs.

These problems are addressed by the SST as depicted in Figure 2.1. it shows the isolated stage that consist of HFT, that efficiently and effectively transfers power in both directions.

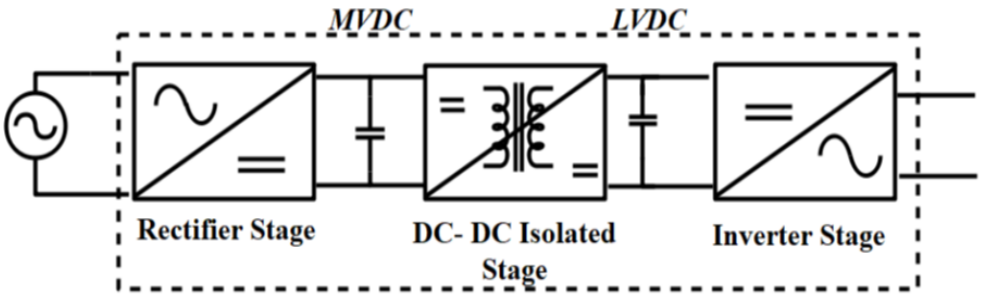

Figure 2.1: The SST major component configuration

(Agrawal et al., 2019; She et al., 2011; Agrawal et al., 2019) proposed that the SST is capable of mitigating voltage swag, voltage swell, and harmonics inherent in the power system and the smart energy system for wide application of the SST. (Bifaretti et al., 2011; Gheisarnejad et al., 2021; Merabet et al., 2015) noted that SST can mitigate these power quality problems using the DC-DC converter multilevel rectifier, and an AC rectifier controller to receive constant or variable DC/AC

power and supply pure sinusoidal AC waveform and constant DC. This is observed to be very useful in the wind turbine, where variable speed produced by the unsteady wind generates variable electrical power outputs.

The DC-DC converter with HFT in it as shown in Figure 2.1, constitutes a very important part of the SST, because it reduces harmonics, corrects pf problems, reduces distortion in the waveform, and offers an opportunity for multiple DC inputs. It also plays an important role in the reduction of the size and cost of the SST. However, the optimization of core magnetic materials at high-frequency operation, to mitigate the core and winding losses is an area that needs further study (Carrasco *et al.*, 2006). Another area that needs investigation is the optimization of component values, like IGBT optimized value and power ratings for minimal losses, operating safely at the required frequencies, and effective control (Liang, 2017). The features of SST discussed above by various researchers can be achieved by optimizing the components using an appropriate mathematical model for determining the components and parameter values like the right switching frequency for the best performance and efficiency and using these parameters and component values in the SST architecture, and the control schemes (Hosseinzadeh *et al.*, 2021).

The main aim of designing the SST is to achieve the following (Fernández-Guillamón *et al.*, 2019):

a. Optimized bus-voltage regulation
b. Proper and the best battery management scheme
c. Active, reactive, and apparent power flow control depending on the requirement of the power system
d. Improvement of the smart energy power factor
e. Overall power quality improved performance
f. Fault detection and isolation in the power system.

Due to the above benefits of the SST, it can be applied as follows:

1. Transportation: SST is widely used in the transport sector machines like tracking systems, and locomotives due to the 75% reduction in weight and 40% decrease in size with a phase of 13.8 kV/ 270 V SST, and the losses are halved and one-third of weight and volume reduction for SSTs is achieved when compared with transformers in DC/AC applications (Huber & Kolar, 2014).
2. Wind Turbines application benefits from flexibility and controllability of SST (Guillod et al., 2017). The application of SSTs can be used to suppress voltage fluctuations caused by the irregular nature of wind energy without the need of a compensator for reactive power. A three-stage Dual Primary Dual Secondary (DPDS) AC/DC-DC/AC SST architecture is suitable for wind turbines. The operation of the variable speed of Doubly-Fed Induction

Generator (DFIG) is managed by a rotor side control, which activates super synchronous or sub-synchronous modes.

3. Interconnection of Grid, Reactive Power, and Energy Routing. The deployment of SSTs in the distribution bus or feeder yields 1.4% decrease in losses, hence SST function as energy interconnectors or routers (Huang, 2018)
4. Traction application can be realized by using a fully modular multi-cell AC-DC SST (Besselmann et al., 2014).
5. SSTs are used as an interface for asynchronous loads and grids. A prototype is made by implementing Single Primary Single Secondary (SPSS) AC-AC SST (H. H. Lee et al., 2008).
6. A Grid source at 50Hz supplies a load that works at 60 Hz by applying the finite set Method Predictive Control (MPC) with compensation in the delay angle (Y. Liu *et al.*, 2017).

Due to limitation in the current and voltage handling capabilities of semiconductors, semiconductor failures, thermomechanical failures, measurement errors, control errors, short circuit or over voltage, and lightning surges, SST can be damaged by these effects (Guillod et al., 2017)

2.3. SST Interfacing challenges in the smart energy system

According to (Khan *et al.*, 2018) interfacing challenges are due to the placement of converters in the SST circuit, the type of converters implemented, and the SST architecture adopted for the smart energy system. Therefore, analysis and further research in this area needs to be done. The summarized SST interfacing challenges are summarized in Table 2.1.

Table 2.1: Challenges in interfacing SST in microgrids.

Challenge	Problem	Solution recommended
SST Efficiency	Converter Losses	Mathematical modelling to aid in the optimum switching frequency selection, using IGBT made from SiC Material (She et al., 2013).
	Thermal transmission	Specially made material for proper heat transfer (Ortiz *et al.*, 2017).
Volume-to-weight ratio	Insulators and heat.	Selecting either natural air convection, fan cooled, or liquid cooled thermal sinks (Mogorovic & Dujic, 2019).
Balancing of high current and high voltage	The power electronic switching component should have a support range of 2.5 kV to 35 kV (Bifaretti *et al.*, 2011)	Power converters should be arranged and placed as modules, and energy wide band gap semiconductors should be used like the 4H-SiC (Ahmed *et al.*, 2018).

High-Frequency Transformer	Material for the magnetic core	Using crystalline nanomaterial core
	Coil or winding	Solenoid core type
	High frequency produced Noise	Control scheme ZVS PWM
	Conductor insulator suitable for high voltage	Using the Litz conductors as samples in the design (H. J. Lee & Yoon, 2019; Viktor et al., 2011).
Schematics for SST Control	Isolation and grid connected modes	Implementing the DC-to-DC converter mode of operation
	Complexity in controller applications	SST coordination, energy management schemes, different modular layers of control (Viktor et al., 2011).
	Costs associated with the Material	LFT is cheaper than SST(Kaushik & Pindoriya, 2014).
	Operation, procurement, and efficiency improvement associated cost (Huber & Kolar, 2016).	Complete analysis of these associated cost has not been done (Yu *et al.*, 2014)
Over-current related behaviour	The SST is not compatible with the traditional protection schemes, and shorter life span of power electronic switches causes issues with the SST (Huber & Kolar, 2016, 2019)	Modern intelligent and technology improved circuit breaker protection is compatible with the SST (Guillod et al., 2017)
Over-voltage Management	Sensitive power electronic circuit protection (Awili & O'Donnell, 2016) (Huber & Kolar, 2019).	Active protection technology for the SST (Guillod *et al.*, 2015).

2.4. SST Architecture

According to (Hannan *et al.*, 2020), the SST structure is classified based on three important properties or characteristics of the SST connection to High Voltage or Medium Voltage to at least one port, MF isolation stage, and control of input or output electrical variables, being universal to incorporate any type of SST. Thus, the classifications of SST are as follows:

1. Single stage SST with no Direct Current Link
2. Two-stage SST with Medium Voltage Direct Current-link
3. Two-stage SST with Low Voltage Direct Current-link and
4. Three-stage SST with Medium and Low Voltage DC Link.

These architectures are shown in Figure 2.2.

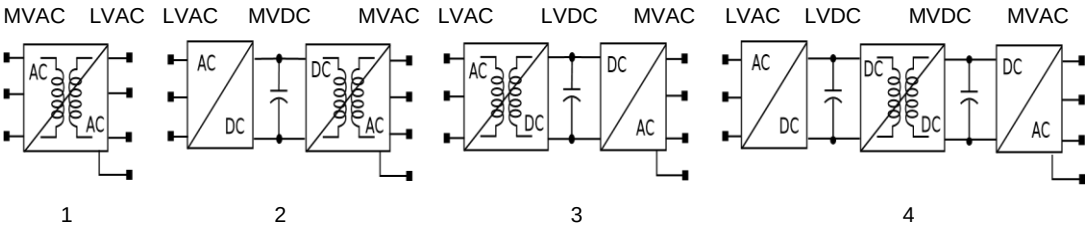

Figure 2.2: SST Architectures.

2.5. Combination of SSTs

(Shamshuddin *et al.*, 2020) proposed that the circuit in Figure 2.3 with a bubble and a cross line represents the isolating SST and the circuit without bubbles but has only a cross, represents a non-isolating SST. Two-stage SST can be constructed using one isolating SST-block and one non-isolating-SST block. This generates a link, which represents a port if the intension is to create an external interconnection, if not, it represents an energy link. Also, more ports can be made at the MFT primary side for back-end isolating-SST-block or at the MFT secondary side for front-end isolating-SST-block. SST topology can be a DPSS AC/DC-AC SST or SPDS AC-DC/AC SST.

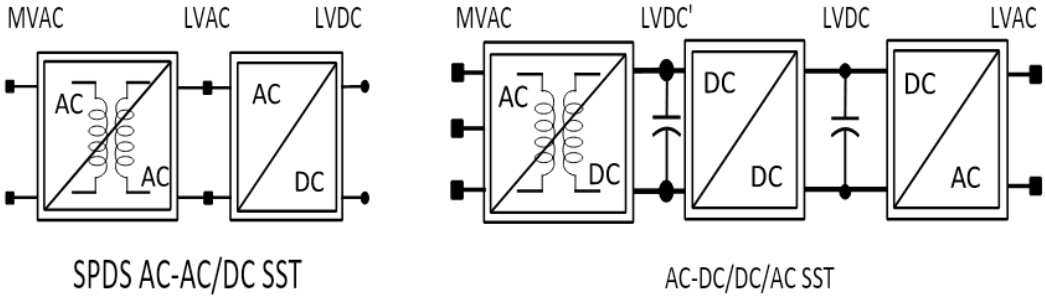

Figure 2.3: Dual primary single secondary (DPSS) AC/DC-AC SST or single primary dual secondary (SPDS) AC-DC/AC SST.

Multiple Input Multiple Output (MIMO) blocks can interface any x-input(s) and y-output ports supplying energy. The voltage ports for MIMO isolating-SST-block have the same the same form, that is AC or DC. This model is depicted in Figure 2.4:

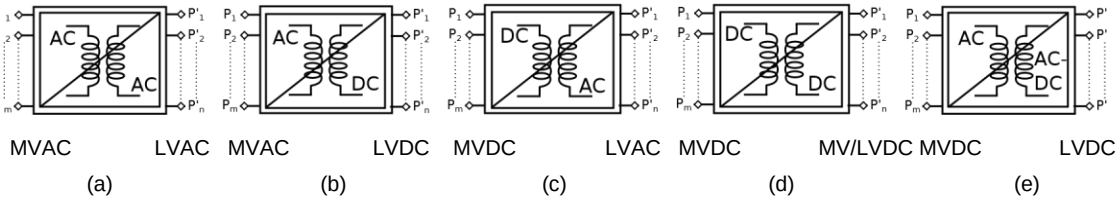

Figure 2.4: SST Multiple Input Multiple Output (MIMO) blocks.

The integration of SST cells that forms a module, modular combinations that forms a converter, and the overall integration of these converters that form the system level integration of the SST is shown in Figure 2.5.

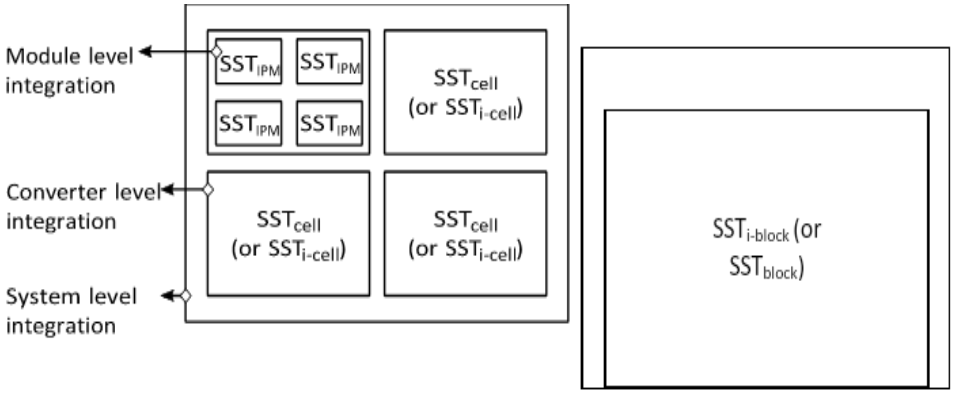

Figure 2.5: Integration for composition of an SST.

2.6. Modular converter level technology for the SST

According to (Baek and Bhattacharya, 2019; al Hadi and Challoo, 2020; el Shafei *et al.*, 2020; Zheng *et al.*, 2020; Sun *et al.*, 2022) the modularity of SST can be enhanced using modules and levels of the converter layers of application as shown in Figure 2.5. This is because of the limited ratings of the power electronic converter components, and their switching frequency limitations. The AC-DC converter stage, half and full bridge connections represent a topology in a single module. Then Half-bridge converter module and two transistors can output two voltage levels, and a full bridge converter module can output three voltage levels, making the conversion of AC to DC, a multi-level modular converter (MMC) as proposed by (Farnesi et al., 2019; Gajowik et al., 2017). The SST topology in Figure 2.6 is often used (Rodrigues *et al.*, 2017).

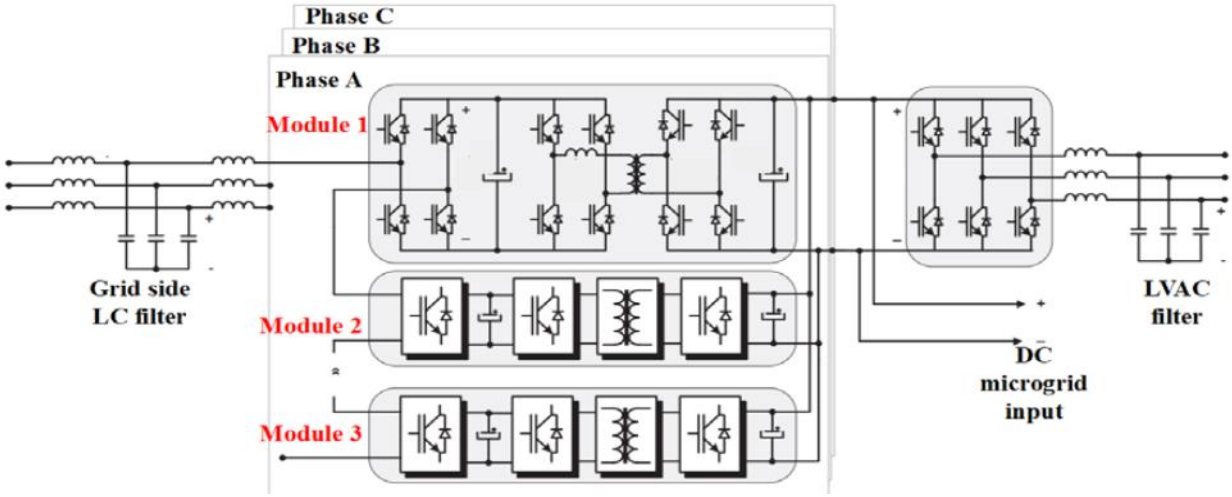

Figure 2. 6: The commonly used SST topology for smart energy.

(Costa et al., 2017; Farnesi et al., 2019; Gajowik et al., 2017) showed that DAB, Tri-Active-Bridge (TAB), Quadruple Active Bridge (QAB), and Penta-Active-Bridge (PAB) (or Multiple Active Bridges (MAB)) are excellent active bridge converters and can be used with high-frequency transformer to achieve high efficiency at high switching performance.

2.7. The SST power flow control strategies

The controllability and coordination of the SST for smart energy is a need that must be fulfilled for the operation of the SST under different conditions and modes. The coordination of the DC and AC power sources will give rise to load power that is equal to the DC power and AC power, assuming there are very small or low losses. (Bifaretti *et al.*, 2011) proposed that a UNIFLEX system will use a remote sensor to get the reference active power and reactive power, then through comparison, control the active, reactive, and apparent power flow in the microgrid or smart energy system. A multi-loop system allows both DC voltage and AC power to flow at the same time and be controlled. This control system constitutes Phase Locked Loop (PLL), reference generators that produce reference signals, the subsystem for prediction, and Pure Sine Wave Modulation (PWM) generator. According to (B. Liu et al., 2016) Fuzzy Logic Controller of the DAB improves its voltage loop. This predictive current control scheme is shown in Figure 2.7:

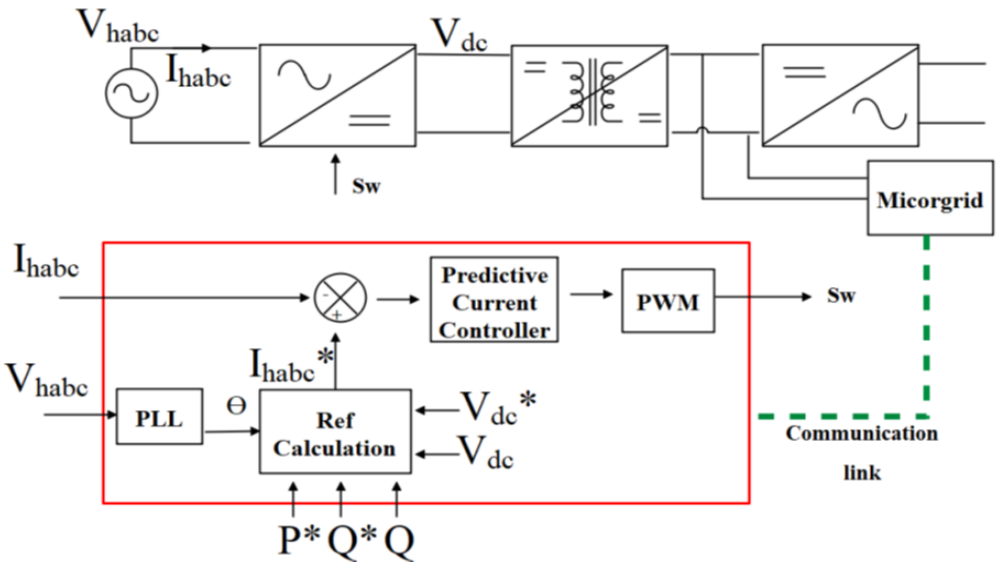

Figure 2.7: The predictive current controller scheme for the SST.

(Olivares *et al.*, 2014) showed that a decentralized current predictive system is also useful, and it involves the generation of a PWM signal (Sw1) at the rectifier stage by using input parameters of the SST Medium Voltage AC side (V_{habc} and I_{habc}). The switching signal (Sw3) at the inverter is produced by using the SST output parameters (V_{labc} and I_{labc}). The decoupled control(dq) is used

as shown in Figure 2.8, for the inverter stage. The medium and low voltage dq axis currents are denoted as I_{hd}/I_{hq} and I_{ld}/I_{lq}, with reference axis currents (I_{hd^*} and I_{ld^*}) calculated from the DC bus voltage (respective) controller but I_{hq^*}/I_{lq^*} are calculated from the needed power factor (pf). The aim is to keep $I_{hq^*} = 0$ and $I_{lq^*} = 0$ to ensure that the inverter and rectifier operate at unity pf. Thus, Sw2 switching signal is produced by the PSM.

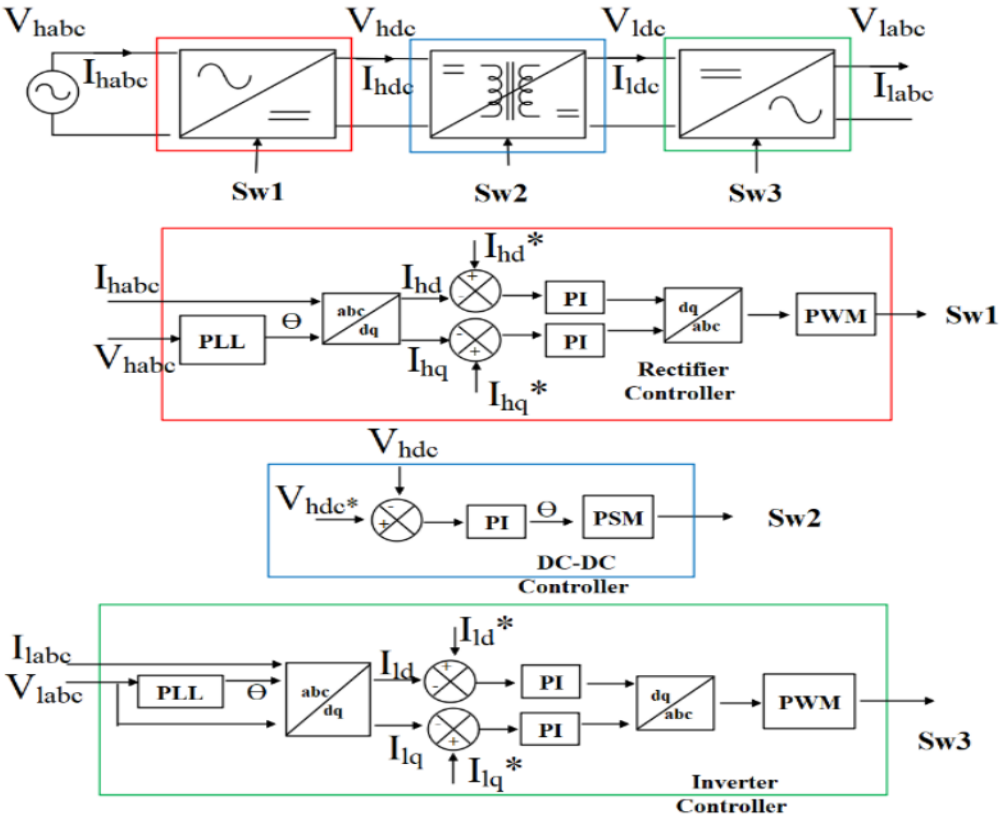

Figure 2.8: The SST decentralized predictive controller (three control levels per stage).

Figure 2.9 shows that the phase angle of HFT medium voltage side and the low voltage side can control the power flow vector (Rodrigues *et al.*, 2017). Through the adjustment of the phase shift between MV and LV sides, the magnitude of the power flow can be adjusted accordingly. D_1 and D_2 are the inner phase shift, the DAB outer phase shift ratio, Θ is controlled according to the requirement of the smart energy system to produce a switching signal by applying PSM. If Θ is zero, power will not flow in the converter. When Θ > 0, power flow to the microgrid from the grid and when Θ < 0, the power flow to the grid from the microgrid. This is shown in (2.1) and (2.2). P_{in} and P_{out} represent input and output power, V_{in} and V_{out} are the input and output voltages, f is the frequency, L is the inductor, D_1 and D_2 are the inner and outer phase shift respectively.

$$\frac{V_{in}V_{out}}{4fL}\left(D_2(1-D_1)-\left(\frac{1}{2}\right)(D_2)^2\right) \text{----------(2.1)}$$

$\frac{V_{in}V_{out}}{4fL}\left(D_2\,(1-D_2)-\left(\frac{1}{2}\right)(D_1)^2\right)$; 0 < $\boldsymbol{D1}$ < $\boldsymbol{D2}$ < 1----------(2.2)

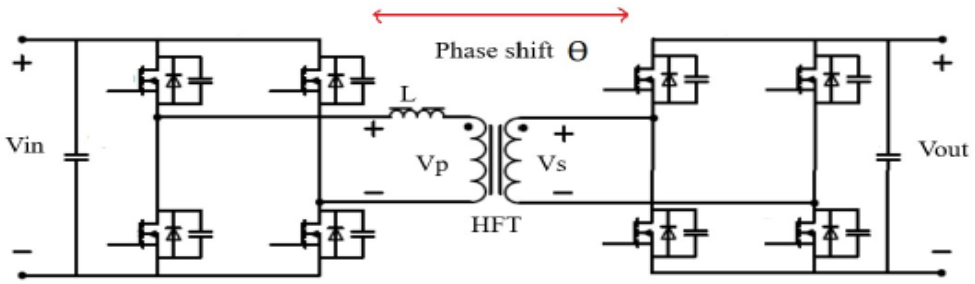

Figure 2.9: The Phase shift power flow control of the SST.

2.8. The classification of SSTs

According to (She *et al.*, 2012) SSTs can also be classified based on:

1. Power stages
2. Voltage levels
3. Control of the isolation stage
4. Modularity
5. Number of ports per power stage

The detailed classification is shown in Figure 2.10:

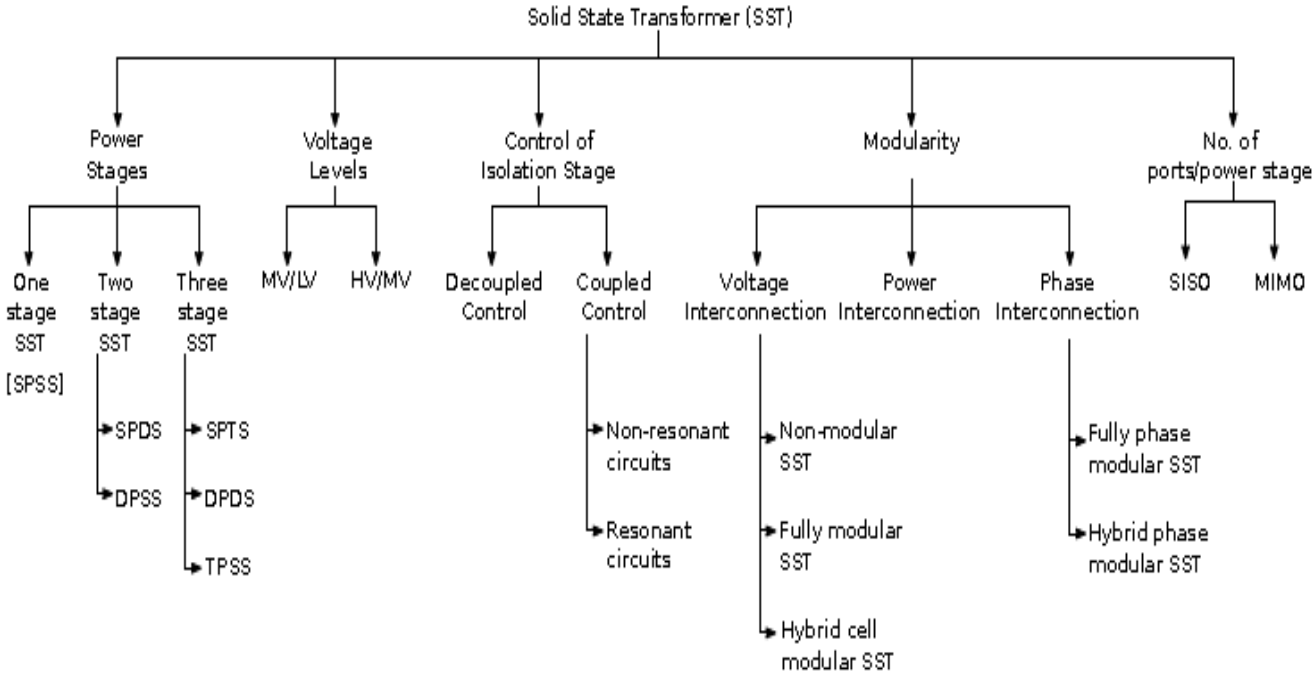

Figure 2.10: The classification of SSTs.

2.9. Medium Voltage or High Voltage Side Solid State Transformer cells

(H. H. Lee et al., 2008) proposed medium Voltage level can be interconnected or interfaced by implementing these procedures:

1. Low Voltage, series-connected semiconductor devices.
2. Wideband gap-based semiconductor devices.
3. Multilevel configured converters.
4. Multi-cell method or approach.

2.10. Construction of SST

The following should be considered for selecting appropriate semiconductor devices for SST:

1. Voltage ratings.
2. Current ratings.
3. Switching frequency.
4. Maximum junction temperature.
5. High blocking voltage capability, and low on-state losses.

2.11. MFR-Medium Frequency Transformer

(Pipolo *et al.*, 2016) noted that this device is a key element in SSTs. An MFT connected to a power converter yields a low footprint with a higher power density with improved efficiency.

2.12. Core Material

The core material is made from a soft magnetic material, which is easy to magnetize and demagnetized, and it has the following features:

1. Low core losses.
2. High saturation flux density and thin hysteresis loop area.
3. High continuous operating temperatures capability.
4. High relative permeability. Soft magnetic materials.
5. Iron in powdered form and very fine small particles of iron alloy.
6. Composites of silicon and silicon-derived nanomaterials.
7. Derivatives of ferrite and pure ferrite material.
8. Magnetic materials in Amorphous form.
9. Nanomaterials used as Nanocrystalline based cores.

2.13. Winding Material and Arrangement of the SST

The choice of coil material is copper or aluminum because of the low electrical resistance. The Insulation and Thermal Considerations, High dielectric factor and thermal conductivity respectively, with tolerance to partial discharge are required for good insulation material selection. Air is normally used for cooling and epoxy is used as dielectric material, especially where the air is insufficient for handling high voltage levels.

2.14. The ongoing research in SST

- ✓ Future Renewable Electric Energy Delivery and Management system (FREEDM) system is thought to be a game changer with novel technological breakthroughs in the design of the control strategies, and the best design for the SST (Das et al., 2019; B. Liu et al., 2017), and 3.6 kV–120 V/10 kVA SST sample was produced and verified using hierarchical control strategy, integrated with FREEDM center (She, 2013).
- ✓ The LEMUR Project consists of 150 kW SST, one DC link (750 Volts DC) that connects DC microgrid. In addition, there are two AC links (375 Volts AC, 750 Volts AC) with multiple connected nano microgrids. The DC microgrid is connected to the LVAC and LVDC links. It recorded an efficiency of 97.17%, even with the IGBT losses at a loading level of 100%. It uses TAB with a centralized predictive controller for current and voltage regulation.
- ✓ The Highly Efficient and Reliable smart Transformer (HEART) project uses a modular approach to make the smart transformer or SST mitigates the challenges of reliability and efficiency. A simplified three-phase SST sample of 100 kW, 1.5 kV, 800 Volts AC, 800 Volts DC with a QAB converter is manufactured. It consists of three cells of cascaded half-bridge per phase with the control objectives of managing local loads and sources while at the same time controlling the MV and LV network. The researchers propose soft load-shedding to mitigate the issues of grid instability during excessive power demand from the grid. It was practically implemented, and it replaced a conventional LFT in a distribution feeder, achieving a 60% improvement in Distributed Generation (DG) wind generation hosting capacity (Costa et al., 2017; de Carne et al., 2018; Ellabban, 2019).

2.15. Ethical considerations

Ethical considerations need not be taken, as quantitative data will be retrieved from the model simulation experiment using software technology (primary data). This is compared to the publicly available data on similar model data (secondary data).

2.16. Summary

Based on the review of many literatures in this area, SST is optimized and designed to incorporate different converter topologies. Each of these topologies consists of modules of cell combination, to enhance control and performance of the SST system. To fully analyze the SST role in the Smart Energy System, the SST application, configuration, coordination or control, and model is reviewed.

The SST application supports rapid development in the transportation sector like the electric vehicle revolution, traction system modernization, and the rollout of charging stations. Thus, the SST can mitigate the following problems associated with the current power system transformers, which include: the integration to the hybrid grid system, isolation mode of operation, transfer of power at unity power factor, transfer of operation from standalone mode to the grid-connected mode, fault isolation and advanced protection, the increase in DC power supply because of high solar PV penetration and usage in the race towards renewable energy applications, mitigation of CO2 and other GHGs. The combination of the SST is done using both the isolating and non-isolating SST block to produce more connection interface or points. this results in DPSS AC/DC-AC SST or SPDS AC-DC/AC SST or MIMO SST topology. The modular converter levels in SST are necessary because of limited power electronic component rating and limited frequency of operation. The AC-DC converter stage, half and full bridge connections represent a topology in a single module. Then Half-bridge converter module and two transistors can output two voltage levels, and a full bridge converter module can output three voltage levels, making the conversion of AC to DC, a multi-level modular converter (MMC). The controllability and coordination of the SST for smart energy is achieved using UNIFLEX system that use a remote sensor to get the reference active power and reactive power, then through comparison, control the active, reactive, and apparent power flow in the microgrid or smart energy system. A multi-loop control system allows both DC voltage and AC power to flow at the same time and be controlled. It constitutes PLL, reference generators that produce reference signal, the subsystem for prediction, and Pure Sine Wave Modulation (PWM) generator. Fuzzy Logic Controller of the DAB is used to control its voltage loop.

CHAPTER 3

THE MATHEMATICAL DIMENSIONS OF THE SST MODEL FOR SMART ENERGY

3.1. Introduction

To observe and verify the behaviour of the SST in certain dynamic conditions that suits a smart and modern energy system, the SST should be modelled, and its role envisaged in a smart energy system. Also, to properly design SST model, some parameters like the switching frequencies, power electronics devices power ratings based on the voltage and power levels, respectively, to be handled in the smart energy system, and the rating of all other passive devices, should be first analyzed mathematical. The dynamic characteristic of a solid-state transformer is preferably analyzed to design a first-order SST design. This is valuable for estimating the values of the parameters needed to design the SST, while making useful assumptions with regards to design process optimization and various losses like the power electronics semi-conductor conduction band and energy barrier properties, and its inherent losses.

Thus, the main aim of this chapter is to find the required parameters for a first order design of SST for smart energy, modelled in mathematical and circuit design approach. Therefore, the first part deals with a constructive overview of assumptions, specifications, and a generalized requirement in the SST design pattern, then filter reduction of distortion is analyzed and described. The converters, which forms an important part of the smart energy transformation is analyzed as a CHB, 3P4L, and the DAB converters, respectively. This is followed by the development of applicable converter equations that will be applied to a particular scenario of the SST. The overall design of the SST is produced, and its modules combinations analyzed.

3.2. The smart energy SST system Specifications, Assumptions, and Requirements

The mathematical parameters and calculation to realize the SST first order design is done based on case study specifications, and where these parameters cannot be directly retrieved or calculated, erudite assumptions are made depending on requirements.

3.2.1. The SST Requirements

The overriding requirement in the design of the SST is that it should be capable of handling medium level voltage on one side and low-level voltage on the other side in the smart energy system, while operating either as standalone (i) or grid connected (ii) as follows:

i. Medium level voltage in the $AC\ grid \leftarrow\rightarrow SST \leftarrow\rightarrow Low\ voltage\ in\ the\ AC\ grid$
ii. Medium level voltage in the $AC\ grid \leftarrow\rightarrow SST \rightarrow Load$

Also, the other important requirements for the SST include power transfer capabilities, fast dynamic response, the harmonic content analysis that is based on the Institute of Electrical Electronics Engineering (IEEE) guidelines, implementation, scalability, and practicability of SST calculated parameters values.

3.2.2. Assumptions made.

Certain assumptions are made to make simplification and calculations of components parameters easier to model, and these parameters includes the following:

i. Wattless components are used.
ii. Zero switching times of the electronic switches (cut-off region for OFF and saturation region ON switching time is zero seconds) are assumed.
iii. The power electronic components operate within the active region (linear region or predictable region).
iv. The impedance of the electronic component is matched based on the maximum power transfer theorem, ensuring that maximum power is transferred between the power electronic devices and the transformer.
v. The power electronic components are operating at unity Power Factor (pf) as depicted in (3.1).
vi. The power electronic components are capable of transferring both active power (P) and reactive power (Q) components of apparent power (S) as shown in (3.2).
vii. If only active power is specified, then it is equal to the apparent power maximum value and reactive power is equal to zero as depicted in (3.3).
viii. The smart energy SST operates in four areas as follows:

$Area\ 1\ (+P,+Q), area\ 2\ (-P,+Q), area\ 3\ (-P,-Q), and\ area\ 4\ (+P,-Q)$ as shown in Figure 3.1.

$pf = \cos\varphi = 1$, if $S_{max} = P_{rated}$ ----------(3.1)

P_{rated} is the rated active power in watts, kilowatts, or megawatts.

S_{max} is the maximum value of the apparent power in VoltAmpre (VA), kiloVoltAmpre (kVA), or MegaVoltAmpre (MVA).

The phase angle between P and S vector components is $\varphi = tan^{-1}\left(\frac{Q}{P}\right)$ ----------(3.2)

The magnitude of $S = |S| = (P^2 + Q^2)^{\frac{1}{2}} \leq |P_{rated}|$ ----------(3.3)

Figure 3.1 shows a circle with a unit radius vector, representing the S, and with a magnitude of 1 per unit (p.u), this is the vector sum of P and Q. the basic trigonometric ratios cos(φ), sin(φ), and tan(φ) of areas (±P, ±Q) is positive in the first quadrant of the circle, with a rotating S vector from right to left. In the second quadrant only sin(φ) is positive. In the third quadrant only tan(φ) is positive, and in the fourth or last quadrant only cos(φ) is positive (this forms the CAST acronym). It can be deduced that only pf (cos (-φ) = cos (-φ) if -90°≤ φ ≤ +90°) in the first quadrant and fourth (last) quadrant has a positive value. Also, according to (3.2), φ will be positive in the first and third quadrant, respectively. Based on the range -90≤ φ≤90, using the reduction techniques of trigonometric functions, and cos(-φ) = cos(φ) = pf, the SST is capable of handling and transferring power in all areas or quadrants of the unit circle shown in Figure 3.1.

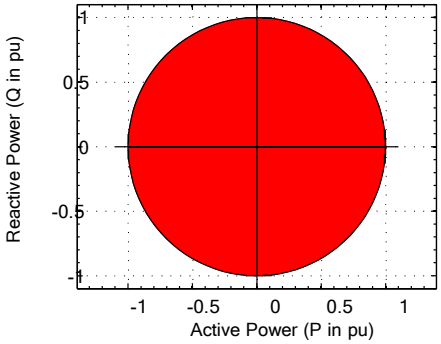

Figure 3.1: Power transfer capability of the SST.

3.2.3. The SST specifications

The SST parameters that need to be specified include the following:

i. P_{rated}
ii. Medium (Line to Line) Voltage (V_{MV}) of the smart energy system
iii. The Alternating Current (AC) frequency of the smart energy grid (f_{grid})
iv. Low Voltage (Line to Line) (V_{LV}) of the smart energy system
v. Power electronic voltage rating of the SST components

These specifications will assist in revealing the voltage limits and how many H-bridges that are required in configuration of CHB, DAB, and the optimal 3P4L converter configuration.

3.3. Waveform distortions and filters

3.3.1. Disturbances and Signal distortion in the waveform

Power electronic components and devices are used as high frequency switches, capable of operating at high frequencies of up to 10 kHz. Since, there is a time delay in the open and contact times of the switching action of power electronics devices or switches, harmonics are presents. These harmonics produce distortion in the voltage and current waveforms. This causes dissipation of heat in the power electronics switches, transmission lines and distribution lines. It further generates oscillations in rotating electrical machines.

The oscillations in power electronics switching devices is depicted in Figure 3.2 (Kanjanavirojkul *et al.*, 2017). It takes very small amount of time (the period (T_c)) to make or break contacts in electronic switches at high frequency (f). the voltage fluctuates and oscillates, and the reactive power increases, before the output voltage magnitude normalizes. This action represents distortions and harmonics in power electronic circuits, and they cause undesirable effects like decrease in the overall efficiency of the SST, and ripple voltages generation. Hence, this distortion needs to be analyzed.

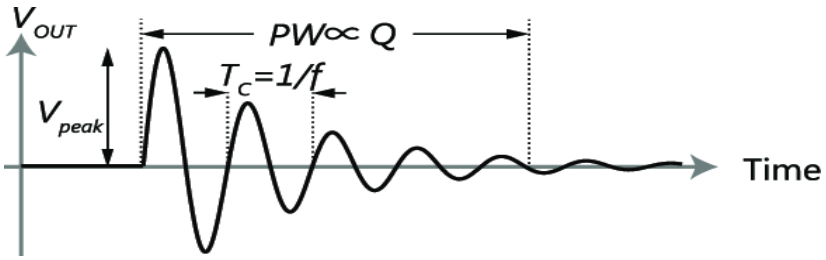

Figure 3.2: oscillations in power electronics switching devices.

The sum of all these distortions caused by these power electronic switches is called Total Harmonic Distortion (THD). THD reveals the ratio of the sum of individual Root Mean Square (RMS) values to the fundamental harmonic RMS value. Additional harmonics can flow into the power system as a whole from the use of non-linear loads like Light Emitting Diode (LEDs) (Yang *et al.*, 2021). Another parameter of interest in the analysis of distortion is the Total Demand Distortion (TDD), which reveals the THD in full load conditions. Thus, THD and TDD are similar, except that TDD is retrieved or calculated under conditions of full load. Based on IEEE 519-1992 standards for harmonics in inverters (Shi and Le, 2021), the harmonics recommended range for SST design is shown in Table 3.1 (Devineni *et al.*, 2022).

Table 3.1: IEEE odd harmonics current distortion limit and range of values in %, with even harmonics limited to 25% of odd harmonics.

I_{SC} / I_L	**h < 11**	**11 ≤ h < 17**	**17 ≤ h < 23**	**23 ≤ h < 35**	**35 ≤ h**	**TDD**
< 20	**4**	**2**	**1**	**0.6**	**0.3**	**5**
20 < 50	7	3.5	2.5	1	0.5	8
50 < 100	10	4.5	4	1.5	0.7	12
100 < 1000	12	5.5	5	2	1	15
> 1000	15	7	6	2.5	1.4	20

The ratio of short circuit current (I_{sc}) to load current (I_L) is taken to be ≤ 19.99 with a distortion limited to only 80% of IEEE 519-1992 values (0.2 * odd harmonics values). The reason behind these assumptions is to allow the SST to operate safely will transferring power at any value of the I_{sc} and harmonic order (h). this chosen parameters is boldened and green colored in Table 3.1.

3.4. The Smart Energy Grid Filters

A filter is necessary because the ripples and harmonic contents need to be isolated and removed from the system. A low voltage filter and a high voltage filter are required and will be implemented. These filters, in addition to the functions elucidated earlier, allows the flow and control of both the active power component, the reactive power component, and the management of pf. In the case of the SST, the three filters needed are:

i. Grid L-filter

This is a filter that produces a damping of -20 decibels (dB) over the whole range. To obtain an optimal attenuation, this filter should be combined with a high frequency switching converter. This type of filter is the commonest among other filters for SST design, and it is shown in Figure 3a.

ii. Grid LC-filter

It is configured using a capacitor for achieving up to -40dB attenuation. It is useful and implemented where impedance of the connected load is high and above frequency of the power electronic switch operation. It is shown in Figure 3b.

iii. Grid LCL-filter

The grid LCL-filter functions better under frequencies above resonance frequency, with an attenuation of -60dB. It is very good at reducing distortion associated with lower switching frequency and configured with passive elements. The downside of this filter is that it can generate

steady and dynamic state current distortions, respectively, because of resonance. This is shown in Figure 3c (Quan *et al.*, 2021).

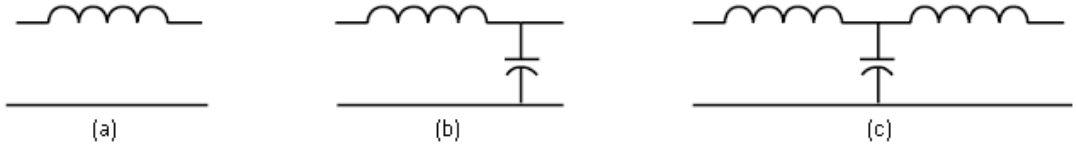

Figure 3.3: Filter types: (a) L-type filter (b) LC-type filter (c) LCL-type filter.

For proper functioning of the SST, two filters are needed as follows:

i. The CHB needs to be connected to the MV grid using L-filter

This is because as H bridges increase in numbers, their individual frequency is summed up, so that high frequency total is achieved. This property is very useful in configuration of modules for the SST, producing sinusoidal waveform with a wave form factor (FF) of 1.11, with reduced distortion factor (DF). Hence, smaller filters are required per module and for the combined SST modules. Using this method ensures that there is a proper filtration of harmonics, low voltage drop due to smaller components values of the filters used, and low cost of SST design.

ii. The 3P4L converter connection needs an LCL-filter

The 3P4L converter has low voltage rating, and high-power rating, which means that the current flow through it is high. To reduce switching loss from operation of the converter at high current flow, the switching frequency needs to be low, and higher filter inductances is needed. These result in high cost and poor dynamic behaviour. The L-type and LC-type filters respectively, need AC grid operating at constant impedance value. However, the SST is required to perform in isolated and grid connected modes respectively, while managing small changes in the grid. Thus, the LCL-type filter is the appropriate filter for the 3P4L converter operation. But LCL-type converter has issues with regards to current distortions. Thus, the damping required are:

i. Active damping

This entails the modification of the structure of the controller through the addition of an existing control branch or scheme. This damping method are sensitive to uncertainties in the parameter's values but does not produce losses. This is suitable for the 3P4L converter damping.

ii. Passive damping

The filter capacitor needs to be connected in series or parallel with more inductor (L), Capacitor (C), or Resistor (R) component to achieve passive damping. Because of the inherent losses in the

components, the overall efficiency of the 3P4L converter is reduced, resulting in lower filter effectiveness. This makes it difficult to achieve damping of frequencies close to resonance frequency.

3.5. Direct Current (DC) link Capacitance

As shown in figure 3.4, a DC link is used in between CHB, and DAB and another DC link is used in between DAB and 3P4L.

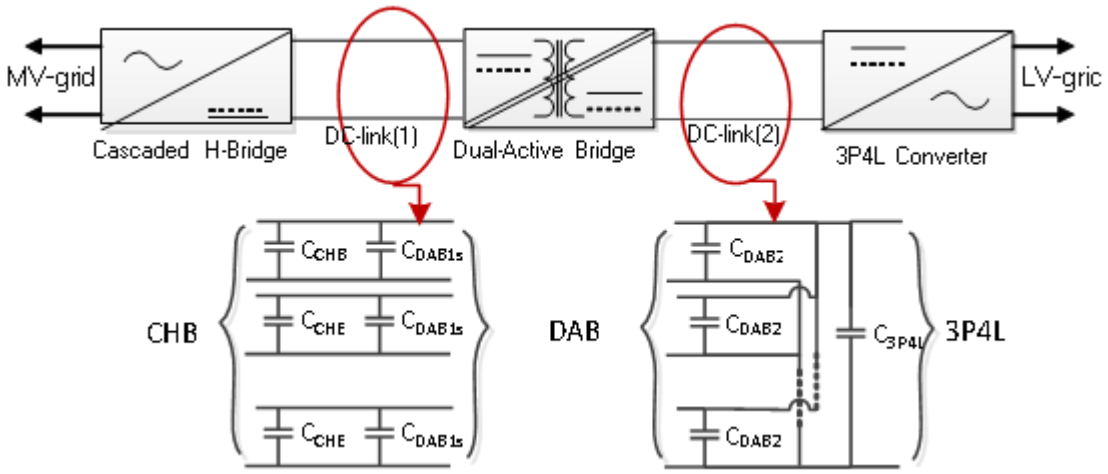

Figure 3.4: The DC links and capacitors topology for the SST.

The rectified voltage flow through link 1 and link 2 are not constant. For a constant voltage to be achieved, infinite capacitance value is required. However, filter capacitor achieves a smooth value of the DC flow through the DC links that is very sufficient for operation of the SST. Due to inability to realize infinite capacitance value, small ripple and distortion is unavoidably present, limited to 10% peak to peak value (Soodi and Vural, 2021). The minimum filter capacitance calculation (Krein, Balog and Mirjafari, 2012), is as follows:

$$C_{min-sin} = \frac{P}{2\pi f \times V_{DC} \times \Delta V} \text{ ----------(3.4)}$$

Where P represents DC link power, V_{DC} is the DC link Voltage, f is the sine waveform frequency, $C_{min\text{-}sin}$ is the minimal capacitance, and ΔV is the DC peak to peak ripple voltage.

The value of minimum filter capacitance for DAB is:

$$C_{min-DAB} = \frac{(50\ P)}{{V_{DC}}^2 \times f_{sw}} \text{ ----------(3.5)}$$

Where P represents the DC link Power, V_{DC} is the DC link Voltage, and f_{sw} is the switching frequency.

3.6. Cascade H-Bridge (CHB)

The CHB is an important constituent of the SST, used for conversion of Alternating Current (AC) electricity to Direct Current (DC) electricity in the smart energy system. CHB constitute input filter, many cascaded H-bridges and output filter as shown in Figure 3.5.

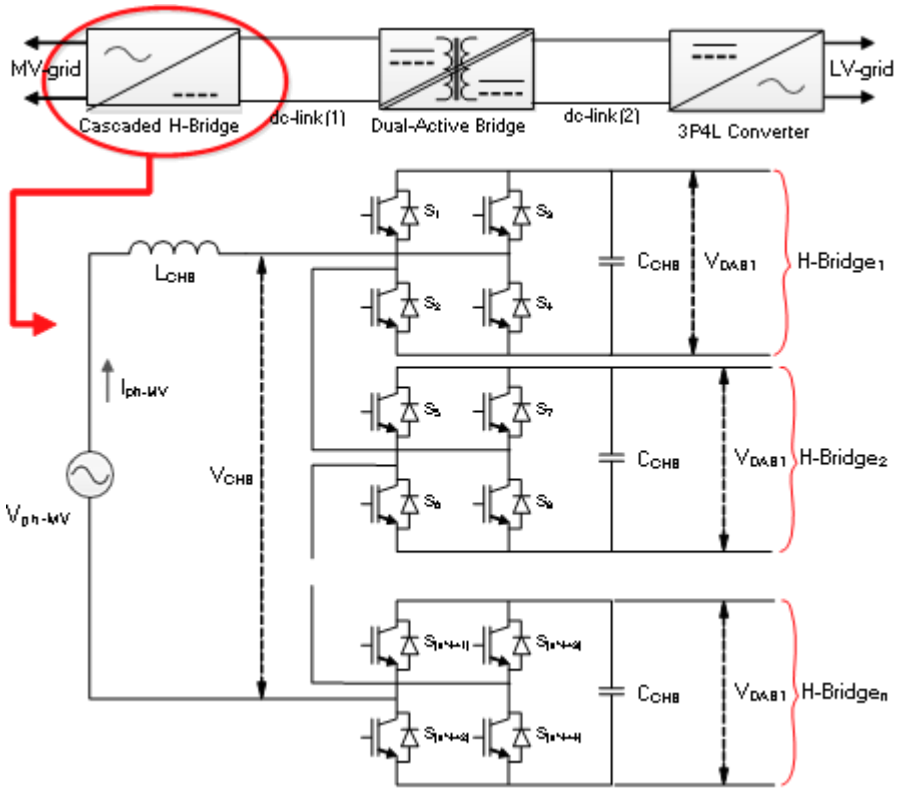

Figure 3.5: (One of three identical phases in an) n-modules of a Cascaded H-Bridge.

Individual H-Bridge is controlled by a controller circuit, that can trigger the Insulated-Gate Bipolar Transistor (IGBT) ON or OFF to achieve the required waveform at variable conduction and delay angles. To design CHB, the following parameters are required:

i. H-bridge numbers needed (n-modules, which is expressed as an integer)
ii. The DC link voltage required (based on the specified requirement to be met)
iii. The filter capacitor value (based on the required parameter analysis and substitutions in the appropriate function)
iv. The grid filters (based on the frequency and distortion levels required)
v. The switching frequency (correlated to the resonance frequency in other to unveil the best way to mitigate (distortion and harmonics)

3.6.1. The CHB Power Control

A single-phase analysis of the power exchange between CHB and the grid is done using only the fundamental harmonics, replacing CHB with an AC voltage source as depicted in Figure 3.6.

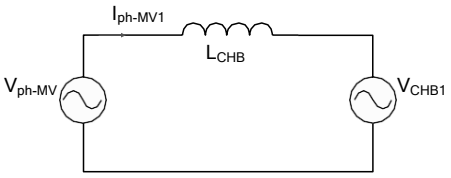

Figure 3. 6: The CHB representation in terms of a single phase.

The power vector analysis of figure 3.7 yields the following:

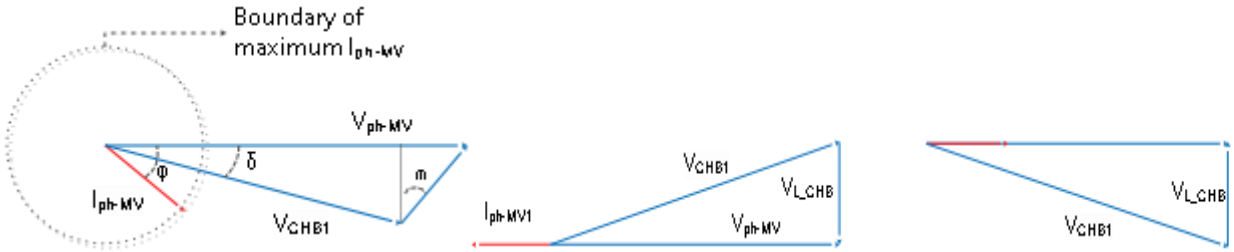

(a) (b) (c)

Figure 3.7: The various vector relationship between the voltages and the current.

(a) representation of arbitrary current, (b) the flow of Power from CHB to MV grid at pf = 1 & (c) Flow of power from MV grid to CHB at pf = 1, and medium phase current ($I_{ph-MV)}$ is in phase with medium phase voltage (V_{ph-MV}).

The mathematical equations depicting power flow from MV grid to CHB as shown in (3.6 and (3.7) as follows:

$$P = 3V_{ph-MV} \times I_{ph-MV1} \times \cos(\varphi) = \frac{[3V_{ph-MV} \times V_{CHB1} \times \sin(\delta)]}{[2\pi f_{grid} L_{CHB}]} \quad \text{----------(3.6)}$$

$$Q == 3V_{ph-MV} \times I_{ph-MV1} \times \sin\varphi = \frac{[3V_{ph-MV} \times V_{CHB1} \times \cos\delta)]}{[2\pi f_{grid} L_{CHB}]} \quad \text{----------(3.7)}$$

It follows that P and Q are the active and reactive power flow from MV grid to CHB, V_{ph-MV} is the MV grid phase to phase voltage, $V_{L\text{-}CHB1}$ is the voltage across L_{CHB1}, V_{CHB1} is the DC link 1, I_{ph-MV1} is the inductor current, V_{CHB} is the CHB AC side voltage, L_{CHB} is the inductor used as a filter, C_{CHB} is the DC link capacitor, φ is the phase angle between the MV grid voltage and current, and δ is the phase angle between the MV grid voltage and the CHB voltage.

Using (3.8), while $V_{ph\text{-}MV}$ and f_{grid} are maintained by the grid, the amount of load gives the value of $I_{ph\text{-}MV}$ absorbed. φ or V_{CHB1} needs to be adjusted or changed to enable the adjustment of reactive power and active power.

$$M_{a-CH} = \frac{\sqrt{2} \times V_{CHB1} \times V_{CHB1}}{N_m * V_{DAB1}} \text{ ----------(3.8)}$$

$m_{a\text{-}CH}$ is the CHB modulation index, and N_m is the parallel H-Bridges number.

3.6.2. The CHB Number of H bridges and DC link Voltage

The number of the H-bridges is an important aspect of the design of the SST, because in CHB, increase in the number of these bridges leads to greater modularity and performance. But the trade-off is that the resulting SST will have more volume, mass, incurred expenses, and complexity respectively. To maintain affordability and simplicity, the number of H-bridges is kept low. For the design of DC-link voltage, the following is considered below:

i. The retrieved DC link ripple voltage is used to set the limits of the DC link voltage value. In other to maintain the DC link ripple voltage at 10%, the inductor is assumed to be a wattless component with a zero voltage drop value, and the AC peak voltage lower limit ($V_{DAB1-min}$) value in each H-bridge is maintained at 95% of the value of the DC link voltage, to avoid the combination of this ripple voltage and the AC voltage peak value.

ii. The IGBT switches rating is used as indication of the DC-link upper voltage limit value. To ensure safety and optimal operation of SST, the DC link voltage ($V_{DAB1-max}$) is set at 80% of the IGBT switch voltage rating value.

The mathematical model is shown in (3.9), (3.10), and (3.11) below:

$$V_{DAB1-max} = \frac{80}{105} \times V_{rated-IGBT} \text{ ----------(3.9)}$$

$$V_{DAB1-min} = \frac{100}{95} \times \frac{\sqrt{2V_{ph-MV}}}{N_m} \text{ ----------(3.10)}$$

The number of required modules (N_m) = (3.10) / (3.9)

$$N_m = \frac{100\sqrt{2V_{ph-MV}}}{95V_{DAB1-max}} \text{ ----------(3.11)}$$

The margin between (3.9) and (3.10) values is very useful in choosing a value for DC link voltage and in optimizing the DAB transformer ratio.

3.6.3. The Capacitor filters.

To obtain optimum smoothening of the DC link waveform, the rectified power in each H-bridge per phase is analyzed below:

$$P = \frac{P_{DAB\,(rated)}}{3N_m} \text{ ----------(3.12)}$$

Substituting (3.4) and (3.12) gives:

$$C_{CHB} = \frac{P_{rated}}{0.6N_m \times \pi \times f_{grid}(V_{DAB1})^2} \text{ ----------(3.13)}$$

3.6.4. The inductor filter and carrier frequency

The inductor filter (L_{CHB}) and carrier frequency (f_{CHB}) are retrieved based on CHB harmonic distortions. As f_{CHB} increase, harmonic distortions decrease, but the switching losses increases. Also, as L_{CHB} increases, the harmonic distortion decreases, but the L_{CHB} size, cost, and voltage drop increases.

The modulation and structure of CHB is unpacked to realized where the maximum switching losses are occurring. To achieve this objective, the Phase Shifted Pure Sine Wave Modulation (PS-PWM) scheme is used. Using this technique, each of the H-bridges is attributed to two signal carriers, having a frequency of f_{CHB}. Thus, the effective frequency ($f_{CHB-effective}$) is shown in (3.14).

$$f_{CHB-effective} = 2N_m f_{CHB} \text{ ----------(3.14)}$$

Based on the IEEE standard for distortion caused by harmonics, the frequency of the 35th harmonic order should not exceed 1750Hz. To comply with this thumb rule, f_{CHB} and L_{CHB} is used to checkmate the distortion level, and according to (3.14), increase in N_m increases the $f_{CHB-effective}$ and inherent harmonic distortion.

The flow chart model for decision on the L_{CHB} and f_{CHB} selection is shown in Figure 3.8. According to Figure 3.8, many combinations of f_{CHB} and L_{CHB} results yield values close enough to the IEEE thumb rule. However, the size and mass of the inductor, and its voltage drop, plus switching losses needs to be considered in these selections.

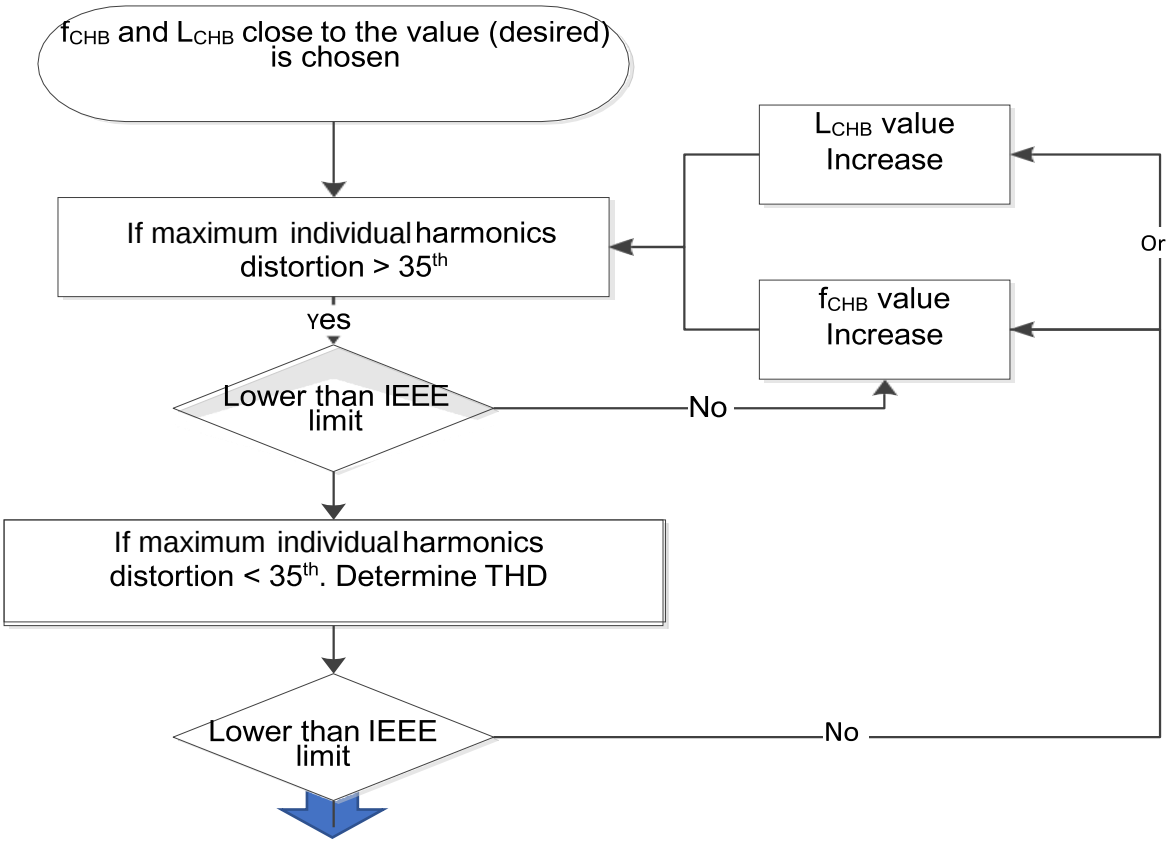

If yes, f_{CHB} and L_{CHB} values are chosen and used in the design.

Figure 3.8: flow chart model for decision on the L_{CHB} and f_{CHB} selection.

3.7. The design parameters of the Dual Active Bridge

To realize galvanic isolation in the SST high voltage side, and low voltage side, the DAB is used. It is made of DC/AC to AC/DC converter, and a HFT situated in between the DC/AC and AC/DC. The CHB H-bridge numbers is equal to the DAB modules, where individual DAB module is directly connected to one CHB H-bridge, and the DAB outputs are connected to DC bus as shown in Figure 3.9. the required parameters are as follows:

i. The switching frequency of DAB (f_{DAB})
ii. The DAB leakage inductance (L_{DAB})
iii. The transformer turns ratio (n_{Tr})
iv. DAB capacitor filter (C_{DAB1s}) and (C_{DAB2})

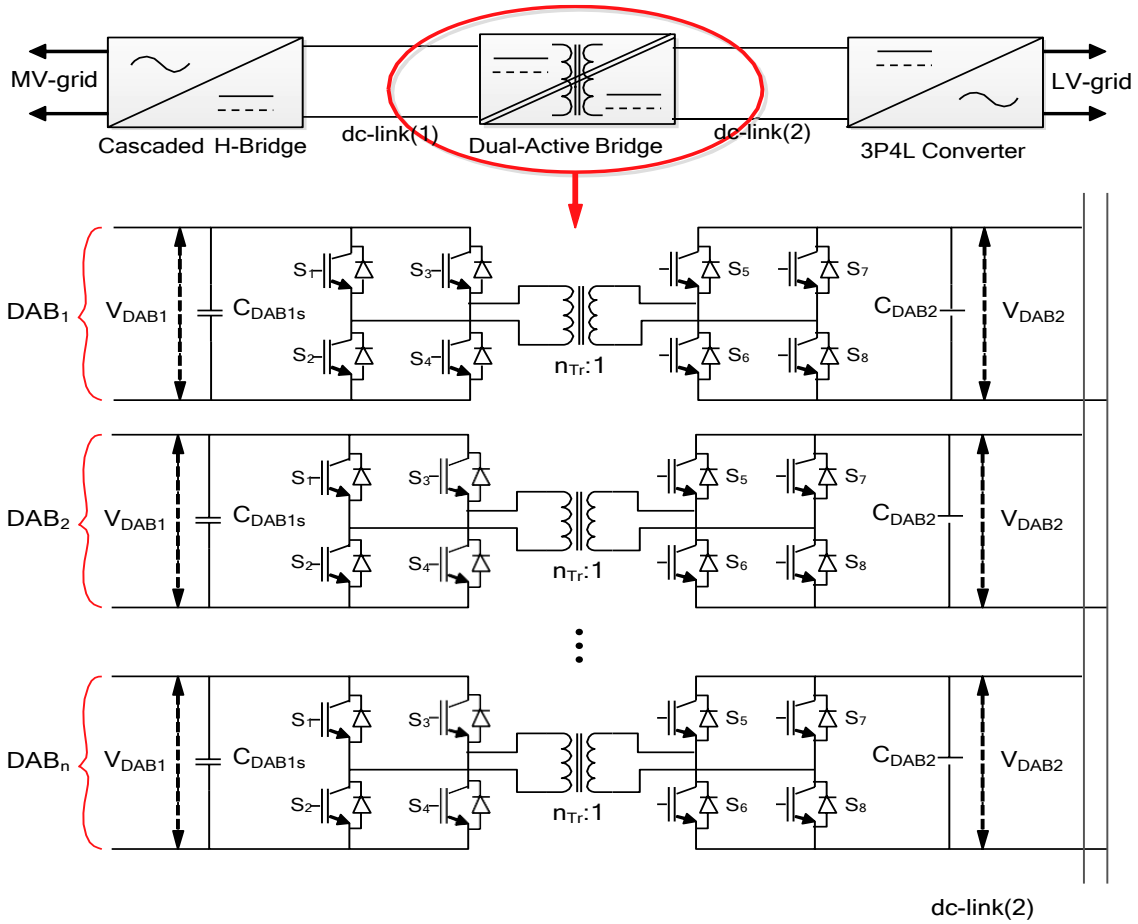

Figure 3.9: The design of N-Number of DAB modules.

The design of N-Number of DAB modules is depicted in Figure 3.9. The $V_{ac\text{-}DAB1}$ = transformer primary side voltage, $V_{ac\text{-}DAB2}$ = transformer secondary side voltage, R_{DAB1} = primary winding resistance, R_{DAB2} = secondary resistance winding, L_M = transformer magnetizing inductance, R_c = core magnetic resistance, L_{DAB1} = primary winding leakage inductance, and L_{DAB2} = secondary winding inductance leakage.

3.7.1. The DAB Power control

To control the DAB power flow, the phase shift method is employed, to control transformer high voltage side and low voltage side power flow, respectively. The transformer analysis is done by considering the transformer equivalent circuit (Sen, 2012) shown in Figure 3.10.

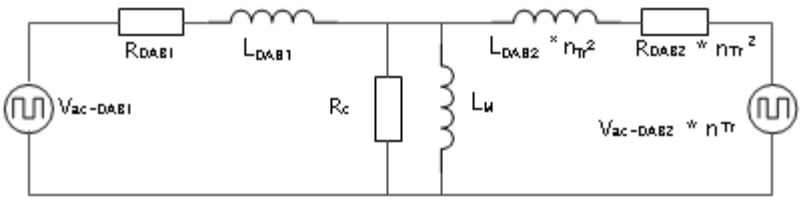

Figure 3.10: DAB transformer equivalent circuit.

The sum of two DAB leakage ($L_{DAB1} + L_{DAB2}$) inductances (L_{DAB}) = $L_{DAB1} + (L_{DAB2}(n_{Tr})^2)$. The DAB transferred power (assuming no losses) is given in (3.15).

$$P_{DAB} = \frac{n_{\times}Tr_{\times}V_{DAB_1}D_{DAB}{\times}V_{DAB2}(1-D_{DAB})}{2f_{DAB}{\times}L_{DAB}} \text{ ---------- (3.15)}$$

Duty cycle, $D_{DAB} = 2t_{on-DAB} \times f_{DAB} = {t_{on-DAB}}\Big/{\left(\frac{T_{s-DAB}}{2}\right)}$ ----------(3.16)

P_{DAB} represents the power flow in the DAB, f_{DAB} is the switching frequency of DAB, D_{DAB} represents the DAB phase-shift (duty cycle), V_{DAB1} is the CHB-side DAB voltage, $t_{on\text{-}DAB}$ is the switch ON delay time, $T_{s\text{-}DAB}$ is DAB switching period, and V_{DAB2} is the 3P4L converter side voltage of the DAB.

The waveform for the DAB output and input transformer voltages respectively, is shown in Figure 3.11. The rated power for the DAB ($P_{DAB\text{-}rated}$) is the same with (3.12).

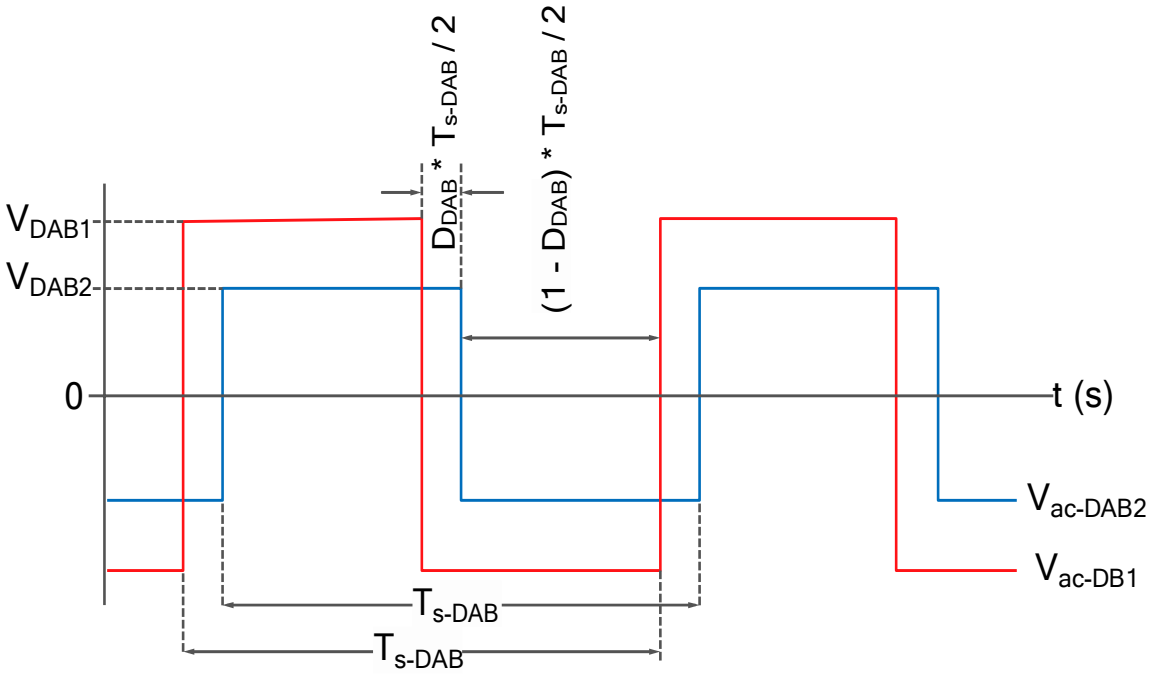

Figure 3.11: The waveform for the DAB output and input transformer voltages.

3.7.2. The operation of the soft DAB switching

To achieve high frequency switching, the DAB offers a soft switching approach that ensures that at switching points of ON and OFF, either the voltage is zero or the current is zero, so that losses associated with switching is minimal or at best negligible. The transformer size is drastically reduced at this high frequency switching of the IGBT. The active region of the IGBT must ensure that DAB

switching is occurring within the correct range. To unveil this range, DC conversion ratio is used according to (3.17)

$$DC_{RATIO} = \frac{n_{\times}T_{r}\times V_{DAB2}}{V_{DAB1}} \text{ ----------(3.17)}$$

As shown in Figure 3.12 (Mi *et al.*, 2008) the variation that results in soft switching (DC_{RATIO} = 1.0 and R = 3 (pu)) is selected for the best switching operation of the DAB.

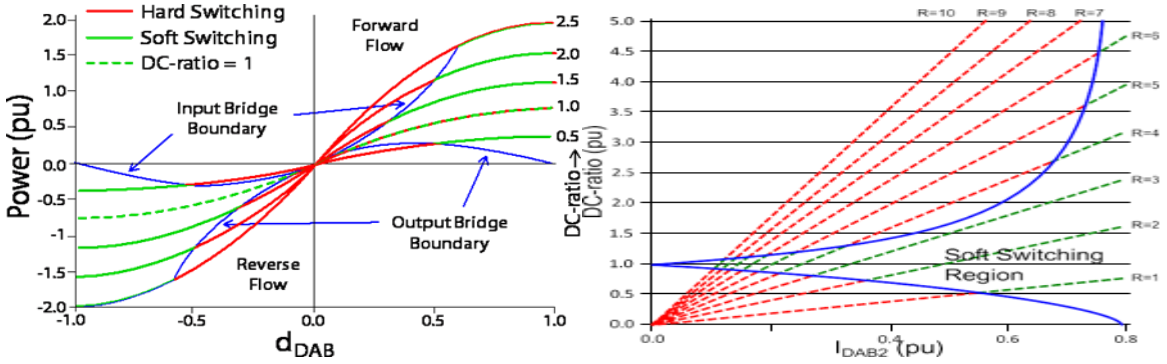

Figure 3.12: (a) the Power output vs Duty Cycle (b) the normal output voltage vs current output.

(3.18) and (3.19) (Atkar *et al.*, 2022) are used to calculate $I_{DAB2(pu)}$ and R.

$$I_{DAB2(pu)} = {I_{DAB2}}/{V_{DAB2} \times n \times T_{r} \times 2\pi \times L_{DAB} \times f_{DAB2}} \text{ ----------(3.18)}$$

$$R_{(pu)} = {V_{DAB2(pu)}}/{I_{DAB2(pu)}} \text{ ---------- (3.19)}$$

3.7.3. The transformer Ratio of the windings

The DAB transformer performs the role of isolation, impedance matching, and voltage matching. The Transformer turn ratio (n_{Tr}) is used to show the windings and voltage relationships on both the high and the low voltage transformer side as shown in (3.20).

$$n \times T_{r} = {V_{DAB1}}/{V_{DAB2}} \text{ ----------(3.20)}$$

The n_{Tr} is represented in its simplest ratio and it is dependent on the parameters of CHB and 3P4L converter. To get the optimal n_{Tr}, $V_{DAB1(minimum)}$ and $V_{DAB2(minimum)}$ is used.

3.7.4. The DAB switching frequency.

The switching frequency is dependent on the type of switching power electronic device used, transformer characteristics, and the efficiency required. A review of works done in this regard shows that for a power rating from 10^3 watts to 10^6 watts, requires a switching frequency of 20kHz, to

reduce acoustic noise associated with high-frequency operation (Zeljkovic *et al.*, 2015)(De Oliveira Filho, *et al.*, 2013)(Mi *et al.*, 2008). Thus, 20kHz will be used as the DAB switching frequency.

3.7.5. The Leakage Inductance

For optimal operation of the DAB, the leakage inductance (L_{DAB}) is computed from (3.15). to maximize the DAB power transfer, D_{DAB} is assumed to be equal to half.

Thus, $L_{DAB} = [n \times T_r * V_{DAB1} * V_{DAB2}] \times [0.5 \times (1 - 0.5)] / [2 \times f_{DAB} \times P_{DAB}]$

$$L_{DAB} = [nT_r \times V_{DAB1} \times V_{DAB2}] / [8 \times f_{DAB} \times P_{DAB\,(rated)}] \quad \text{----------(3.21)}$$

This shows that the maximum L_{DAB} varies inversely as the rated power ($P_{DAB\,(rated)}$), and there will be 80% restriction on the L_{DAB} to achieve the best duty cycle. This is applied to (3.21) to give (3.22).

$$L_{DAB\,(MAX)} = [n \times Tr \times V_{DAB1} \times V_{DAB2}] / [10 \times f_{DAB} \times P_{DAB\,(rated)}] \quad \text{----------(3.22)}$$

3.7.6. The capacitor for filter operation

The two DAB capacitors for DC link 1 and Dc link 2 are calculated from (3.24), then the CHB side capacitor is calculated from (3.25), and 3P4L side from (3.23)

$$C_{3P4L} = P_{rated} / 2\pi \times f_{grid} \times 0.1 \times (V_{DAB2})^2 \quad \text{----------(3.23)}$$

$$C_{DAB1} = 50 \times P_{DAB\,(rated)} / f_{DAB} \times (V_{DAB1})^2 \quad \text{----------(3.24)}$$

$$C_{DAB2} = 50 \times P_{DAB\,(rated)} / f_{DAB} \times (V_{DAB2})^2 \quad \text{----------(3.25)}$$

The switching actions of DAB and CHB is smoothened by their respective capacitors (C_{DAB} (high frequency operation) and C_{CHB} (low frequency operation)). The sum of each CHB H bridge and individual DAB is shown in (3.26).

$$C_{DAB1} = C_{CHB} + C_{DAB1} \quad \text{----------(3.26)}$$

3.8. The Three Phase Four Leg Converter (3PF4L)

The 3P4L converter receives DAB DC electricity and transform it int AC. It is connected in stand-alone mode (Load), or grid connected mode, and it consist of 4 half bridges (each for phase mode and another for neutral mode) as shown in Figure 3.13. To model the 3P4L converter, DC link, grid filter values, switching frequency, and filter capacitors parameters, respectively, are needed.

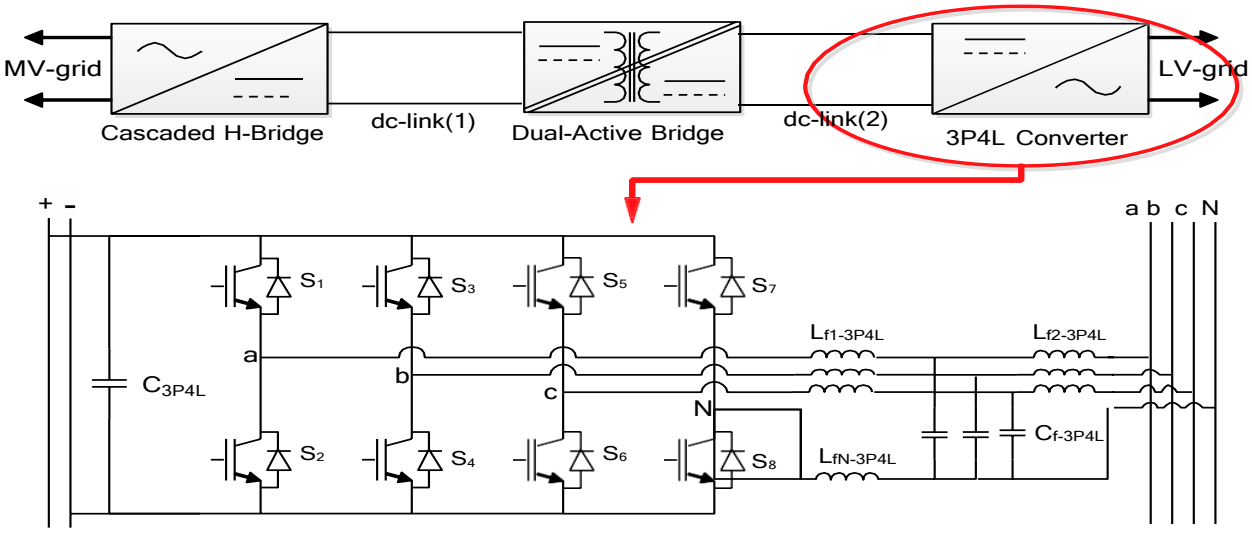

Figure 3.13: The 3P4L converter circuit.

3.8.1. The 3P4L converter control

To simplify the analysis of the control of the 3P4L converter, current flow mesh analysis is done based on Figure 3.14, resulting in (3.27)

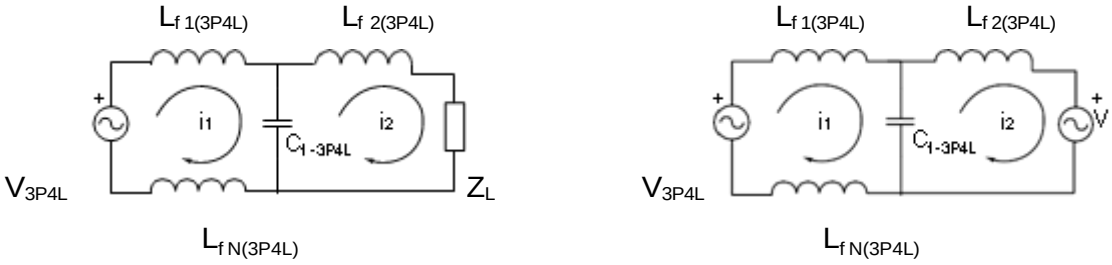

(a) Mesh circuit for stand-alone scheme (b) Mesh circuit for grid connected

Figure 3.14: The mesh circuit control scheme for 3P4L converter.

The inductors and capacitors represent the passive parameters, i_1 and i_2 are the 3P4L converter output phase current and grid side or load side phase current respectively. The grid phase voltage is V and V_{3P4L} is the 3P4L converter output voltage.

3.8.2. Analysis of the grid connected is as follows:

$$(i_1 - i_2)\, X_{cf} + i_1\,(X_{Lf1} + X_{Cf}) = V_{3P4L} \quad \text{----------(3.27)}$$

$$i_2\,(X_{Lf2} + X_{Cf})(i_2 - i_1)X_{Cf} = V \quad \text{----------(3.28)}$$

Where X is the reactance ($2\pi fL$ or $2\pi fC$)

The combination of (3.27) and (3.28) gives the (3.29) below:

$V_{3P4L} = \{ [V + i_2(X_{Lf2} + X_{cf})]/X_{Cf} \} \times \{(X_{Lf2} + X_{LfN} + X_{Cf}) - i_2 X_{Cf}\}$ ----------(3.29)

Also, $i_2 = \frac{P}{3V \times \cos\varphi}$ ----------(3.30)

3.8.3. The stand-alone analysis is as follows:

$\{i_1(X_{LfN} + X_{Lf1} + X_{Cf}) - i_2 X_{Cf}\} = V$ ----------(3.31)

$i_2(X_{Lf2} + X_{Cf} - Z_L)(i_2 - i_1)X_{Cf} = V$ ----------(3.32)

the combination of (3.3.1) and (3.3.2) gives:

$\{[i_2(Z_L + X_{Cf} + X_{Lf2})/X_{Cf}](X_{LfN} + X_{Lf1} + X_{Cf})\} - [i_2 X_{Cf}]$ ----------(3.33)

Also, the grid voltage is equal to load voltage, thus $i_2 = V/Z_L$ ----------(3.34)

The analysis of DC link Voltage is as follows:

According to (3.35) DC link and AC fundamental output voltages respectively are related (Mohan and Kamath, 1997).

LCL filter capacitor should have a voltage drop of not more than 10% of the voltage in the grid, and DC link capacitor ripple voltage should around 5% (Sahoo, Otero-De-Leon and Mohan, 2013).

$V_{DAB2} \geq \sqrt{3} \times (\sqrt{2} V_{3P4L1}) \geq \sqrt{6} V_{3P4L1}$ ----------(3.35)

$V_{DAB2\text{-}min} = [\sqrt{6} \times (100 + 10)\ \% \times V] \,/\, [95\%] = [(22\sqrt{6})/19] \times V$ ----------(3.36)

The analysis of the DC link Capacitor

To calculate the DC link capacitor value, the ripple voltage is set at 10% (Mohan *et al.*, 1994).

$C_{3P4L} = P_{rated} / (2\pi f_{grid} \times 0.1 \times V_{DAB2})^2$ ----------(3.37)

3.8.4. The analysis of the switching frequency

The switching frequency is correlated to the values of the filter, and the switching frequency increase, results in decreased requirements needed for the filter. Also, an increase in the filter parameters causes more voltage drops to occur. The converter of the 3P4L works under low voltage but high current conditions, the frequency needs to be kept under 5kHz to minimize switching losses (Solatialkaran, Khajeh and Zare, 2021). The various filter design is shown in Figure

3.15 (Zabaleta *et al.*, 2016). The switching frequency should be twice the resonance frequency (Azab, 2020) in each of the frames in Figure 3.15. The resonance frequency in Figure 3.15 (c) is greater (thrice) than the resonance frequency in Figure 3.15 (b) and the resonance in Figure 3.15 (b) is greater than the resonance frequency in Figure 3.15 (a). The inductor in Figure 3.15 (c) is three times the inductor in Figure (b), and it accounts for the further reduction in Electromagnetic Interference (EMI) in these two circuits. To improve the filter performance further the switching frequency is increased to four times of the resonance frequency.

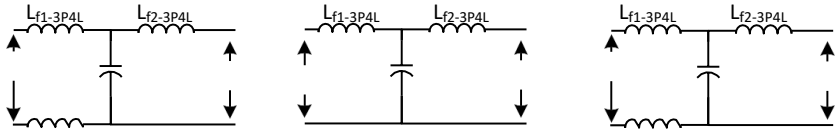

(a) *abc* frame (b) αβ frame (c) γ frame

Figure 3.15: LCL filter with (V_{3P4L}) input voltage, Filter capacitor ($C_{f(3P4L)}$), and V_{LV} output (voltage) in the *abc*, and the αβ-γ frames respectively.

3.8.5. The SST Grid filter

The LCL filter type converter is used to connect the 3P4L converter to the low voltage grid, its parameter analysis and most importantly selection for a particular SST is paramount. The LCL filter THD should be compliant to IEEE1547 standard, $C_{f(3P4L)}$ value should be lower than 5% of impedance base value (Z_b), voltage drop has to be lower than 10% of the low voltage grid value, and $10 * f_{grid} \geq f_{resonance} \geq 0.5 f_{3P4L}$ (switching frequency)(Miveh *et al.*, 2016)(Lin *et al.*, 2019)(Ismail and Mishra, 2018)(Shri *et al.*, 2013) to avoid harmonic and resonance issues.

3.8.6. Control strategy for the LCL type filter

To obtain optimal control scheme for the LCL type filter, the $f_{resonance} \leq 0.25 * F_{grid}$, to realize a enough bandwidth that ensures that a Proportional Integral (PI) controller is implemental in the control module of the SST (Gao *et al.*, 2020)(Zhang, Tang and Yao, 2014). Using (3.38) to (3.44) LCL filter parameters are optimized and retrieved (Sen, Yenduri and Sensarma, 2014)(Liserre, Blaabjerg and Dell'aquila, 2004).

$$f_{res\text{-}\alpha\beta} = \sqrt{(L_{f1(3P4L)} + L_{f2(3P4L)}) / [2\pi\sqrt{(L_{f1\text{-}3P4L} L_{f2\text{-}3P4L} C_{f(3P4L)})}]} \quad \text{----------(3.38)}$$

$$f_{res\text{-}\gamma} = \sqrt{(L_{f1(3P4L)} + L_{f2(3P4L)} + 3L_{fN\text{-}3P4L}) / [2\pi\sqrt{(3L_{f2\text{-}3P4L} L_{fN\text{-}3P4L} C_{f\text{-}3P4L} + L_{f1\text{-}3P4L} L_{f2\text{-}3P4L} C_{f(3P4L)})}]} \quad \text{----(3.39)}$$

$$L_{fres\text{-}\alpha\beta} = f_{grid}\sqrt{(2/xy)} \quad \text{----------(3.40)}$$

The factor x and y are expressed in (3.41) and (3,42)

$L_{f1\text{-}3P4L} = L_{f2\text{-}3P4L} = y(Z_b/2\pi f_{grid})$ ----------(3.41)

$C_{f\text{-}3P4L} = (x) \ / \ (2\pi f_{grid} Z_{base})$ ----------(3.42)

$Z_{base} = (V_{ph\text{-}LV})^2 / P_{rated}$ ----------(3.43)

$f_{res\text{-}\gamma} = w \times f_{res\text{-}\alpha\beta}$ ----------(3.44)

$L_{fN\text{-}3P4L} = [2L_{f1\text{-}3P4L} - (2\pi f_{res\text{-}\gamma})^2 (L_{f1(3P4L)})^2 C_{f\text{-}3P4L}] / [(3(2\pi f_{res\text{-}\gamma})^2 L_{f1(3P4L)} C_{f\text{-}3P4L}) - (3)]$ --------(3.45)

From (3.38) to (3.45) LCL filter parameters are small and cost less, however, the harmonics are high. Thus, to optimize this design, $f_{res-\gamma} = f_{res-\alpha\beta}$, with large values and w = 1. The flow chart MATLAB c++ progamming algorithm is used to implement and test the parameters for the design of the LCL type filter is depicted in Figure 3.16. the nested if statements algorithm can be used to fully simplify and automate this LCL type filter design parameter selection.

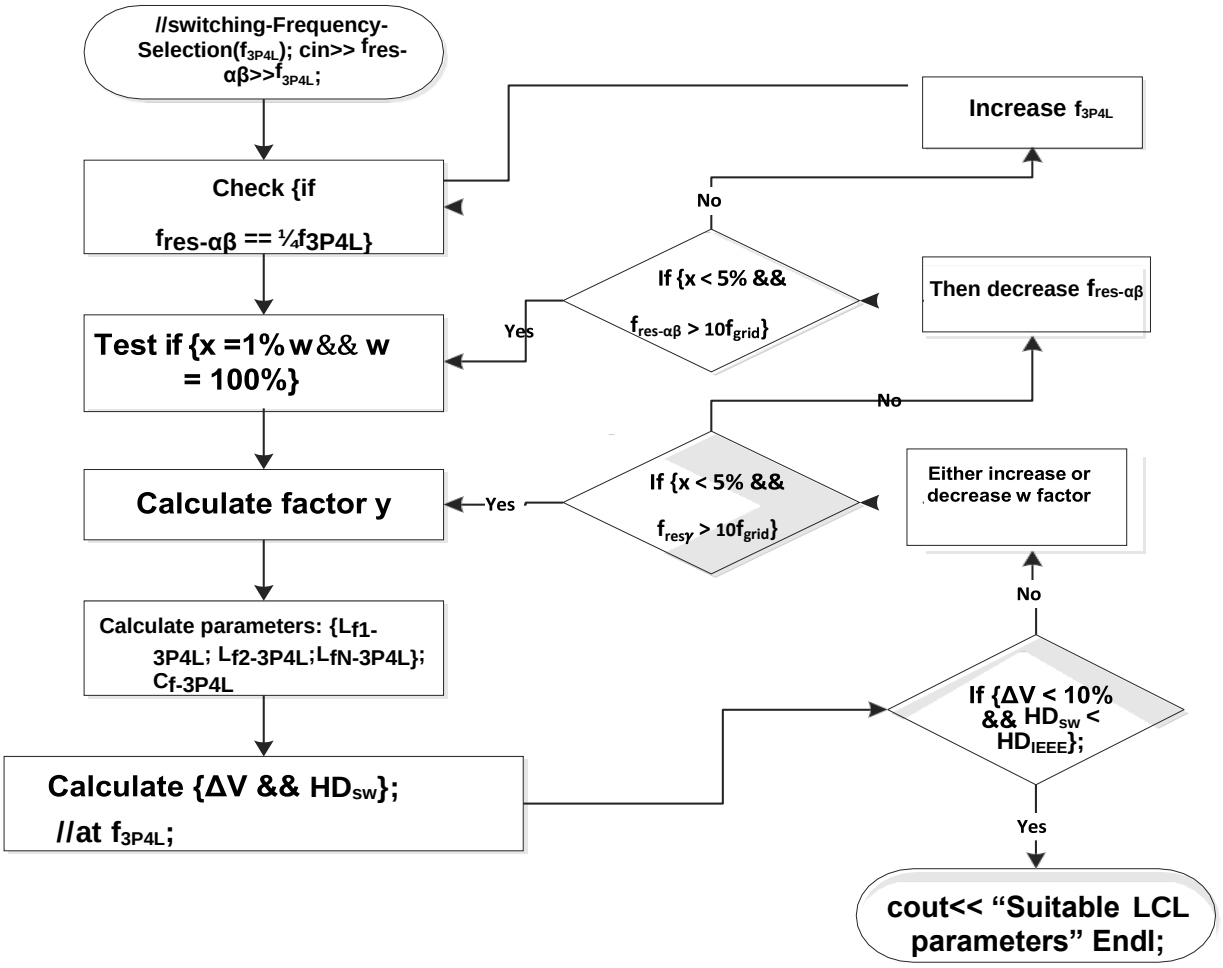

Figure 3.16: The flow chart MATLAB c++ programming algorithm.

3.9. Results of the mathematical dimensions of the SST design

The results from the complex mathematics involved in the SST design is creatively and innovative done and presented in a simple format that is easy to study, and most importantly, can be used to design a programming flow chart algorithm and whole decision-making software capable of minimizing the effort and time constraint associated with the design and modeling of the SST for smart energy. The results of these mathematical dimensions in the design of the SST are shown in (3.1) to (3.44) and Figure 3.1 to Figure 3.15. These mathematical dimensions are implemented in the next chapter for calculating the values of all the required parameters for the design, simulation, and modelling of the SST.

3.10. Summary

The behaviour of the SST in dynamic conditions that is suitable for a smart and modern energy system was carried out, by the analysis of the SST vital components (converters) and their parameters which should be designed first. This is done by mathematical analysis, culminating in various equations representing their behaviour, function, control strategies, and their ratings. The required voltage, current and power rating of each component are represented by corresponding equations that unveil the impedance matching requirement, which ensures that maximum power is transferred between connecting components of the SST in the smart energy system. The components and parameters determined include the filter values and the required filter types, DC capacitors values, switching frequency, and the CHB, DAB, and 3P4L converters, respectively. To model these three converters, DC link, grid filter values, switching frequency, and filter capacitors and inductors parameters, respectively, are needed. This converter's specialized functions of the SST are a game changer in the distributed energy system of the hybrid microgrid and smart grid parts of the smart energy system.

This chapter unveils a mathematical dimension of calculating the number of modules needed in each SST converter, thereby solving the complex problem of SST modularity, voltage levels and power rating in a creative and innovative approach. Finally, the equations, mathematical functions, and algorithms developed in this study helped in the design of converters' DC links, and the combinations of these components culminated in the design of the SST in an erudite manner.

CHAPTER 4: THE SST MODEL DESIGN PARAMETERS FOR SMART ENERGY FROM THE MATHEMATICAL DIMENSIONS

4.1. Introduction

The mathematical and technical functions derived from chapter three is implemented in the component value determination for the individual power electronic components which includes the Hybrid bridge, CHB, and DAB, culminating in SST design.

4.2. The SST specifications

The SST rated and specified parameter values that is used to design the CHB, DAB, and the 3P4L converter topologies are listed in table 4.1.

Table 4.1: The SST rated and specified parameter values.

Parameter	Value	Unit	Denotation
Apparent Power	1.0	MVA	S_{rated}
Desired Power Factor	1.0	Dimensionless	pf
Real Power	1.0	MW	P_{rated}
Reactive Power	0	KVAr	Q
Grid Frequency	50	Hz	f_{grid}
Medium Level Voltage	10	KV	V_{ML}
Low Level Voltage	400	V	V_{LV}

4.3. The mathematical design for CHB

The number of the hybrid bridges or modules should be kept minimum, to reduce complexity, and the associated voltage drop. Also, high rating of IGBT component will reduce the number of IGBT required, and associated cost.

Using (3.11), $N_m = (100 \times \sqrt{2} \times 10000/\sqrt{3}) \,/\, (95 \times 1261.5) = 6.8131 = 7$ modules.

According to the IGBT ratings when $m = 7$, $V_{rated\text{-}IGBT} = 1700V$ for each IGBT, using

$V_{DAB1(max)} = (80 \,/\, 105) \times V_{rated\text{-}IGBT})$ ----------(3.9)

$V_{DAB1(min)} = (100 \,/\, 95) \times \sqrt{2} \times V_{ph\text{-}MV} / N_m)$ ----------(3.10)

$V_{DAB1(max)} = 1295.2831V$ and $V_{DAB1(min)} = 1227.8144V$, and the V_{DAB1} chosen as average between two minimum and maximum values $= [V_{DAB1(min)} + V_{DAB1(max)}] \,/\, 2 = 1261.5V$.

In addition, if $V_{DAB1} = 1260 \pm 4\ V$, and $V_{DAB2} = 720\ V$, then the transformer turns ratio $(n_{Tr}) = V_{DAB1} / V_{DAB2} = 4{:}7$.

$C_{CHB} = P_{rated} / [0.6 N_m \times \pi \times f_{grid} (V_{DAB1})^2]$ ----------(3.13)

$$C_{CHB} = 1000000 / [06 \times 7 \times (22/7) \times 50 \times (1261.5)^2 = 953\ \mu F$$

The maximum distortion in percentage corresponding to various values of inductors at different frequencies are shown in Figure 4.1 and Figure 4.2. Also, the CHB harmonic profile in Figure 4.3 shows maximum distortion of 0.255 at a harmonic order of 270, but on average, distortion order of 0.2 corresponds to an average harmonic order of 300. Hence, percentage distortion ranges from 0.15 to 0.255 within harmonic order of 270 to 320.

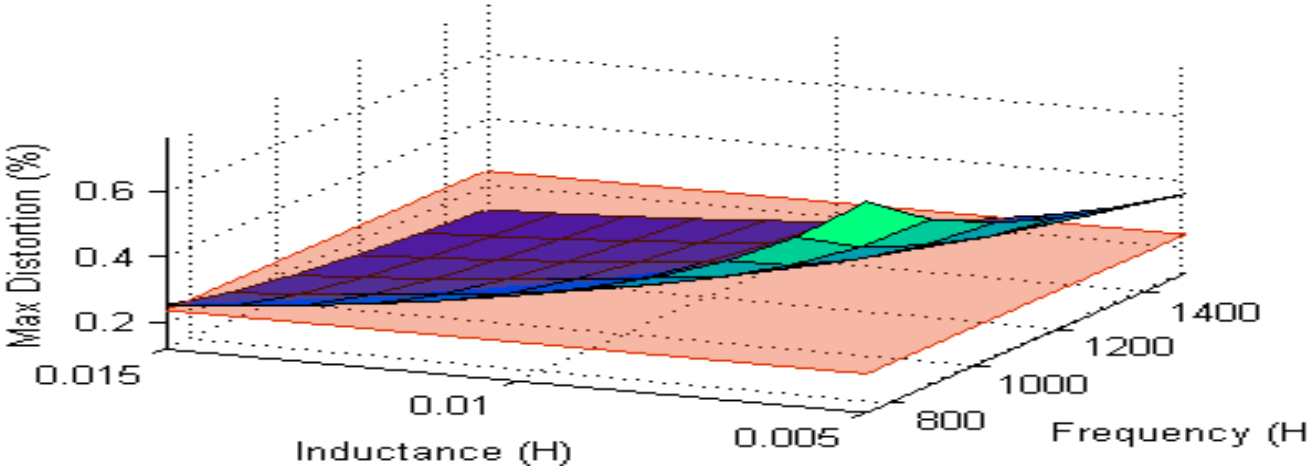

Figure 4. 1: The 3D flow graph of maximum distortion, inductance, and frequency for the CHB.

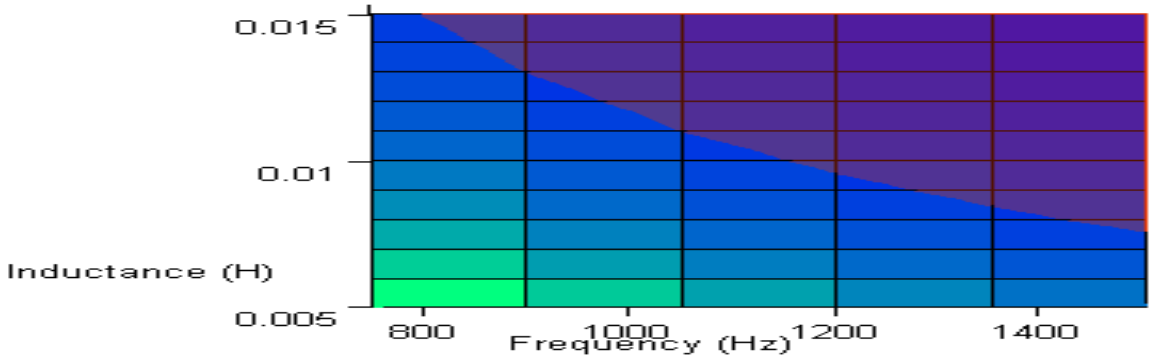

Figure 4. 2: The top view of the 3D flow graph.

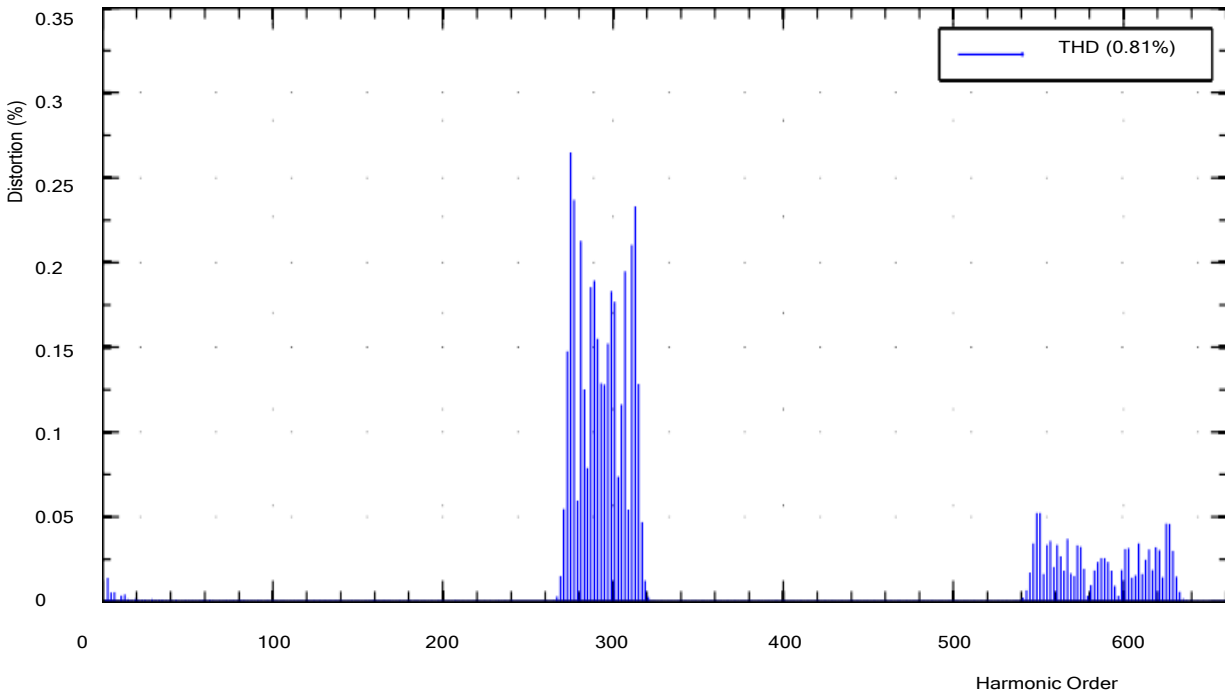

Figure 4. 3: The CHB harmonic distortion and profile.

Analysis of the graph representation in Figure 4.1 and Figure 4.2 shows that the three-graph function overlapped at f_{CHB} = 1055Hz, and L_{CHB} = 10.5mH.

4.4. The mathematical design of Dual Active Bridge

The power in the DAB is the sum of the individual power in each of the DAB modules, and the DAB minimum and maximum values are $V_{DAB2min}$ and $V_{DAB2max}$, evenly spread out around the V_{DAB2} value ($V_{DAB2min} < V_{DAB2} < V_{DAB2max}$ $(1.1 \times V_{DAB2max})$), and $V_{DAB2} = [V_{DAB2min} + V_{DAB2max}] / 2 = V_{DAB2}$.

$V_{DAB2min} = 2V_{DAB2} - V_{DAB2max} = (2 \times 720 - 1.1 \times 720) = 648$ V.

Using $P_{DAB\,(rated)} = (P_{rated})/(3N_m)$ ----------(3.12)

$$P_{DAB(rated)} = 1000000 / [3 \times 7] = 47619.0476 = 47.6\text{kW}$$

Using $L_{DAB} = [n_{Tr} \times V_{DAB1} \times V_{DAB2}] / [8f_{DAB} \times P_{DAB\,(rated)}]$ ----------(3.21)

$L_{DAB} = [(4/7) \times 1261.5 \times 720] / [8 \times 20000 \times 47619.0476] = 68.121\ \mu H.$

$C_{DAB1} = 50 \times P_{DAB\,(rated)}] / [f_{DAB}\,(V_{DAB1})^2]$ ----------(3.24)

$C_{DAB1} = [50 \times 47619.0476] / [20000 \times (1261.5)^2] = 74.8077\ \mu F.$

$C_{DAB2} = [50 \times P_{DAB\,(rated)}] / [f_{DAB} \times (V_{DAB2})^2]$ ----------(3.25)

$CDAB2 = [50 \times 47619.0476] / [20000 \times (720)2] = 229.64443\ \mu F.$

The voltage output waveform is shown in Figure 4.4

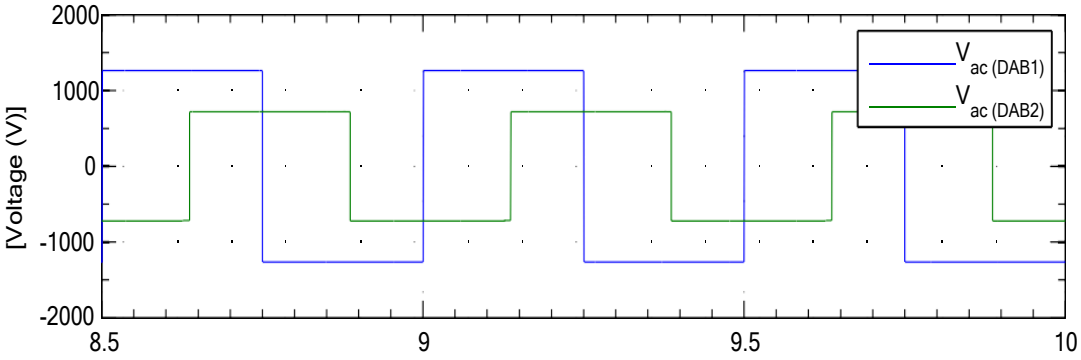

Figure 4. 4: The voltage waveform of the Dual Active Bridge.

The voltage output waveform shown in Figure 4.4 has a vertical displacement from minimum value to maximum value of DAB voltages as follows:

$V_{DAB1\ (min)} = 648V \times 2 = 1296$ peak-peak Volts with period, $T = (9.15 - 8.65)\ x\ 10^{-4} = 0.00005$ seconds, frequency, $F = 1/t = 1/0.00005 = 20kHz$.

$V_{DAB2} = 1296V * 2 = 2592$ peak-peak volts, period $(T) = 0.0009$ seconds, frequency $(F) = 1/f = 1/0.0009 = 1111.1111Hz = 1.1kHz$.

The current waveform of the Dual Active Bridge is shown in Figure 4.5.

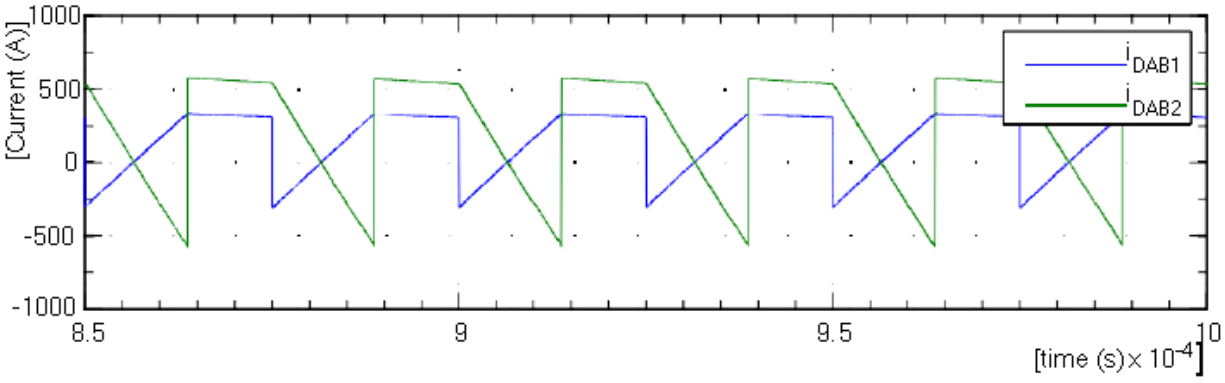

Figure 4. 5: The current waveform of the Dual Active Bridge.

The current (i_{DAB2}) has a period $(T) = 0.00075$ seconds, frequency $(f) = 1333.3333Hz = 1.3kHz$, peak-peak current $= 1020$ Amperes, and the current (i_{DAB1}) has the same period, frequency $(f) = 1333.3333Hz = 1.3kHz$, peak-peak current $= 520$ Amperes according to Figure 4.5.

4.5. The Three Phase Four Leg (3P4L) Converter

The 3P4L converter component parameters can be calculated from the various equations as follows:

The $V_{3P4L} = V_{DAB2} = 720V$.

The second DC link capacitor, $C_{3P4L} = P_{rated} / [2\pi f_{grid} \times 0.1 \times (V_{DAB2})^2]$

$C_{3P4L} = 1000000 / [2\pi \times 50 \times 0.1 \times (720)^2] = 61.40mF.$

$Z_{base} = (V_{LV\,(ph)})^2 / P_{rated} = (400/\sqrt{3})^2/1000000 = 0.0533pu.$

Also, $Z_{base\,(maximum)} = (720/\sqrt{3})^2/1000000 = 0.1728\Omega.$

Hence, factor $x_{minimum}$ depicting per unit impedance as follows:

$Z_{pu} = C_{3P4L} \times 2\pi f_{grid} \times Z_{base} = 0.0614 \times 2\pi \times 50 \times 0.0533 = 1.0281pu.$

And $x_{maximum} = 0.0614 \times 2\pi \times 50 \times 0.1728 = 3.332pu.$

Thus, x is taken as 1.5% and $w = 96\%$.

$C_{f\text{-}3P4L} = (x) / (2\pi f_{grid} \times Z_{base}) = 0.015 / [2\pi \times 50 \times 0.0533] = 895 \times 10^{-6}\,F = 895\mu\,F.$

The switching frequency (f_{3P4L}) should be below 5000Hz and resonance frequencies in frame αβ and frame γ should be less than one fourth of the switching frequency to reduce the distortions. f_{3P4L} = 3500Hz is chosen, and the resonance in the two frames is calculated below:

$$f_{res(\alpha\beta)} = 0.25 \times 3500 = 875 \text{ Hz, and } f_{res(\gamma)} = w \times f_{res(\alpha\beta)} = 0.96 \times 875 = 840 \text{ Hz.}$$

$$f_{res(\alpha\beta)} = (1/2\pi)\sqrt{[(2) / (L_{f1(3p4L)} \times C_{f(3p4L)})]}, \text{ and it yields } [2\pi F_{res(\alpha\beta)}]^2 = [(2) / (L_{f1(3p4L)} \times C_{f(3p4L)})]$$

$$L_{f1(3p4L)} = [(2) / ([2\pi \times F_{res(\alpha\beta)}]^2 \times C_{f(3p4L)})] = [(2) / ([2\pi \times 875]^2 \times 895 \times 10^{-6})] = 73.9318 \times 10^{-6}\,H$$

$$L_{f1(3p4L)} = 73.9318\ \mu H = L_{f2(3p4L)}.$$

$$f_{res(\gamma)} = \sqrt{(L_{f1(3P4L)} + L_{f2(3P4L)} + 3L_{fN\text{-}3P4L})} / [2\,\pi\,\sqrt{(3L_{f2\text{-}3P4L} \times L_{fN\text{-}3P4L} \times C_{f\text{-}3P4L} + L_{f1\text{-}3P4L} \times L_{f2\text{-}3P4L} \times C_{f(3P4L)})}]$$

$$[2\pi \times 840]^2 = \frac{[2 \times 73.9318 \times 10^{-6} + 3L_{fN\text{-}3P4L}]}{[(3 \times 73.9318 \times 10^{-6} L_{fN\text{-}3P4L} 895 \times 10^{-6} + 73.9318 \times 10^{-6} \times 73.9318 \times 10^{-6} \times 895 \times 10^{-6})]}$$

$$5.5297L_{fn(3P4L)} + 1.3627 \times 10^{-4} = 1.4786 \times 10^{-4} + 3L_{fn(3P4L)}$$

$$L_{fn(3P4L)} = (1.4786 \times 10^{-4} - 1.3627 \times 10^{-4}) / (5.5297 - 3) = 4.58157 \times 10^{-6}\,H = 4.58\ \mu H.$$

The isolated voltage mode (V_{3P4L}), the grid-connected mode voltage (V_{grrid}), and the currents waveforms, respectively are shown in Figure 4.6.

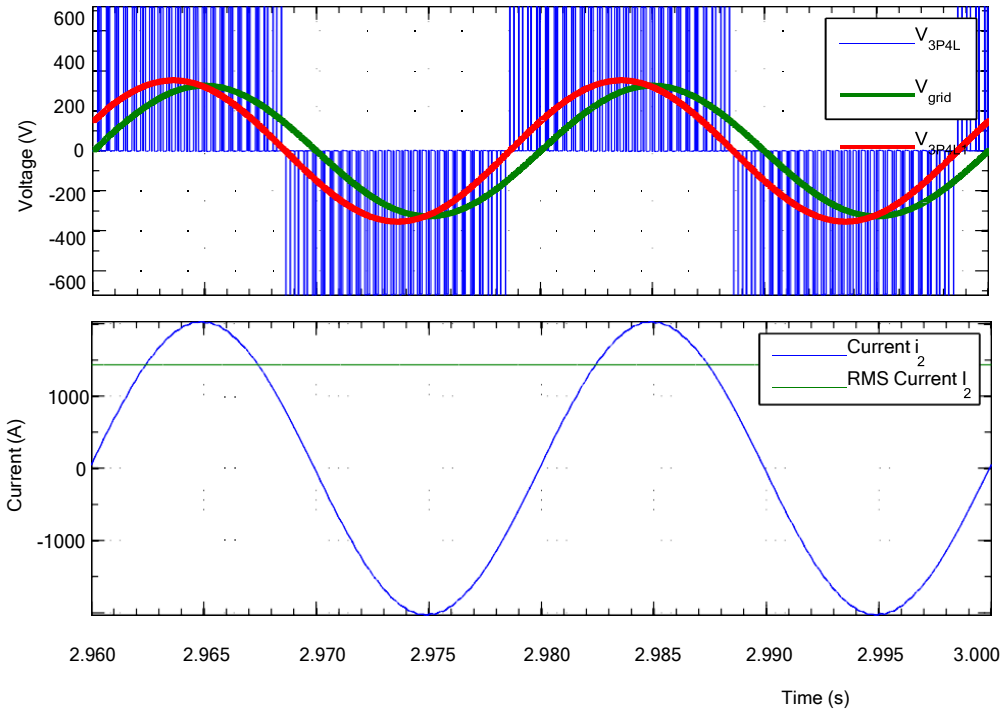

Figure 4. 6: The isolated voltage mode (V_{3P4L}) waveform, the grid-connected mode voltage (V_{grid}) waveform, the current waveform, and the RMS current waveform.

The Harmonic profile and the distortion of the waveforms is low in the isolated or stand-alone mode compared to the grid-connected mode as shown in Figure 4.7 (a) and Figure 4.7(b).

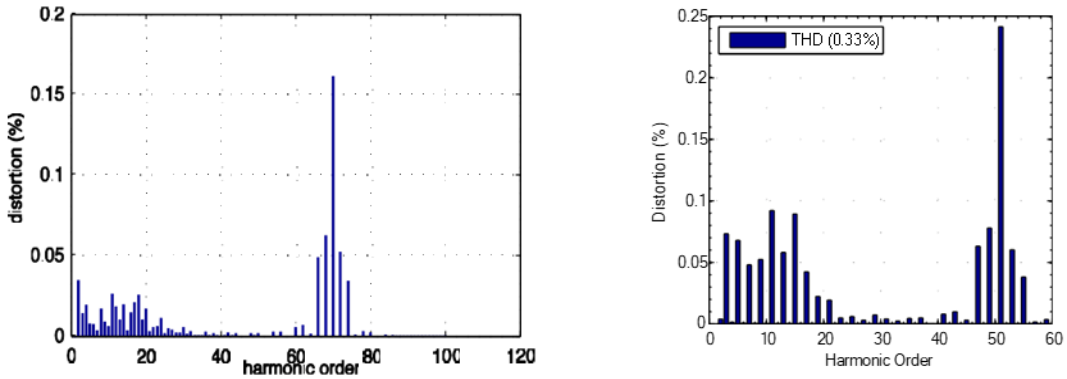

(a) (b)

Figure 4. 7: The harmonic profile of the 3P4L converter output waveforms in the isolated (a) and connected mode (b).

4.6. Results

The summarized results of the component values are shown in Table 4.2 for the SST parameters and ratings, Table 4.3 for the CHB retrieved parameters, Table 4.4 for the DAB retrieved parameters and Table 4.5 for 3P4L converters parameters, respectively.

Table 4.2: SST parameters and ratings.

Ratings specified	Denotation	Rated value
SST Power rating	$P_{(rated)}$	10^6 W
SST line-to-line Medium-Voltage	$V_{(MV)}$	10^4 V
SST line-to-line Low-Voltage	$V_{(LV)}$	400 V
Frequency of the grid	$F_{(grid)}$	50 Hz
Equivalent phase voltage	$V_{(ph)}$	230.94 V

Table 4.3: The retrieved CHB parameters.

Variable	Denotation	Resulted value
H-Bridges numbers	$N_{[m]}$	7.0000
Voltage of the DC link	$V_{(DAB1)}$	1261.5000 V
CHB Capacitor	$C_{(CHB)}$	953.0000 µF
CHB Frequency	$f_{(CHB)}$	1055.0000 Hz
CHB Inductance	$L_{(CHB)}$	10.5000 mH
Rated IGBT voltage required	$V_{(rated\text{-}IGBT)}$	1700.0000 V
DAB minimum voltage required	$V_{[DAB1(min)]}$	1227.8144V
DAB maximum voltage required	$V_{[DAB1(max)]}$	1295.2831V

Table 4.4: The retrieved DAB components values.

Parameter Name	Symbol	Value
The required Power in DAB	$P_{(DAB)}$	47.60 kW
Winding or turn ratio of the HF Transformer	$n_{(tr)}$	4:7
The DAB switching frequency	$F_{(DAB)}$	20 kHz
Leakage or Linking inductance	$L_{(DAB)}$	68.121 µH
First DC link capacitor filter	$C_{(DAB1)}$	74.8077 µF.
Second DC link capacitor filter	$C_{(DAB2)}$	229.64443 µF

Table 4.5: The retrieved components value of the 3P4L converter.

Parameter Name	Symbol	Value
Voltage of the DC link	$V_{(DAB2)}$	720.00 V
The Capacitor in the Second DC link	$C_{(3P4L)}$	61.40 mF
X-factor	x	1.50%
W-factor	w	96.00%
αβ frame resonance frequency	$f_{[res(\alpha\beta)]}$	875.00 Hz
γ frame resonance frequency	$F_{[res(\gamma)]}$	840.00 Hz
First Filter inductor	$L_{[f1(3p4L)]}$	73.9318μH
Second Filter inductor	$L_{[f2(3p4L)}]$	73.9318μH
Neutral Leg Inductor	$L_{[fn(3P4L)]}$	4.58 μH
Capacitor Filter	$C_{[(f3P4L)]}$	895μ F

4.7. SST design for smart energy

The overall SST design for smart energy application from the components in modular forms is shown in Figure 4.8.

4.8. Summary

The SST has been analyzed using power electronic equations applicable to the power electronic components like the IGBT, and these equations and models provides the basis for the evaluated component values for the filters, DC-link capacitors, CHB, DAB, and 3P4L converters. The converters are combined to for a single SST cell, the cells are joined in parallel or series to form the SST modules, and the modules are merged to form the required SST system according to the voltage and current level requirements.

The components and parameter values are verified, and the proposed model is designed accordingly. The results shows that LCL type filter is the most suitable, the modular design of the SST provides for three phases from three single phases, and that the SST model equations are suitable for optimizing and modelling of the individual component parameters, culminating in the SST design, complying with the IEEE standards for reducing the harmonics and distortions, and MATLAB simulation of the converters.

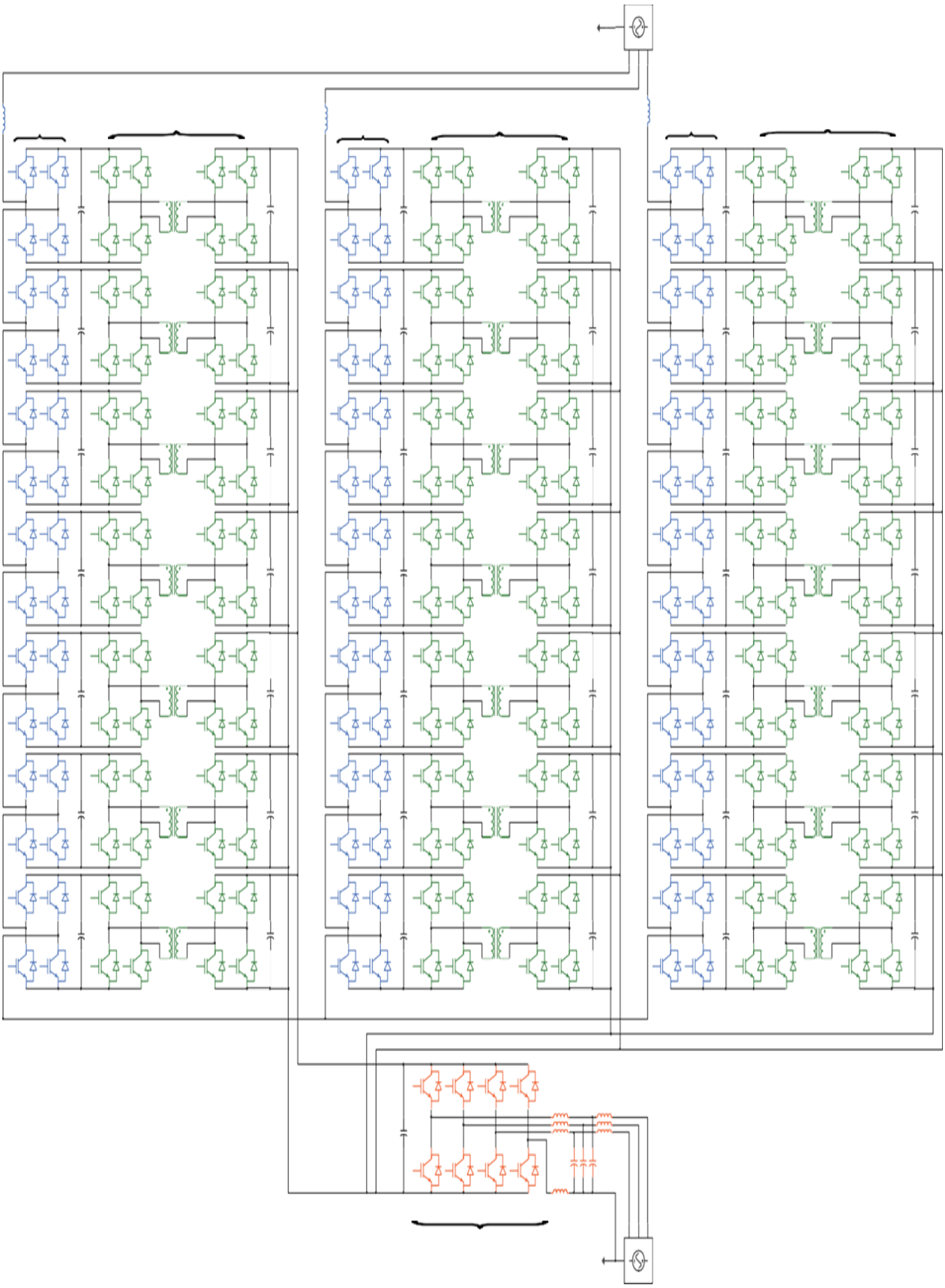

Figure 4.8: The SST design for smart energy.

CHAPTER 5

THE SST CONTROL MODEL DESIGN PARAMETERS FOR SMART ENERGY FROM THE MATHEMATICAL DIMENSIONS

5.1. Introduction

The SST is modelled as a rectifier circuit, high frequency converter circuit, and inverter circuit, with bi-directional power flow from sources to loads as shown in Figure 5.1. The SST is modular and can be combined to produce multi-phase sources with high voltage rating, high power capacity, and high current rating. Voltage control loop and current control loop is used to control the SST AC to DC, DC to DC (high frequency transfer of power from the high voltage DC power to low voltage DC power), and DC to AC modules respectively as shown in Figure 5.2.

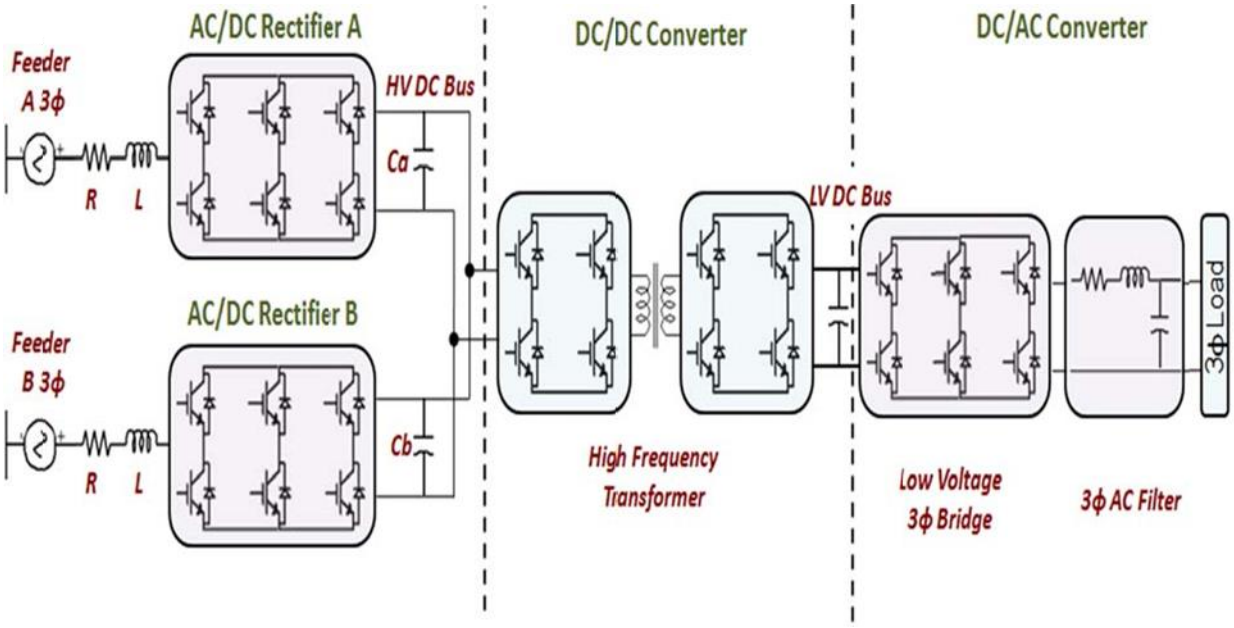

Figure 5.1: The block diagram of SST for smart energy depicting the three converter stages and the transmission lines (3-Phase).

The single phase or per phase analysis can be implemented to simplify the differential equation involved in control engineering modelling of not only the rectifier but the other two converters (DC to DC and DC to AC converters). The single-phase model for retrieving the control engineering for the SST is shown in Figure 5.2. The electrical energy sources from feeder A and feeder B, which is a single-phase source is feed into AC/DC rectifier A, and the output High Voltage DC (HVDC) is transferred through HVDC bus with smoothening capacitance (Ca and Cb). The smoothened HVDC is feed into the DC/DC high frequency converter with a high frequency transformer

sandwiched in between the two sides of the DC/DC converter stage, with Low Voltage DC (LVDC) output fed into the DC/AC converter through the LVDC bus with another smoothening capacitor. A single-phase LV hybrid bridge does the conversion, the RLC rectifier smoothens the three-phase output to the load. The bidirectional power flow through each of the converter stages provides control strategies that is analyzed and modelled to generate a control scheme for the SST.

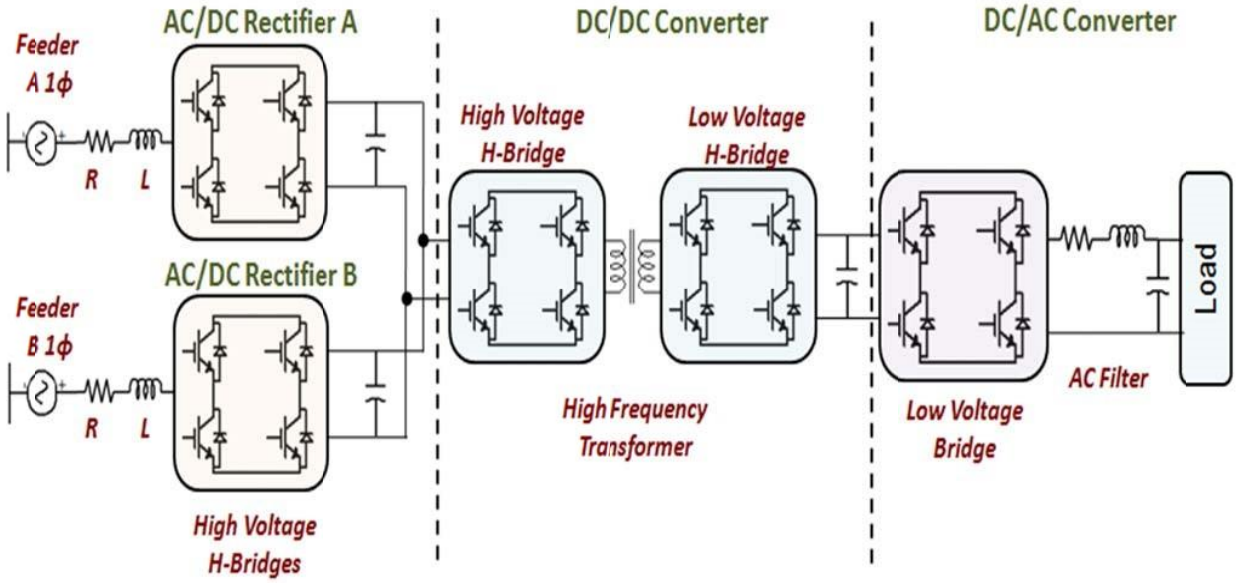

Figure 5.2: The per-phase analysis of the SST for modelling the control system.

5.2. The SST Rectifier Control

The rectifier constitutes the ability to allow bi-directional operation on the electrical power conversion process. This converter operates in the following modes:

5.2.1. The rectifier mode of operation: This entails the management of power drawing from the grid in such a way as to allow reactive and active power flow from the grid to the converter, however only the real power is utilized. This ensure that the power factor of the SST is unity and overall power quality from of the SST is optimized.

5.2.2. The regenerative mode: In this mode the rectifier block functions as a converter, ensuring that both active power and reactive power flow to the grid based on the control instructions implemented or control feedback from the SST requirements.

The controlling of the SST rectifier is modelled as follows:

$$d[i_{g1}(t)]/d(t) = [R_{g1}/L_{g1}][i_{g1}(t)] - [v_{1(n1)}(t)]/L_{g1} + [e_{g1}(t)]/L_{g1} - \omega_{s1}[\,J][i_{g1}(t)] \quad \text{----------(5.1)}$$

$$d[i_{g2}(t)]/d(t) = [R_{g2}/L_{g2}][i_{g2}(t)] - [v_{2(n2)}(t)]/L_{g2} + [e_{g2}(t)]/L_{g2} - \omega_{s2}[\,J][i_{g2}(t)] \quad \text{----------(5.2)}$$

$$dv_{hdc}(t)/dt = [i_{g1}(t)]^T[s_{g1}] / C_e + [i_{g2}(t)]^T[s_{g2}] / C_e - [2v_{hdc}(t)] / [3Z_eC_e] \text{ ----------(5.3)}$$

where; [J] is a vector 2X2 matrix consisting of $\begin{bmatrix} 0 & -1 \\ 1 & 0 \end{bmatrix}$, $v_{1(n1)}$ and $v_{2(n2)}$ are voltage switching function to control the rectifier's voltage and currents $i_{g1}(t)$ and $i_{g2}(t)$, $e_{g1}(t)$ and $e_{g2}(t)$ are the feeders voltages, R_{g1}, L_{g1} and R_{g2}, L_{g2} represents input Resistances and input Inductances, C_e is the equivalent Capacitance, ω_{s1} and ω_{s2} signal angular frequency for the control of the current input of the rectifier, v_{hdc} is the high voltage DC, and Z_e is the equivalent Load impedance. Hysteresis control strategy is used to control the fast current through the rectifier, and the Proportional Integral (PI) control is used to control the slow high DC voltage (v_{hdc}). This voltage is network dependent in the regenerative mode, and only the current is controlled in this mode. Based on the equation developed in (5.1) to (5.2) the control model is shown in d-q reference plane in Figure 5.3.

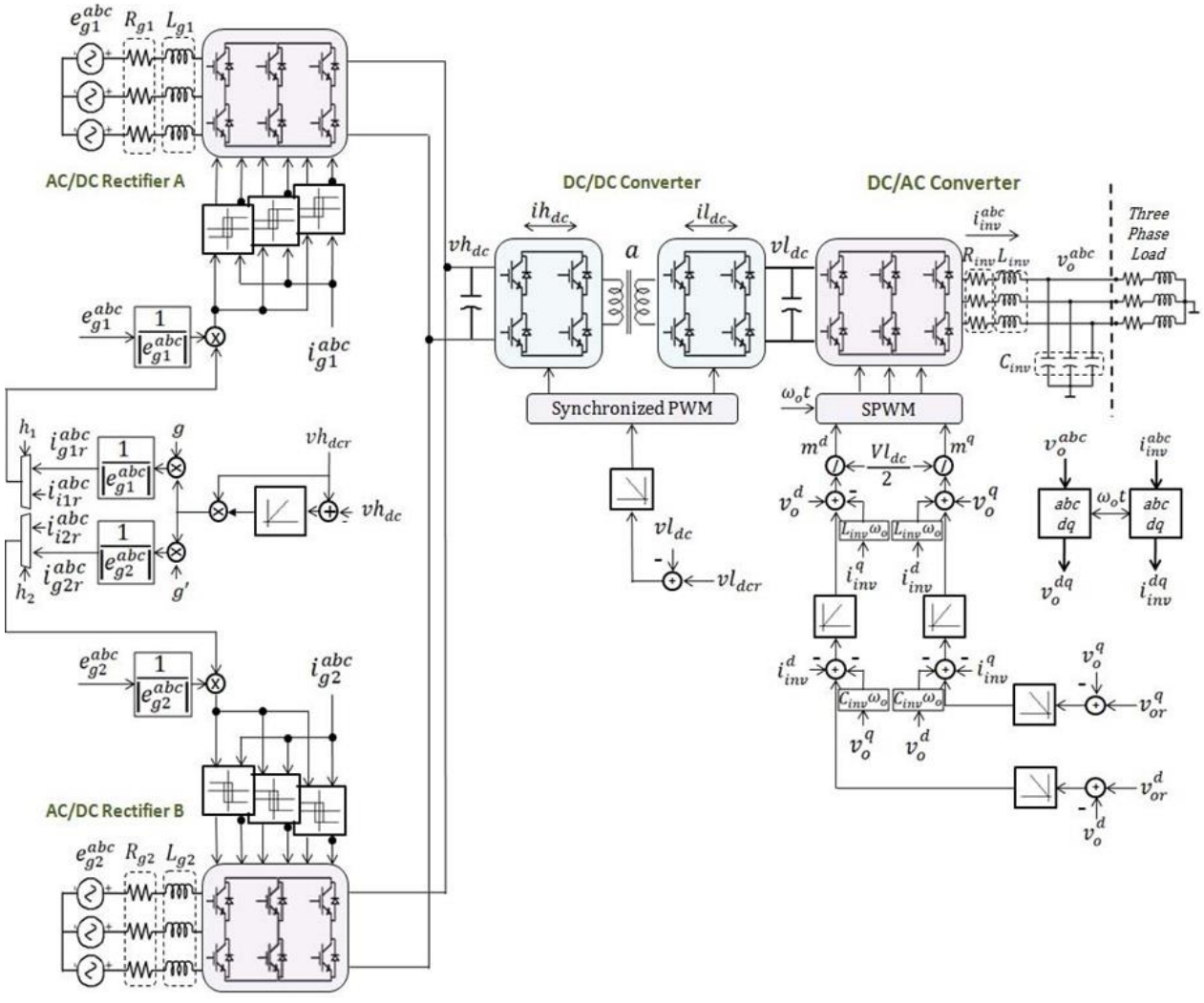

Figure 5.3: the control Block diagram of the SST rectifier, DC to DC converter, and DC to AC converter.

In Figure 5.3, e_{g1}^{abc} and e_{g2}^{abc} are the network feeder voltages, i_{g1}^{abc} and i_{g2}^{abc} are the corresponding feeder link currents, i_{g1r}^{abc} and i_{g2r}^{abc} are the reference network link currents, e_{g1r}^{abc} and e_{g2r}^{abc} are the network reference feeder voltages, g and g/ are power selector handle with values between 1 and 0, and the vh_{icr} is the reference high DC voltage.

5.3. The DC-to-DC converter implemented using Dual Active Converter (DAB) control

To analyze the control of the DC-to-DC converter, a simplified equivalent circuit of the DAB is considered in Figure 5.4 below:

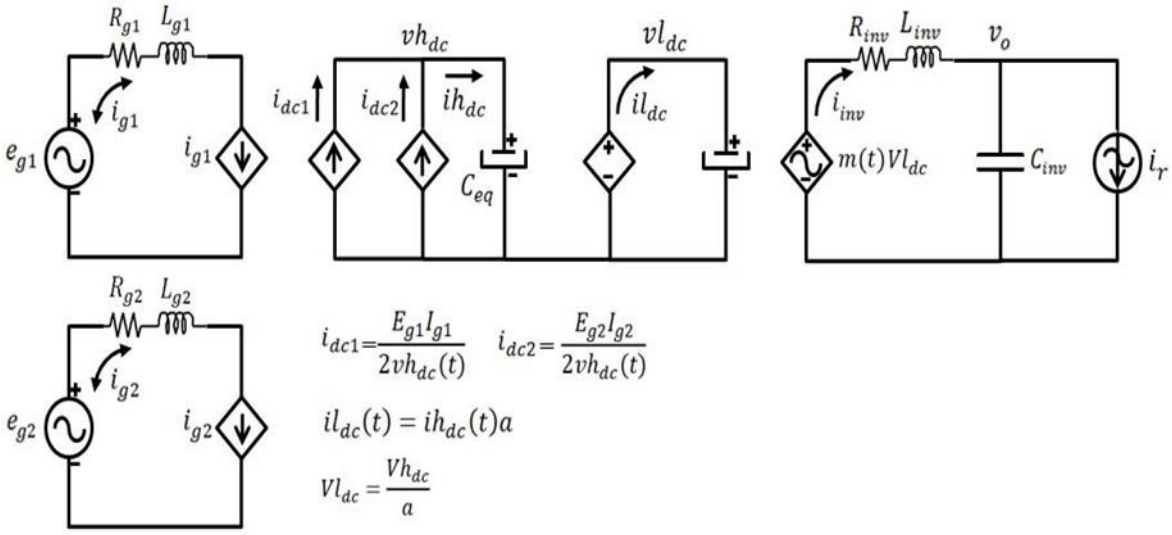

Figure 5.4: The control model of a DAB.

Assuming forward flow of current in the DAB, the current in the input (i_{dc1}, i_{dc2}, i_{hdc}), the voltages (vl_{dc} and vh_{dc}), and factor a (representing the ratio of input line currents il_{dc} and ih_{dc}) are related. Based on the circuit analysis of the equivalent circuits, their relationships are depicted in (5.4) to (5.9).

$I_{dc1} = [E_{g1} \times I_{g1}] \,/\, [2 \times vh_{dc}(t)]$ ----------(5.4)

$I_{dc2} = [E_{g2} \times I_{g2}] \,/\, [2 \times vh_{dc}(t)]$ ----------(5.5)

Thus, (5.4) / (5.5) gives the ratio of i_{dc1} to i_{dc2} as follows:

$[i_{dc1} \,/\, i_{dc2}] = [E_{g1} \times I_{g1}] \,/\, [E_{g2} \times I_{g2}]$ ----------(5.6)

$vl_{dc} = [vh_{dc} \,/\, a]$ ----------(5.7)

$il_{dc}(t) = [ih_{dc}(t) \times a]$ ----------(5.8)

$ih_{dc} = I_{dc1} + I_{dc2}$ ----------(5.9)

Where factor a represents steady state gain, ih_{dc} is the high DC current from the combination of the two input currents, vl_{dc} is the output DC voltage, and il_{dc} is the output voltage.

5.4. The DC-to-AC converter using 3P4L converter

The control for this SST output stage block is to ensure constant output voltage irrespective of the load inherent changes and input voltage variations. To achieve this set objective, two loops are produced in the DC-to-AC control block of Figure 5.3. the two loops consist of an outer loop and an inner loop. The outer loop is designed to function as a voltage controller, and the inner loop is designed as a current controller, that is capable of tracking current reference in few milliseconds and ensure voltage stability in the d-q reference. The differential equations depicting these scenarios are a s follows:

$di_{(inv)}(t)/d(t)=[-(R_{(inv)}/L_{(inv)})(i_{(inv)}(t))]+[(vl_{dc}/2L_{(inv)})(m(t))]-[v_0(t)/L_{(inv)}]-[\omega_o \times [J] \times i_{(inv)}(t)]$-(5.10)

$[C_{(inv)} \times (dv_0(t) / d(t))] = [(i_{(inv)}(t)] - [\omega_o \times [J] \times v_0(t)] - [i_r(t)]$ ----------(5.11)

$[C_e \times dvh_{dc}(t) / d(t)] = [i_{dc1}(t)] + [i_{dc2}(t)] - [i_{load}(t)]$ ----------(5.11)

$[C_e \times dvh_{dc}(t) / d(t)] = [E_{g1} \times I_{g1}] / [2vh_{dc}(t)] + [E_{g2} \times I_{g2}] / [2vh_{dc}(t)] - [i_{load}(t)]$ -------(5.12)

Where $C_{(inv)}$, $L_{(inv)}$, and $R_{(inv)}$ are the Capacitance, Inductance, and Resistance output parameters of the filter, ω_o is the angular frequency in radians of the voltage and current outputs respectively, $i_{(inv)}(t)$ is the filter inverter input current, $v_o(t)$ is the output 3P4L converter voltage, $i_r(t)$ represents current flow to the load (managed by the control scheme as a disturbance), m(t) represents the modulation index (as known as the input controller), and v_{or} is the desired output voltage reference.

5.5. Simulation of the control scheme

The control of the converter's performance is done using Source-A and Source-B, each delivering apparent power at 19kVA. The simulation shows that the outputs (current and voltage), and the inputs (current and voltage) were maintained at a constant value based on their reference values. The control scheme is shown in Figure 5.5.

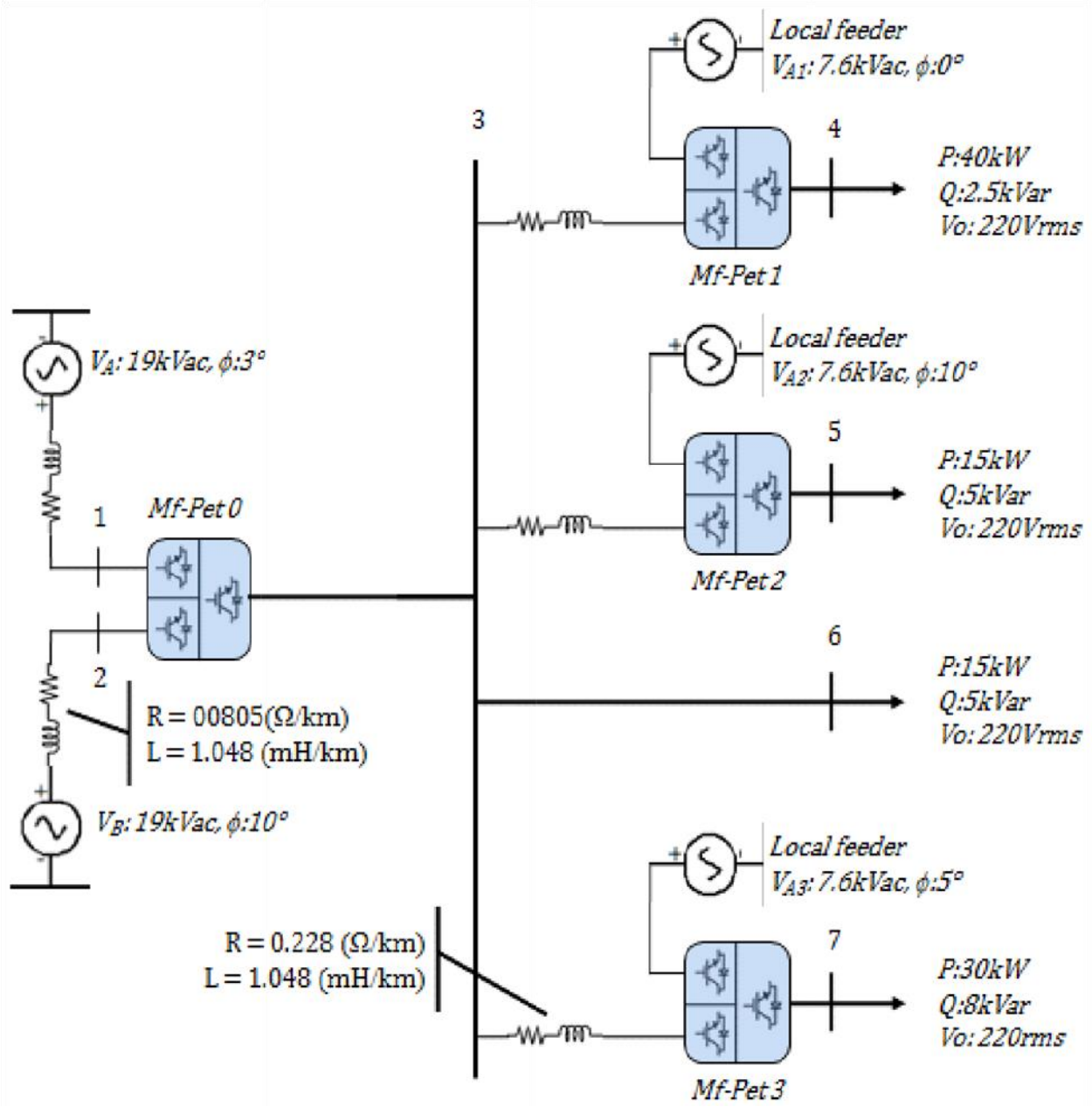

Figure 5.5: The control scheme of the grid connected SST in the smart energy system.

In Figure 5.5. The SSTs are labelled Mf-Pet0, Mf-Pet1, Mf-Pet2, Mf-Pet3. The $\boldsymbol{\pi}$-transmission line parameters are R = 0.22Ω/km and L = 1.047mH/km for the interconnected SSTs, and R = 0,0805 Ω/km and L is kept at the same value for feeder A and feeder B connection to Mf-Pet0, which is connected to other SSTs at 7.6kV in the smart energy distribution system. the voltage supplied to the load is maintained at a constant $220V_{ph(rms)}$, and different load draws different load current from the SST, provided the load power requirement is lower than the power supplied by the SST. The SST ensures that the phase angle of the voltage and current is close

to zero at unity power factor. At a step of 0.6 seconds, the Source-A supplies 75% of the required power, and Source-B supplies the remainder 25% of the load power requirement, and feeders A1, A2, and A3 are not injecting their power to the smart energy system. To equally share supply of power from all sources, a new reference is set at a step of 0.9 seconds. This ensures that the load receives 50% of power from both feeder A and feeder B sources, and another 50% from Feeder A1, A2, and A3 combined sources. This is the distributed generation of the energy pool from all sources, namely energy source A, B, A1. A2, and A3, parallel connected to each other through the SSTs at the same voltages in the distribution grid but different phase angles.

The SSTs ensure that the 7.6kV at unity pf is maintained in the distribution grid, and different load requirements peculiar to each load is met as depicted in Figure 5.6, which shows operation during transient change of reference voltage and current $(\mathrm{VoT1\ and\ IoT1})$, operation during transient change of load voltage and current $(\mathrm{VLB6\ and\ ILB6})$, operation during nonlinear loads $(\mathrm{PoT0\ and\ QoT0})$ which reveals that the active power balances and correspond to the reactive power, and operation during linear load $(\mathrm{PLB6\ and\ QLB6})$.

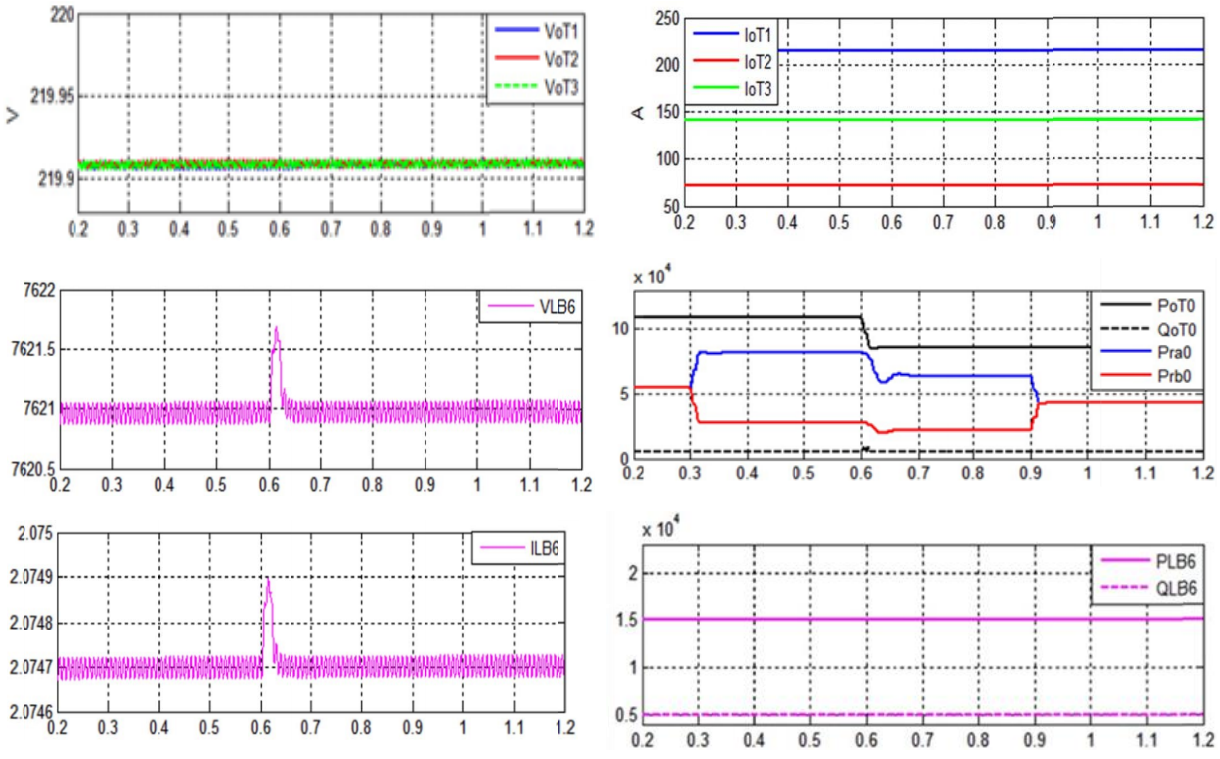

Figure 5.6: The constant voltage, current, and output power (reactive and real power) outputs of the controlled SSTs connected to the loads.

5.6. Summary

To optimally control the SST, the SST was considered as a model consisting of three converter blocks. Each block is modeled as a differential equation and transformed into a control loop. This made the SST to be modular and easy to integrate for performing more functions like a source of high, medium, or low voltage, current, and power respectively, according to the need of the smart energy system. The voltage and current differential equations yield the voltage control loop and the current control loop.

The hysteresis control loop uses the current control scheme to control fast current through the rectifier or the Cascade Hybrid Bridge in the regenerative mode, where network voltage is independent of voltage control. The Proportional Integral (PI) control is implemented using the voltage control pedagogy to seamlessly control the slow DC voltage power flow in the CHB operating in the rectifier mode.

The equivalent circuit is modeled and simulated to verify the load requirements of the constant supply of electrical current, voltage, and power are met. The research results show that using 0.6 seconds step, only feeder A and feeder B are supplying power to the load. The research result, indeed, confirmed that the output current and voltage is constant based on the power absorbed by the load and show the ability of the SST to function as an intelligent power electronic transformer, capable of integrating various energy sources and storage with the load and the grid. Hence, the aim and objective of designing and modeling a SST for smart energy, that can combine various and diverse energy sources and storage together with the grid(s) and the load(s) for smart energy, has been achieved.

CHAPTER 6

CONCLUSION AND RECOMMENDATIONS

6.1 Introduction

The SST consist of HFT, converters (the DAB, CHB, and 3P4L Converters), and DC link capacitors. It allows bi-directional power flow and various control topologies. These SST attributes makes it modular, modern, and an intelligent power system machine. This SST modules can be combined to achieve a higher voltage, current and power ratings respectively. The SST plays a central role in the integration of various electrical energy sources to form a hybrid microgrid system, that guarantees a higher reliability, performance, and economic prospects for both the producers and consumers of energy.

The size of the SST is small, and the energy density is high, when compared to LFT. However, the LFT is cheaper than the SST, currently. As the technology improves, the cost of SST will be similar or cheaper than the LFT. The efficiency of the SST is slightly lower than the LFT, due to power electronic high switching frequencies and voltage drops which is 0.3V for Germanium (Ge) and 0.65V for Silicon (Si).

The SST is a complex power electronic converter system that mitigates problems like the voltage sag, current surge, power quality issues, power factor correction, waveform distortion, and can be classified based on power stages, voltage levels, control of the isolation stages, modularity, and number of ports per power stage. The SST can operate in the stand-alone mode or grid connected mode. The control and coordination of the converters, and other SST components is achieved using phase-controlled power flow, centralized and decentralized predictive power control and other advanced peripheral Integral (PI) schemes. Matrix converters can be implemented to achieve higher efficiency and control of the SST.

This chapter draws conclusion from the work done in this research by giving the overall deliverables from all the chapters in the dissertation. Section 6.1 presents chapter 6 introduction, section 6.2 presents the dissertation aims and objectives, section 6.3 gives the summarized deliverables of all the dissertation chapters, section 6.4 reveals the future work or research that needs to be done, and section 6.5 gives the author’s publications.

6.2 Aim and Objectives of the Dissertation

The aim of the research is the design and modelling of a SST that can integrate diverse energy sources and loads for smart energy applications. The research objectives achieved included an overview and brainstorming of the SST in chapter one, a scholarly literature review of SSTs in chapter two, formulating the advanced mathematics depicting advanced power electronics applicable to SSTs in chapter three, applying the power electronic equations developed to evaluate the component values for the SST model and design in chapter four, designing a control system model for the SST in chapter five, and chapter 6 presents the conclusion drawn from the research results.

6.3 Dissertation deliverables

This section provides a summary of the research work done to achieve the aim and objectives of this research study.

6.3.1 Chapter Two: The Literature Review

The literature review of scholarly articles revealed that the SST functions as an energy router by connecting variable AC and DC sources together and managing their energy or power contents, for eventual supply of constant power to the grid and consumers at unity power factor. This mitigates the issue of sensitivity associated with variable energy sources like wind energy and solar energy. The SST ensures reliability by allowing battery (storage) integration in the energy mix. These provisions are possible because the SST has LVDC, MVDC, LVAC, and MVDC ports. The SST can be combined to achieve HVDC and HVAC. This central role played by SST results in 1.4% reduction in losses, and its application in the transport sector which accounts for 40% Green House Gases (GHGs) emissions in Europe, ensures the use of machines like tracking systems and locomotives, resulting in 75% reduction in weight and 40% decrease in size with a phase of up to 7.6kV/220V_{rms} and 13.8kV/400V_{Line}, the losses are halved, and one third of weight and volume reduction for SSTs is achieved when compared with transformers in DC/AC applications. The combination of the SST was done using both the isolating and non-isolating SST block to produce more connection interfaces or points. This results in DPSS AC/DC-AC SST or SPDS AC-DC/AC SST or MIMO SST topology. The design and modeling of the SST is optimized by deriving and using applicable power electronics formulae and equations. These equations and various formulae yield the mathematical model of the SST. This mathematical model is used to calculate and retrieve the SST parameters and components values of the IGBT, DC- link Capacitors, Transformer Turn Ratio, Switching Frequency, Number of Hybrid Bridges, losses at the rated frequency, and inductances (self, mutual, and leakage inductances, respectively). The

components of the SST analyzed include the CHB converter that converts AC to DC and links this DC via a DC link capacitor to the DAB. In addition, DAB and 3P4L converters are also analyzed.

6.3.2 Chapter Three: The mathematical dimensions of the SST model for smart energy

In chapter three, the design and modelling of the SST is optimized by deriving and using applicable power electronics formulae and equations. These equations and various formulae yield the mathematical model of the SST. This mathematical model is used to calculate and retrieve the SST parameters and components values of the IGBT, DC- link Capacitors, Transformer Turn Ratio, Switching Frequency, Number of Hybrid Bridges, losses at the rated frequency, and inductances (self, mutual, and leakage inductances, respectively). The components of the SST analyzed include the CHB converter that converts AC to DC and links this DC via a DC link capacitor to the DAB. The DAB is another converter that uses a high frequency transformer situated in between the DC/AC and transforms DC/AC to AC/DC, while ensuring galvanic isolation in the SST high voltage side and low voltage side, and it links to the 3P4L converter through a DC link capacitor. The CHB H-bridge numbers is equal to the DAB modules, where individual DAB module is directly connected to one CHB H-bridge, and the DAB outputs are connected to DC bus in the SST. The 3P4L converter is the component of the SST that receives DAB DC electricity and transform it int AC. It is connected in stand-alone mode (Load), or grid connected mode, and it consist of 4 half bridges (each for phase mode and another for neutral mode). To model these three converters, DC link, grid filter values, switching frequency, and filter capacitors and inductors parameters, respectively, are needed. To assist in retrieving the converters filter parameters, the algorithms are written in simple but engineering and mathematical problem-solving centered methodology, for easy implementation in the various programing languages like $c++$, MATLAB, python etc.

6.3.3 Chapter Four: The SST model design parameters for smart energy from the mathematical dimensions

The research results from chapter four shows that the model equation is very important in optimizing the individual component parameters, $\mathrm{MATLAB\ simulation}$ of the converters, reducing the harmonics and distortions, and in the overall compliance to the $\mathrm{IEEE\ standards}$. The SST parameters and components values required and calculated include SST Power rating $(\mathrm{P(rated)} = 1\ \mathrm{MW})$, SST line-to-line Medium-Voltage $(\mathrm{V_{(MV)}} = 10\ \mathrm{kV})$, SST line-to-line Low-Voltage $(\mathrm{V_{(LV)}} = 400\ \mathrm{V})$, Frequency of the grid $(\mathrm{F_{(grid)}} = 50\ \mathrm{Hz})$, and Equivalent phase voltage $(\mathrm{V_{(ph)}} = 230.94\ \mathrm{V})$.

The CHB converter components values retrieved are H-Bridges numbers ($N_{[m]} = 7$), Voltage of the DC link ($V_{(DAB1)} = 1261.5000V$), CHB Capacitor ($C_{(CHB)} = 953.0000\mu F$), CHB Frequency ($f_{(CHB)} = 1055Hz$), CHB Inductance ($L_{(CHB)} = 10.5mH$), Rated IGBT voltage ($V_{(rated\text{-}IGBT)} = 1700V$), DAB minimum voltage ($V_{[DAB1(min)]} = 1227.8144V$), and DAB maximum voltage ($V_{[DAB1(max)]} = 1295.2831V$).

The DAB converter components are parameters retrieved include the Power in DAB ($P_{(DAB)} = 47.60\ kW$), Winding or turn ratio of the HF Transformer ($n(tr) = 4{:}7$), The DAB switching frequency ($F_{(DAB)} = 20kHz$), Leakage or Linking inductance ($L_{(DAB)} = 68.121\mu H$), First DC link capacitor filter ($C_{(DAB1)} = 74.807\mu F$), Second DC link capacitor filter ($C_{(DAB2)} = 229.6444\mu F$). The voltage waveform in the DAB converter is a pure square waveform, and the current is a partial triangular and square waveform.

The 3P4L converter components and parameters retrieved are Voltage of the DC link ($V_{(DAB2)} = 720.00V$), The Capacitor in the Second DC link ($C_{(3P4L)} = 61.40\ mF$), x-factor (1.5%), w-factor (96%), αβ frame resonance frequency ($f_{[res(\alpha\beta)]} = 875Hz$), γ frame resonance frequency ($F_{[res(\gamma)]} = 840Hz$), First Filter inductor ($L_{[f1(3p4L)]} = 73.9318\mu H$), , Second Filter inductor $L_{[f2(3p4L)]} = 73.9318\mu H$), Neutral Leg Inductor ($L_{[fn(3P4L)]} = 4.58\mu H$), Capacitor Filter ($C_{[(f3P4L)]} = 895\mu\ F$). The voltage and current waveforms are pure sinusoidal waveforms with an average percentage distortion of 0.15 at a harmonic order of 300. Based on these results, the Filter implemented in reducing the distortion in grid connected mode is the LCL type filter in the 3P4L converter.

6.3.4 Chapter Five: The SST control model design parameters for smart energy from the mathematical dimensions

Chapter five reveals that the SST is optimally controlled as a model that has three converters (CHB, DAB, and 3P4L converters) differential equations, transformed into a control loop. This approach makes the SST modular, with both voltage and current control loop. While the hysteresis loop uses the control loop scheme to control fast current changes through the CHB rectifier mode, the voltage control is achieved through the regenerative mode. The Proportional Integral (PI) control is used to control voltage in CHB rectifier mode.

The power selector handles (g and g/), the reference voltage and the reference current are used to set the desired reference point in the SST converters. This is implemented by deriving the required differential equation linking the parameters, variable and constants in a relationship that is transformed into a comprehensive control system. The equivalent circuit is modelled to simulate and verify the load requirements of constant supply of electrical current, voltage, and power. The

simulation confirmed that the output current and voltage is constant based on the power absorbed by the load. The SST model and design is shown at the appendices A to B.

The equivalent circuit is modelled and simulated to verify the load requirements of constant supply of electrical current, voltage, and power are met. At 0.6 seconds step only the feeder A and feeder B are supplying power to the load. Feeder A contributes 75%, and feeder B contributes 25% of the load power requirement, while isolating independent feeder $A1$, $A2$, and $A3$, respectively, in the smart energy system. $At\ 0.9$ seconds step, 75% load power requirement is met by the feeder A and B, while the previously isolated feeder $A1$, $A2$, and $A3$ supplies the remaining 25%. The simulation confirmed that the output current and voltage is constant based on the power absorbed by the load and shows the benefits of designing and modelling SST for a smart energy integration.

6.4 Future Works

The real-time interaction and communication using information and communication technology between the SSTs need more research to fully make the SST an intelligent Power electronics converter. The integration of artificial intelligence in the SST should be explored.

More scholarly articles and literature for the SST applications in distribution systems that supports four wire options are needed.

Due to power electronic components extensive use in the SSTs, failures, protection, reliability, efficiency, and lifespan cost analysis of SSTs are areas that needs more research.

6.5 AUTHORS PUBLICATIONS

1. Asiegbu A, Almaktoof A. The Design and Modelling of a Solid-State Transformer for Smart Energy. Cape Peninsula University of Technology Post Graduate Conference 2023, South African Renewable Energy Technology Centre (SARETEC), Belville, City of Cape Town· Mar 1, 2023 (Presented and Published).

2. Asiegbu A, Almaktoof A. A Review of Solid-State Transformer for Smart Energy. Wattnow June 2023 issue, South African Institute of Electrical Engineers [City of Johannesburg] · May 23, 2023 (Published).

3. Asiegbu A, Almaktoof A, Abougarair W. The Hybrid Analysis of Solar Energy, Energy Storage and Waste-To-Energy (WTE) for Cost-Effective Power Generation in Muldersdrift. International Conference – Electrical Engineering and Information Technology (ICEEIT) [Benghazi, Libya]. May 11, 2023 (Submitted).

4. Asiegbu A, Almaktoof A, Aboalez K. Energy Savings from Energy Audit of a Residential Building in the Forest Hill City of Johannesburg. 10th International Conference on Advanced Technologies Proceedings [Turkey] · Nov 28, 2022 (Published).

5. Asiegbu A, Almaktoof A, Adonis M. An Energy Access Assessment Report Focusing on Resource and Cost Assessment for Rwanda. Africa and International Use of Energy (AIUE) Proceedings of the 3rd Industrial and Commercial Use of Energy Conference 2022 [City of Cape Town] · Nov 29, 2022 (Published).

6. Asiegbu A, Almaktoof A, Adonis M. Analysis of a Hybrid Renewable Energy Microgrid for Ruzizi Rural Community in Rwanda Using HOMER Pro. South African Association of Wind Energy (WindAc 2022) International Conference [City of Cape Town] · Oct 23, 2022. (Accepted).

7. Asiegbu A, Almaktoof A, Aboalez K. Energy Efficiency Policy and Standards. Africa and International Use of Energy (AIUE) Proceedings of the 2nd Energy and Human Habitat Conference 2021 [City of Cape Town] · Jul 26, 2021. (Published).

8. Asiegbu A. Comparison of Biodiesel and Green Ammonia. Wattnow June 2022 issue, South African Institute of Electrical Engineers [City of Johannesburg] · Jun 13, 2022 (Published).

9. Asiegbu A, Almaktoof A, Adonis M. The Design and Analysis of an Advanced Hybrid Renewable Energy Microgrid for Cyangugu Remote Rural Community in Rwanda using Homer Pro. Innovation and Technological Advances for Sustainability (ITAS 2023) [Doha, Qatar] (Published).

10. Asiegbu A, Almaktoof A, Adonis M, Atanda R. An Innovative and Cost-Effective Power Generation Solution Using Waste-To-Energy (WTE) For Muldersdrift. Enlit Africa (17th May) 2023 [City of Cape Town], (Accepted (Speaker), Presented, and Published).

11. Asiegbu A, Almaktoof A, Tariq K. The Green Hydrogen as a Renewable Energy Source and Storage in the Transportation Sector of Germany. Southern Africa Universities Power Engineering Conference (SAUPEC) 2023 [University of Johannesburg, City of Johannesburg] (Presented and published in IEEE explore).

12. Asiegbu A, Almaktoof A, Khalat A. Energy Access Assessment Report Focusing on Energy Poverty and Energy Demand for Rwanda. 2023 IEEE 3rd International Maghreb Meeting of the Conference on Sciences and Techniques of Automatic control and Computer Engineering. MI-STA 2023 May 21 – 23, 2023 – BENGHAZI – LIBYA. (Presented and published)

13. Asiegbu A, Atanda R. Benefits Assessment and Sustainability Assessment Summarized Implementation of the Sustainable Energy Access Planning (SEAP) Framework. Wattnow February 2023 issue, Magazine publication of the South Africa Institute of Electrical Engineers. (Published)

14. Afeef B, Asiegbu A, Almaktoof A. Design and Implementation of LoRa based IoT Smart Irrigation System. 2023 IEEE 3rd International Maghreb Meeting of the Conference on Sciences and Techniques of Automatic control and Computer Engineering. MI-STA 2023 May 21 – 23, 2023 – BENGHAZI – LIBYA. (Submitted for Publication).

REFERENCES

A. Hirsch and J. Guerrero, Y.P. (2018) *Microgrids: A review of technologies, key drivers, and outstanding issues," Renew. Sustain. Energy Rev., vol. 90, no. April, pp. 402–411*, *Renewable and Sustainable Energy Reviews*.

Abu-Siada, A., Budiri, J. and Abdou, A.F. (2018) 'Solid state transformers topologies, controllers, and applications: State-of-the-art literature review', *Electronics (Switzerland)*. Available at: https://doi.org/10.3390/electronics7110298.

Agrawal, A., Nalamati, C.S. and Gupta, R. (2019) 'Hybrid DC-AC Zonal Microgrid Enabled by Solid-State Transformer and Centralized ESD Integration', *IEEE Transactions on Industrial Electronics*, 66(11). Available at: https://doi.org/10.1109/TIE.2019.2899559.

Ahmed, K.Y. *et al.* (2018) 'Development of power electronic distribution transformer based on adaptive PI controller', *Institute of Electrical Electronics Engineers Access*, 6. Available at: https://doi.org/10.1109/ACCESS.2018.2861420.

al Hadi, A. and Challoo, R. (2020) 'Voltage and current loop controlled three-stage three-port solid state transformer', in *ASEE Annual Conference and Exposition, Conference Proceedings*. Available at: https://doi.org/10.18260/1-2--35491.

Atkar, D. D. *et al.* (2022) 'Optimal Design of Solid State Transformer-Based Interlink Converter for Hybrid AC/DC Micro-Grid Applications', *IEEE Journal of Emerging and Selected Topics in Power Electronics*, 10(4). doi: 10.1109/JESTPE.2021.3099625.

Awili, S. and O'Donnell, T. (2016) 'Integrating smart solid state transformers into distribution substations', in *CIGRE Session 46*.

Azab, M. (2020) 'Multi-objective design approach of passive filters for single-phase distributed energy grid integration systems using particle swarm optimization', *Energy Reports*, 6. doi: 10.1016/j.egyr.2019.12.015.

Baek, S. and Bhattacharya, S. (2019) 'Isolation Transformer for 3-Port 3-Phase Dual-Active Bridge Converters in Medium Voltage Level', *Institute of Electrical Electronics Engineers Access*, 7. Available at: https://doi.org/10.1109/ACCESS.2019.2895818.

Banaei M., Salary E. (2014). Mitigation of voltage sag, swell and power factor correction using solid-state transformer-based matrix converter in output stage, *Alexandria Engineering Journal*, Volume 53, Issue 3, Pages 563-572, ISSN 1110-0168. https://doi.org/10.1016/j.aej.2014.06.003.

Besselmann, T., Mester, A., Dujic, D. (2013). Power electronic traction transformer: Efficiency improvements under light-load conditions. *IEEE T Power Electronics., P29, 3971– 3981.*

Besselmann, T., Mester, A. and Dujic, D. (2014) 'Power electronic traction transformer: Efficiency improvements under light-load conditions', *IEEE Transactions on Power Electronics, 29(8).* Available at: https://doi.org/10.1109/TPEL.2013.2293402.

Bifaretti, S. *et al.* (2011) 'Advanced power electronic conversion and control system for universal and flexible power management', *IEEE Transactions on Smart Grid*, 2(2). Available at: https://doi.org/10.1109/TSG.2011.2115260.

Carrasco, J.M. *et al.* (2006) 'Power-electronic systems for the grid integration of renewable energy sources: A survey', *IEEE Transactions on Industrial Electronics*. Available at: https://doi.org/10.1109/TIE.2006.878356.

Chen H., Prasai A., Divan D., (2017). Dyna-C: A minimal topology for bidirectional solid-state transformers. *IEEE T Power Electronics* 32: 995–1005.

Costa, L.F., Buticchi, G. and Liserre, M. (2017) 'Quad-active-bridge dc-dc converter as cross-link for medium-voltage modular inverters', *IEEE Transactions on Industry Applications*, 53(2). Available at: https://doi.org/10.1109/TIA.2016.2633539.

Das, D., Hrishikesan, V.M. and Kumar, C. (2019) 'Smart Transformer-based Hybrid LVAC and LVDC Interconnected Microgrid', in *2018 IEEE 4th Southern Power Electronics Conference, SPEC 2018*. Available at: https://doi.org/10.1109/SPEC.2018.8635923.

de Carne, G. *et al.* (2018) 'Load Control Using Sensitivity Identification by Means of Smart Transformer', *Institute of Electrical Electronics Engineers Transactions on Smart Grid*, 9(4). Available at: https://doi.org/10.1109/TSG.2016.2614846.

De Oliveira Filho, H. M., De Souza Oliveira, D. and Praca, P. P. (2013) 'Soft-switching bidirectional isolated three-phase DC-DC converter with dual phase-shift and variable duty cycle', in *2013 Brazilian Power Electronics Conference, COBEP 2013 - Proceedings*. doi: 10.1109/COBEP.2013.6785105.

Devineni, G. K. *et al.* (2022) 'THD Optimization with Low Switching Frequency Control for 15-Level Reduced Switch Asymmetric Multilevel Inverter', in *Lecture Notes in Electrical Engineering*. doi: 10.1007/978-981-16-4943-1_9.

Ellabban, O. (2019) 'A Solid-State Transformer as Enabling Technology for Microgrids for Integration into the Power Distribution System: An Overview', in. Available at: https://doi.org/10.5339/qfarc.2016.eepp1689.

el Shafei, A. *et al.* (2020) 'Design and Implementation of a Medium Voltage, High Power, High Frequency Four-Port Transformer', in *Conference Proceedings - Institute of Electrical Electronics Engineers Applied Power Electronics Conference and Exposition - APEC*. Available at: https://doi.org/10.1109/APEC39645.2020.9124337.

Farnesi, S. *et al.* (2019) 'Solid-state transformers in locomotives fed through AC lines: A review and future developments', *Energies*. Available at: https://doi.org/10.3390/en12244711.

Fernández-Guillamón, A. *et al.* (2019) 'Power systems with high renewable energy sources: A review of inertia and frequency control strategies over time', *Renewable and Sustainable Energy Reviews*. Available at: https://doi.org/10.1016/j.rser.2019.109369.

Gajowik, T., Rafał, K. and Malinowski, M. (2017) 'Review of multilevel converters for application in solid state transformers', *Przeglad Elektrotechniczny*. Available at: https://doi.org/10.15199/48.2017.04.01.

Gao, T. *et al.* (2020) 'A novel active damping control based on grid-side current feedback for LCL-filter active power filter', *Energy Reports*, 6. doi: 10.1016/j.egyr.2020.11.027.

Gheisarnejad, M., Farsizadeh, H. and Khooban, M.H. (2021) 'A Novel Nonlinear Deep Reinforcement Learning Controller for DC-DC Power Buck Converters', *IEEE Transactions on Industrial Electronics*, 68(8). Available at: https://doi.org/10.1109/TIE.2020.3005071.

González-Molina F., Martin-Arnedo J., Alepuz S., et al. (2015). EMTP model of a bidirectional multilevel solid-state transformer for distribution system studies. Power & Energy Society General Meeting. *IEEE Power electronics*, 1–5.

Grider, D., Agarwal, A., Ryu, S.-H., Cheng, L., Capell, C., Jonas, C., Burk, A., O'Loughlin, M., Das, M., Palmour, J. (2012). Advanced SiC Power Technology for High Megawatt Power Conditioning; Technical Report; Cree, Inc.: Durham, NC.

Guillod, T., Krismer, F., Färber, R., Franck, M., Kolar, J. (2015). Protection of MV/LV solid state transformers in the distribution grid. In Proceedings of the IECON 2015-41st Annual Conference of *the IEEE Industrial Electronics Society*, Yokohama, Japan, 9–12 November 2015; IEEE: Hoboken, NJ, USA, 2015; pp. 3531–3538.

Gupta E., Sinha S., Vates U., Chavan S. (2021). A high-performance solid-state transformer for an efficient electric grid application. Page 1. ISSN 2214-7853. Available at: https://doi.org/10.1016/j.matpr.2021.02.469.

Guillod, T. *et al.* (2015) 'Protection of MV/LV solid-state transformers in the distribution grid', in *IECON 2015 - 41st Annual Conference of the IEEE Industrial Electronics Society*. Available at: https://doi.org/10.1109/IECON.2015.7392648.

Guillod, T., Krismer, F. and Kolar, J.W. (2017) 'Protection of MV Converters in the Grid: The Case of MV/LV Solid-State Transformers', in *IEEE Journal of Emerging and Selected Topics in Power Electronics*. https://doi.org/10.1109/JESTPE.2016.2617620.

Hannan, M.A. *et al.* (2020) 'State of the art of solid-state transformers: Advanced topologies, implementation issues, recent progress and improvements', *IEEE Access*, 8. Available at: https://doi.org/10.1109/ACCESS.2020.2967345.

Hirsch, A., Parag, Y. and Guerrero, J. (2018) 'Microgrids: A review of technologies, key drivers, and outstanding issues', *Renewable and Sustainable Energy Reviews*. Available at: https://doi.org/10.1016/j.rser.2018.03.040.

Hooshmand R., Ataei M., Rezaei M. (2012). Improving the dynamic performance of distribution electronic power transformers using sliding mode control, *Journal of Power Electronics*, 12 (1) pp. 145-156.

Hosseinzadeh, N. *et al.* (2021) 'Voltage stability of power systems with renewable-energy inverter-based generators: A review', *Electronics (Switzerland)*. Available at: https://doi.org/10.3390/electronics10020115.

Hopkins D. and Safiuddin M. (2010). Power Electronics in a Smart Grid Distribution System. http://www.dchopkins.com/professional/open_seminars/PowerElectronics_SmartGrid.pdf. Retrieved on 25/04/2023.

Huang, A.Q. (2018) 'Solid state transformers, the energy router and the energy internet', in *The Energy Internet: An Open Energy Platform to Transform Legacy Power Systems into Open Innovation and Global Economic Engines*. Available at: https://doi.org/10.1016/B978-0-08-102207-8.00002-3.

Huang A. (2019). Solid state transformers, the Energy Router, and the Energy Internet,

Woodhead Publishing. Page 21, ISBN 9780081022078. https://doi.org/10.1016/B978-0-08102207-8.00002-3.

Huang, A. (2019). Solid state transformers, the Energy Router, and the Energy Internet. *In the Energy Internet*; Elsevier: Amsterdam, The Netherlands, pp. 21–44.

Huang, A.Q. *et al.* (2011) 'The future renewable electric energy delivery and management (FREEDM) system: The energy internet', *Proceedings of the IEEE*, 99(1). Available at: https://doi.org/10.1109/JPROC.2010.2081330.

Huber E., Kolar J. (2014). Volume/weight/cost comparison of a 1MVA 10 kV/400 V solid-state against a conventional low-frequency distribution transformer. In Proceedings of the 2014 *IEEE Energy Conversion Congress and Exposition (ECCE),* Pittsburgh, PA, USA, IEEE: Hoboken, NJ. pp. 4545–4552.

Huber, J.E. and Kolar, J.W. (2014) 'Volume/weight/cost comparison of a 1MVA 10 kV/400 V solid-state against a conventional low-frequency distribution transformer', in *2014 Institute of Electrical Electronics Engineers Energy Conversion Congress and Exposition, ECCE 2014*. Available at: https://doi.org/10.1109/ECCE.2014.6954023.

Huber, J.E. and Kolar, J.W. (2016) 'Solid-State Transformers: On the Origins and Evolution of Key Concepts', *Institute of Electrical Electronics Engineers Industrial Electronics Magazine*, 10(3). Available at: https://doi.org/10.1109/MIE.2016.2588878.

Huber, J.E. and Kolar, J.W. (2019) 'Applicability of Solid-State Transformers in Today's and Future Distribution Grids', *Institute of Electrical Electronics Engineers Transactions on Smart Grid*, 10(1). Available at: https://doi.org/10.1109/TSG.2017.2738610.

Ismail, N. M. and Mishra, M. K. (2018) 'Study on the design and switching dynamics of hysteresis current controlled four-leg voltage source inverter for load compensation', *IET Power Electronics*, 11(2). doi: 10.1049/iet-pel.2017.0118.

Krause C. (2012). Power transformer insulation—history, technology, and design*. IEEE Transformer, Dielectric, Electric, Insulation.*, 19, 1941–1947.

Martinez-Velasco A., Alepuz S., Gonzalez-Molina F., et al. (2014). Dynamic average modelling of a bidirectional solid-state transformer. https://isiarticles.com/bundles/Article/pre/pdf/57495.pdf. Retrieved on 25/06/2021.

Merwe D., Mouton T. (2009). Solid-state transformer topology selection*. IEEE International Conference on Industrial Technology*. IEEE, 1–6.

Moonem A., Krishnaswami H. (2014). Control and configuration of three-level dual-active bridge DC-DC converter as a front-end interface for photovoltaic system. 29th IEEE Applied Power Electronics Conference and Exposition (APEC). IEEE, 3017–3020.

Lee H., Nguyen H., Chun T. (2008). Implementation of direct torque control method using matrix converter fed induction motor, *Journal of Power Electronics*, 8 (1) pp. 74-80.

Liserre, M., Buticchi G., Andresen M., De Carne G., Costa L., Zou Z. (2016). The smart transformer: Impact on the electric grid and technology challenges. *IEEE Ind. Electron. Mag*. 2016, 10, 46–58.

Liu Y., Liu Y., Abu-Rub H., Ge B. (2016). Model predictive control of matrix converter based solid state transformer. In Proceedings of the 2016 *IEEE International Conference on Industrial Technology (ICIT)*, Taipei, Taiwan, 14–17 March 2016; pp. 1248–1253.

Kanjanavirojkul, P. *et al.* (2017) 'Design, analysis and implementation of pulse generator by CMOS flipped on glass for low power UWB-IR', in *IEICE Transactions on Fundamentals of Electronics, Communications and Computer Sciences*. doi: 10.1587/transfun.E100.A.200.

Kaushik, R.A. and Pindoriya, N.M. (2014) 'A hybrid AC-DC microgrid: Opportunities & key issues in implementation', in *Proceeding of the IEEE International Conference on Green Computing, Communication and Electrical Engineering, ICGCCEE 2014*. Available at: https://doi.org/10.1109/ICGCCEE.2014.6922391.

Khan, M.O. *et al.* (2018) 'A load flow analysis for AC/DC hybrid distribution network incorporated with distributed energy resources for different grid scenarios', *Energies*, 11(2). Available at: https://doi.org/10.3390/en11020367.

Kotb, M.F., El-Saadawi, M. and El-Desouky, E.H. (2018) 'Over Current Protection Relay using Arduino Uno for Future Renewable Electric Energy Delivery and Management (FREEDM) System', *European Journal of Electrical Engineering and Computer Science*, 2(5). Available at: https://doi.org/10.24018/ejece.2018.2.5.39.

Krein, P. T., Balog, R. S. and Mirjafari, M. (2012) 'Minimum energy and capacitance requirements for single-phase inverters and rectifiers using a ripple port', *IEEE Transactions on Power Electronics*, 27(11). doi: 10.1109/TPEL.2012.2186640.

Lee, H.H., Nguyen, H.M., and Chun, T.W. (2008) 'Implementation of direct torque control method using matrix converter fed induction motor', *Journal of Power Electronics*, 8(1).

Lee, H.J. and Yoon, Y.D. (2019) 'Intelligent Transformer Unit Topology Using Additional Small Power Converter Based on Conventional Distribution Transformer', in *2019 Institute Electrical Electronics Engineers Energy Conversion Congress and Exposition, ECCE 2019*. Available at: https://doi.org/10.1109/ECCE.2019.8912672.

Liang, X. (2017) 'Emerging Power Quality Challenges Due to Integration of Renewable Energy Sources', *IEEE Transactions on Industry Applications*, 53(2). Available at: https://doi.org/10.1109/TIA.2016.2626253.

Lin, Z. *et al.* (2019) 'Optimized Design of the Neutral Inductor and Filter Inductors in Three-Phase Four-Wire Inverter with Split DC-Link Capacitors', *IEEE Transactions on Power Electronics*, 34(1). doi: 10.1109/TPEL.2018.2812278.

Liu, B. *et al.* (2016) 'Fuzzy logic control of dual active bridge in solid state transformer applications', in *IET Conference Publications*. Available at: https://doi.org/10.1049/cp.2016.1183.

Liu, B. *et al.* (2017) 'Solid state transformer application to grid connected photovoltaic inverters', in *2016 International Conference on Smart Grid and Clean Energy Technologies, ICSGCE 2016*. Available at: https://doi.org/10.1109/ICSGCE.2016.7876063.

Liu, Y. *et al.* (2017) 'Real-time implementation of finite control set model predictive control for matrix converter based solid state transformer', *International Journal of Hydrogen Energy*, 42(28). Available at: https://doi.org/10.1016/j.ijhydene.2017.04.293.

Liserre, M., Blaabjerg, F. and Dell'aquila, A. (2004) 'Step-by-step design procedure for a grid-connected three-phase PWM voltage source converter', *International Journal of Electronics*, 91(8). doi: 10.1080/00207210412331306186.

Maitra A., Sundaram A., Gandhi M., Bird S., Doss S. (2009), 'Intelligent Universal Transformer Design and Applications', in Proc. 2009 20th International Conference on Electrical Distribution, Prague, 8-11 June 2009, Paper 1032.

Merabet, A. *et al.* (2015) 'Multivariable control algorithm for laboratory experiments in wind energy conversion', *Renewable Energy*, 83. Available at: https://doi.org/10.1016/j.renene.2015.04.031.

Mi, C. *et al.* (2008) 'Operation, design and control of dual H-bridge-based isolated bidirectional DC-DC converter', *IET Power Electronics*, 1(4). doi: 10.1049/iet-pel:20080004.

Miveh, M. R. *et al.* (2016) 'An Improved Control Strategy for a Four-Leg Grid-Forming Power Converter under Unbalanced Load Conditions', *Advances in Power Electronics*, 2016. doi: 10.1155/2016/9123747.

Mogorovic, M. and Dujic, D. (2019) '100 kW, 10 kHz Medium-Frequency Transformer Design Optimization and Experimental Verification', *IEEE Transactions on Power Electronics*, 34(2). Available at: https://doi.org/10.1109/TPEL.2018.2835564.

Mohan, N. *et al.* (1994) 'Simulation of Power Electronic and Motion Control Systems—An Overview', *Proceedings of the IEEE*, 82(8). doi: 10.1109/5.301689.

Mohan, N. and Kamath, G. R. (1997) 'Active power filters - recent advances', *Sadhana - Academy Proceedings in Engineering Sciences*, 22(pt 6). doi: 10.1007/BF02745842.

Olivares, D.E. *et al.* (2014) 'Trends in microgrid control', *IEEE Transactions on Smart Grid*, 5(4). Available at: https://doi.org/10.1109/TSG.2013.2295514.

Orosz T. (2019). Evolution and modern approaches of the power transformer cost optimization methods. Period. Polytech. Electrical Engineering, Computer Science. p63, 37– 50. https://core.ac.uk/download/pdf/236625564. pdf Retrieved on 25/04/2023.

Ortiz, G. *et al.* (2017) 'Design and Experimental Testing of a Resonant DC-DC Converter for Solid-State Transformers', *IEEE Transactions on Power Electronics*, 32(10). Available at: https://doi.org/10.1109/TPEL.2016.2637827.

Pipolo S., Bifaretti S., Bonaiuto V., Tarisciotti L., Zanchetta P. (2016). Reactive power control strategies for UNIFLEX-PM Converter. In Proceedings of the IECON 2016-42nd Annual Conference of *the IEEE Industrial Electronics Society*, Florence, Italy, 23–26 October 2016; IEEE: Hoboken, NJ, USA, 2016; pp. 3570–3575.

Pipolo, S. *et al.* (2016) 'Reactive power control strategies for UNIFLEX-PM Converter', in *IECON Proceedings (Industrial Electronics Conference)*. Available at: https://doi.org/10.1109/IECON.2016.7793903.

Rodrigues, W.A. *et al.* (2017) 'Analysis of Solid State Transformer based microgrid system', in *2016 12th IEEE International Conference on Industry Applications, INDUSCON 2016*. Available at: https://doi.org/10.1109/INDUSCON.2016.7874543.

Roman E. et al. (2002), 'A Power Electronic-Based Distribution Transformer', IEEE Transactions on Power Delivery, Vol. 17, April 2002, Pages: 537 - 543.

Qin H, Kimball JW (2013) Solid-state transformer architecture using AC-AC dual-activebridge converter. *IEEE T Industrial Electronics* 60: 3720–3730.

Quan, Z. *et al.* (2021) ‘Reconsideration of Grid-Friendly Low-Order Filter Enabled by Parallel Converters’, *IEEE Journal of Emerging and Selected Topics in Power Electronics*, 9(3). doi: 10.1109/JESTPE.2020.3009056.

Ramachandran V., Kuvar A., Singh U., et al. (2014). A system level study employing improved solid state transformer average models with renewable energy integration. *IEEE Power and Energy Society General Meeting*. IEEE, 1–5.

Ronanki D., Williamson S. (2018). Evolution of power converter topologies and technical considerations of power electronic transformer-based rolling stock architectures. *IEEE, Transport Electri* 4: 211–219.

Sabahi M., Goharrizi A., Hosseini S., Sharifian M., Gharehpetian G. (2010). 'Flexible Power Electronic Transformer', IEEE Transactions on Power Electronics, Vol. 25, Issue 8, pp. 2159 – 2169.

Sahoo, A. K., Otero-De-Leon, R. and Mohan, N. (2013) ‘Review of modular multilevel converters for teaching a graduate-level course of power electronics in power systems’, in *45th North American Power Symposium, NAPS 2013*. doi: 10.1109/NAPS.2013.6666895.

Saponara, S. and Mihet-Popa, L. (2019) ‘Energy storage systems and power conversion electronics for e-transportation and smart grid’, *Energies*. Available at: https://doi.org/10.3390/en12040663.

Sen, P. C. (2012) ‘Principles of Electric Machines and Power Electronics 3rd Edition’, *Wiley*.

Sen, S., Yenduri, K. and Sensarma, P. (2014) ‘Step-by-step design and control of LCL filter based three phase grid-connected inverter’, in *Proceedings of the IEEE International Conference on Industrial Technology*. doi: 10.1109/ICIT.2014.6894991.

Shadfar, H., Ghorbani Pashakolaei, M. and Akbari Foroud, A. (2021) ‘Solid-state transformers: An overview of the concept, topology, and its applications in the smart grid’, *International Transactions on Electrical Energy Systems*. Available at: https://doi.org/10.1002/2050-7038.12996.

Shamshuddin, M.A. *et al.* (2020) ‘Solid state transformers: Concepts, classification, and control’, *Energies*. Available at: https://doi.org/10.3390/en13092319.

She, X. *et al.* (2011) ‘Performance evaluation of solid state transformer based microgrid in FREEDM systems’, in *Conference Proceedings - IEEE Applied Power Electronics Conference and Exposition - APEC*. Available at: https://doi.org/10.1109/APEC.2011.5744594.

She, X. *et al.* (2012) ‘Solid state transformer interfaced wind energy system with integrated active power transfer, reactive power compensation and voltage conversion functions’, in *2012 IEEE Energy Conversion Congress and Exposition, ECCE 2012*. Available at: https://doi.org/10.1109/ECCE.2012.6342508.

She, X. (2013) ‘Control and Design of a High Voltage Solid State Transformer and its Integration with Renewable Energy Resources and Microgrid System.’, *Igarss 2014* [Preprint], (1).

She, X., Huang, A.Q. and Burgos, R. (2013) ‘Review of solid-state transformer technologies and their application in power distribution systems’, *IEEE Journal of Emerging and Selected Topics in Power Electronics*, 1(3). Available at: https://doi.org/10.1109/JESTPE.2013.2277917.

Shi, X. and Le, H. T. (2021) 'Mitigating Harmonics from Residential Solar Photovoltaic Systems', in *2021 IEEE PES Innovative Smart Grid Technologies - Asia, ISGT Asia 2021*. doi: 10.1109/ISGTASIA49270.2021.9715578.

She, X., Wang, F., Burgos, R., Huang, A.Q15–20 (September 2012). Solid state transformer interfaced wind energy system with integrated active power transfer, reactive power compensation and voltage conversion functions. In Proceedings of the *2012 IEEE Energy Conversion Congress and Exposition (ECCE)*, Raleigh, NC, USA, IEEE: Hoboken, NJ, USA. pp. 3140–3147.

Shri, A. *et al.* (2013) 'Design and control of a three-phase four-leg inverter for solid-state transformer applications', in *2013 15th European Conference on Power Electronics and Applications, EPE 2013*. doi: 10.1109/EPE.2013.6634666.

Shri A., Popovic J., Ferreira A., et al. (2013). Design and control of a three-phase four-leg inverter for solid-state transformer applications. 15th *European Conference on Power Electronics and Applications* (EPE). IEEE, 1–9.

Solatialkaran, D., Khajeh, K. G. and Zare, F. (2021). 'A Novel Filter Design Method for Grid-Tied Inverters', *IEEE Transactions on Power Electronics*, 36(5). doi: 10.1109/TPEL.2020.3029827.

Sooriyabandara M., Ekanayake J. (2010). 'Smart Grid - Technologies for its realization', in Proc. 2010 IEEE International Conference on Sustainable Energy Technologies (ICSET).

Soodi, H. A. and Vural, A. M. (2021) 'Design, Optimization and Experimental Verification of a Low Cost Two-Microcontroller Based Single-Phase STATCOM', *IETE Journal of Research*. doi: 10.1080/03772063.2021.1875270.

Srdic S. Lukic S., Toward (2019). Extreme Fast Charging: Challenges and Opportunities in Directly Connecting to Medium-Voltage Line*. IEEE*. page 7, 22–31.

Sun, Q. *et al.* (2022) 'Model Predictive Direct Power Control of Three-Port Solid-State Transformer for Hybrid AC/DC Zonal Microgrid Applications', *IEEE Transactions on Power Delivery*, 37(1). Available at: https://doi.org/10.1109/TPWRD.2021.3064418.

Tesla N. (1 May 1888). System of Electrical Distribution. U.S. Patent 381, 970.

Vaca-Urbano F., Alvarez-Alvarado M., Recalde A., Moncayo-Rea F. (2019). Solid-State Transformer for Energy Efficiency Enhancement. IntechOpen, DOI:10.5772/intechopen.84345.

Van der Merwe J. and Mouton H. (Sept 2009). The solid-state transformer concept: A new era in power distribution, in Proceedings of *the IEEE Africon Conference*, Nairobi, Page 3.

Vargas T., Toebe A., Rech C. (2015). Double network control architecture for a modular solid-state transformer. 13th IEEE Brazilian Power Electronics Conference and 1st Southern Power Electronics Conference (COBEP/SPEC). *IEEE*, 1–6.

Viktor, B., Indrek, R. and Tõnu, L. (2011) 'Intelligent Transformer: Possibilities and Challenges', *Scientific Journal of Riga Technical University. Power and Electrical Engineering*, 29(1). Available at: https://doi.org/10.2478/v10144-011-0016-8.

Wang L., Zhang D., Wang Y., et al. (2016). Power and voltage balance control of a novel three phase solid-state transformer using multilevel cascaded H-bridge inverters for microgrid applications. *IEEE T Power Electric* 31: 3289–3301.

Wolf M., (October 2009). Design and implementation of a modular converter with application to a solid-state transformer, Master's thesis, Stellenbosch University, Page 2, 3, 47.

Yang, J. *et al.* (2021) 'Harmonic characteristics data-driven THD prediction method for LEDs using MEA-GRNN and improved-Adaboost algorithm', *Institute of Electrical Electronics Engineers Access*, 9. doi: 10.1109/ACCESS.2021.3059483.

Yu Du SB., Wang G., Bhattacharya S. (2010). Design considerations of high voltage and high frequency three phase transformer for Solid State Transformer application. *Energy Conversion Congress and Exposition (ECCE)*. *IEEE*, 1551–1558.

Yu, X. *et al.* (2014) 'System integration and hierarchical power management strategy for a solid-state transformer interfaced microgrid system', *IEEE Transactions on Power Electronics*, 29(8). Available at: https://doi.org/10.1109/TPEL.2013.2289374.

Zabaleta, M. *et al.* (2016) 'LCL grid filter design of a multimegawatt medium-voltage converter for offshore wind turbine using SHEPWM modulation', *IEEE Transactions on Power Electronics*, 31(3). doi: 10.1109/TPEL.2015.2442434.

Zeljkovic, S. *et al.* (2015) 'Control of SiC-based dual active bridge in high power three phase on-board charger of EVs', in *Electrical Systems for Aircraft, Railway and Ship Propulsion, ESARS*. doi: 10.1109/ESARS.2015.7101454.

Zhang, N., Tang, H. and Yao, C. (2014) 'A systematic method for designing a PR controller and active damping of the LCL filter for single-phase grid-connected PV inverters', *Energies*, 7(6). doi: 10.3390/en7063934.

Zhao T., Zeng J., Bhattacharya S., et al. (2009). An average model of solid-state transformer for dynamic system simulation. IEEE Power and Energy Society General Meeting. *IEEE*, 1–8.

Zheng, L. *et al.* (2020) '7.2 kV Three-Port Single-Phase Single-Stage Modular Soft-Switching Solid-State Transformer with Active Power Decoupling and Reduced DC-Link', in *Conference Proceedings - IEEE Applied Power Electronics Conference and Exposition - APEC*. Available at: https://doi.org/10.1109/APEC39645.2020.9124244.

APPENDICES

Appendix A: The SST Central Role in The Smart Energy Mix

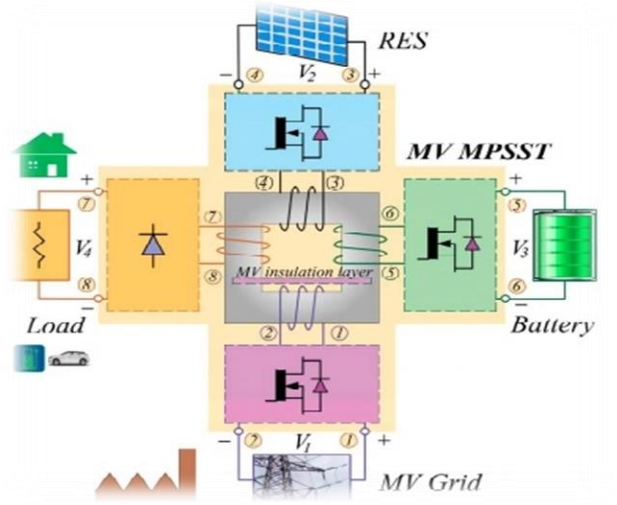

Appendix B: Selection of core materials based on important characteristics of magnetic materials.

Magnetic Core Material (Type of Material)	The Flux Density (Flux Per Unit Area)	The Power Losses	Magnetic Permeability	Readily Availability	The Material Cost (Affordability)
Amorphous	√	X	√	√	√
Silicon grain Steel	√	X	√	√	X
Ferrite	√	√	√	√	√
Nanocrystalline	√	X	√	X	X

Appendix C: MATLAB Simulink SST Model Design for Smart Energy

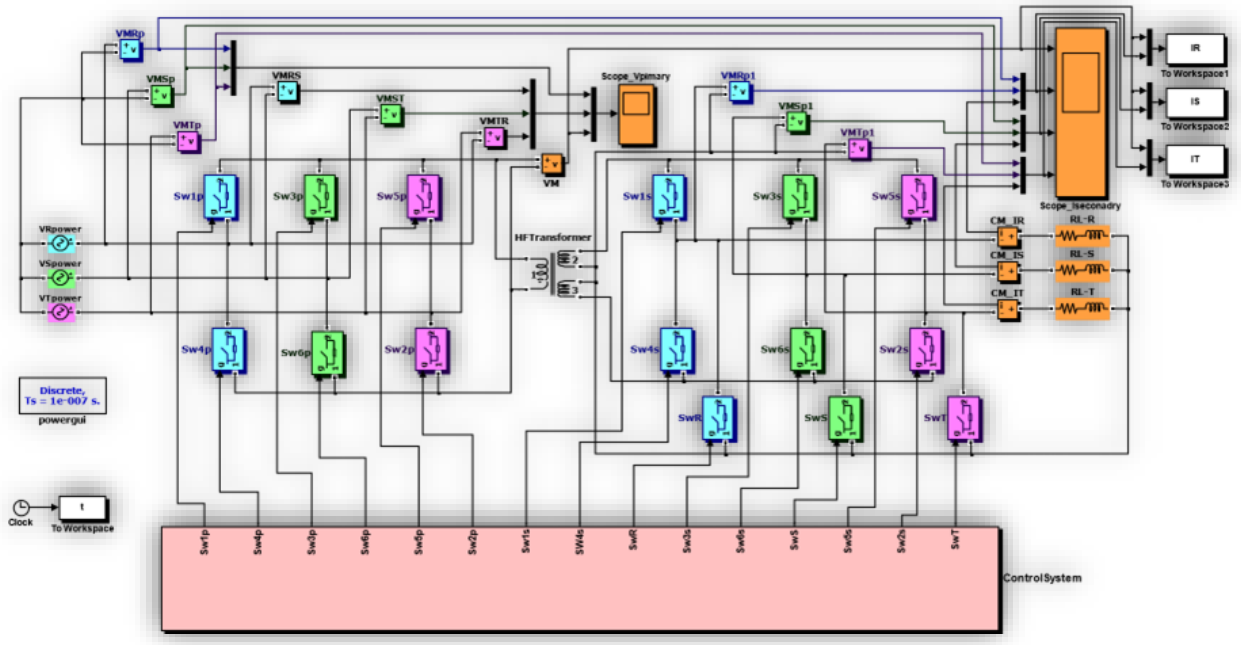

Appendix D: MATLAB embedded code and Simulink Control Sub-System Model and Design

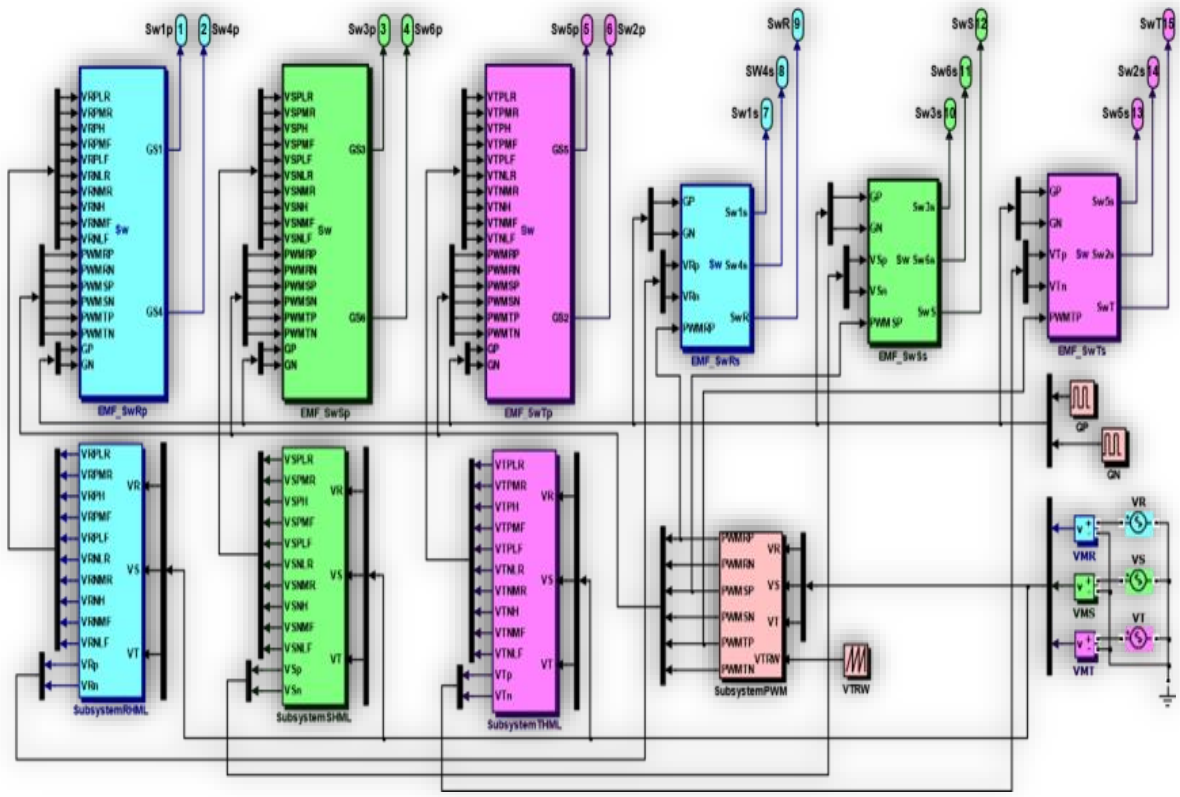

Appendix E: MATLAB Simulink waveforms for High-Frequency Transformer (HFT) primary and secondary terminals